

# Large Tyre Testing and Modelling for Handling

By

Yasheen Babulal

Submitted in partial fulfilment of the requirements for the degree

Master of Engineering  
(Mechanical Engineering)

in the faculty of

Engineering, Built Environment and Information Technology (EBIT)

at the

University of Pretoria

Pretoria  
South Africa  
2015

## Dissertation summary

### Large Tyre Testing and Modelling for Handling

**Yasheen Babulal**

Supervisor: Professor Schalk Els  
Department: Mechanical and Aeronautical Engineering  
University: University of Pretoria  
Degree: Master of Engineering (Mechanical Engineering)

In order to simulate vehicle handling and roll over propensities, tyre characteristics in the form of side-force versus slip-angle curves, as well as suitable tyre models are required. For large tyres these characteristics are not readily available. Tyre manufacturers either do not have these characteristics, or do not openly publish them.

Similarly, the majority of tyre models have been developed and validated for passenger car tyres and their applicability to large tyres are unknown. Furthermore the tests conducted to obtain passenger car tyre data cannot always be performed on large tyres.

The purpose of this study was to measure side-force versus slip-angle characteristics for two large tyres then use the data to parameterise existing tyre models and determine the accuracy of these models. The tyres of interest were the GoodYear Regional 385/65R22.5 tyre, which is a typical truck tyre, and a Michelin 16.00R20 XZL, which is a tyre typically used on military vehicles.

In order to measure these characteristics, existing tyre testing equipment in the form of a tyre test trailer had to be revived, as it had not been used in the past 10 years. The confidence in the equipment was therefore so low that extensive verification tests had to be conducted to develop sufficient confidence in the equipment, to be able to perform these tests and obtain accurate data. In line with this objective, it was envisaged to create a commercial business opportunity for tyre testing utilising the revived equipment, as there is a huge international requirement for data on these tyres.

The above equipment revival was conducted successfully, and the tyre tests were performed at Gerotek Test Facilities. Successful steady state side-force versus slip-angle characteristic tests were performed, and a dynamic double lane change test was performed, and used to validate models.

From the side-force versus slip-angle characteristic data three existing tyre models were parameterised namely, Fiala, UA (University of Arizona) and Pacejka 89 tyre models, as implemented in ADAMS View software.

In order to validate these models, an ADAMS model of the Tyre Tester was developed incorporating physical measured parameters, such as the geometry, mass, centre of mass and moments of inertia.

Correlation between the simulated data of the tyre models and the measured track data was evaluated. The correlation showed that the Pacejka 89 tyre model provided the closest fit for the side-force versus slip angle tests, of all three tyre models. The Pacejka 89 tyre model also showed good correlation on the dynamic double lane change tests.

## Acknowledgement

I wish to express my appreciation to the following organization and persons who made this dissertation possible:

- My supervisor Professor Schalk Els for his enthusiasm and eagerness, guidance and advice throughout this project.
- The fellow students of the Vehicle Dynamics Group (VDG) at the University of Pretoria.
- My colleagues at Gerotek test facilities for their support and advice, and for the use of the facilities.
- The following persons are gratefully acknowledged for their assistance during the course of the study:
  - Adam Rehnberg
  - Carl Becker
  - Theunis Botha
  - Joachim Stallmann
- My family for their encouragement and support.

## Table of Contents

1.	Large Tyre Testing and Modelling for Handling .....	1
1.1	Introduction.....	1
1.2	Organisation of the report .....	2
2.	Technical introduction and literature survey.....	3
2.1	General information about tyres .....	3
2.2	Slip-angle and side-force explained.....	3
2.3	Tyre testers .....	5
2.4	Tyre modelling.....	10
2.5	Tyre models used in this study.....	10
2.6	Large tyres .....	16
2.7	Summary of Technical introduction and literature survey .....	16
3.	The Tyre Tester .....	17
3.1	Description of the Tyre Tester .....	17
3.2	Load cell verification exercise .....	20
3.3	Applying forces to the Tyre Tester.....	22
3.4	Summary of the Tyre Tester.....	27
4.	Track testing.....	28
4.1	Tyres .....	28
4.2	Track testing at Gerotek Test Facilities.....	29
4.3	Instrumentation on the Tyre Tester:.....	31
4.4	Side-force slip-angle testing.....	32
4.5	Characteristic tyre data – side-force slip-angle .....	34
4.6	GoodYear tyre testing data .....	37
4.7	Michelin tyre testing data .....	38
4.8	Double lane change test .....	40
4.9	Summary of Track Testing .....	41
5.	Tyre Tester characterisation and modelling .....	42
5.1	CAD model dimensions.....	42
5.2	Mass of Tyre Tester.....	45
5.3	Centre of gravity .....	46
5.4	Moments of Inertia.....	53
5.5	ADAMS simulation model creation .....	59
5.6	Summary of Tyre Tester characterisation and modelling .....	62
6.	Parameterisation of ADAMS tyre models .....	63
6.1	Determination of general tyre parameters for tyre models.....	63
6.2	Fiala tyre model .....	66
6.3	UA tyre model.....	67
6.4	Pacejka 89 ('Magic Formula') tyre model.....	67
6.5	Summary of parameterisation of ADAMS tyre models .....	71
7.	Simulation results and correlation .....	72
7.1	Simulation results: GoodYear tyre – Side-force versus slip-angle tests: .....	72
7.2	Simulation results: Michelin tyre – Side-force versus slip-angle tests: .....	78
7.3	Pacejka 89: RMSE analysis of Curve-fit and Simulated data compared to Measured data 83	
7.4	Simulation results: GoodYear tyre - Double lane change .....	84
7.5	Simulation results: Michelin tyre – Double lane change .....	90
7.6	Summary of Simulation results and correlation.....	94

8.	Conclusion and recommendations .....	95
8.1	Conclusion.....	95
8.2	Recommendations for future work.....	96

References

Appendix A: ADAMS tyre model files

Appendix B: Load cell calibration certificate

## List of figures

Figure 1: Vehicle cornering (“Car of the week” Hotrod Ramblings Part 2   MyRideisMe.com, 2014)	4
Figure 2: Typical side-force versus slip-angle characteristic graph (Haney, 2003)	4
Figure 3: Forces acting on a tyre (Pacejka 2006)	5
Figure 4: VMI Tire test machine (VMI Group   Force and moment testing, 2014)	6
Figure 5: MTS Flat Trac classic Tyre Tester (Flat-Trac® Tire Test Systems, 2005)	6
Figure 6: FKA’s dynamic tyre test rig (www.ika.rwth-aachen.de, 2007)	7
Figure 7: MTS – Flat-Trac Roadway for Dynamic Road Handling testing on large vehicles (Flat-Trac® Tire Test Systems, 2005)	8
Figure 8: The Delft tyre test trailer (Yunus.hacettepe.edu.tr, (n.d.))	8
Figure 9: Farm tractor tyre testers (Kutzbach et al, 2009)	9
Figure 10: ADAMS Tyre model table (ADAMS View HELP, 2012)	11
Figure 11: Illustration of coefficients contained in the ‘Magic Formula’ (Bakker E et al, 1989)	14
Figure 12: Tyre Tester	17
Figure 13: CAD Model of Tyre Tester	17
Figure 14: Side view of Tyre Tester (dimensions in mm)	18
Figure 15: Top view of Tyre Tester (dimensions in mm)	18
Figure 16: Front view of Tyre Tester (dimensions in mm)	18
Figure 17: CAD model with load cells	19
Figure 18: Tyre Tester load cells	19
Figure 19: Tension verification setup	21
Figure 20: Compression verification setup	21
Figure 21: Load cell verification - serial number: 33443 (Tension test)	22
Figure 22: Lateral force applied perpendicular to wheel hub in the Y direction	23
Figure 23: Analysis of applied lateral force	24
Figure 24: Vertical force applied perpendicular to wheel hub in the Z direction	24
Figure 25: Vertical applied force analysis	25
Figure 26: Longitudinal force applied parallel to wheel hub in the X direction	26
Figure 27: Longitudinal force analysis	27
Figure 28: Gerotek’s Straight Track	30
Figure 29: Close-up view of the surface of Gerotek’s Straight Track	30
Figure 30: Tow vehicle and Tyre Tester	30
Figure 31: View from top of wheel set at a specific slip-angle (GoodYear tyre)	33
Figure 32: Tow vehicle with Tyre Tester performing slip-angle tests (Michelin tyre)	33
Figure 33: Tyre scrub marks (Michelin tyre)	33
Figure 34: Tyre scrub wear (Michelin tyre)	33
Figure 35: Data showing individual values on load cells, speed and slip-angle	35
Figure 36: Data of total lateral force, slip-angle and speed	36
Figure 37: Side-force slip-angle characteristic curve: GoodYear Tyre	38
Figure 38: Side-force slip-angle characteristic curve: Michelin Tyre	39
Figure 39: Double lane change track	40
Figure 40: Double lane change test being performed	41
Figure 41: Mainframe of Tyre Tester	43
Figure 42: Subframe of Tyre Tester	43
Figure 43: Mainframe and subframe detached from each other	44
Figure 44: CAD model of assembled Tyre Tester	44
Figure 45: Tyre Tester with load cells (highlighted) under landing legs	45

Figure 46: Force diagram in longitudinal plane of Tyre Tester .....	46
Figure 47: Side view of Tyre Tester highlighting the Centre of Gravity position.....	47
Figure 48: Force diagram in lateral plane of Tyre Tester .....	48
Figure 49: Top view of Tyre Tester highlighting the Centre of Gravity position.....	49
Figure 50: Lift method to determine vertical position of the centre of gravity .....	50
Figure 51: Force diagram used to determine vertical position of the centre of gravity .....	51
Figure 52: Vertical centre of gravity versus lift angle .....	52
Figure 53: Schematic presentation of the rotational vibration of a rigid body.....	53
Figure 54: Roll moment of inertia setup .....	55
Figure 55: Spring displacement as measured during roll moment of inertia determination .....	55
Figure 56: Determining the moment of inertia at the centre of gravity .....	56
Figure 57: Pitch moment of inertia setup.....	57
Figure 58: Depiction of yaw moment of inertia setup .....	58
Figure 59: Graphic of the Tyre Tester ADAMS model .....	59
Figure 60: Illustration of Tyre Tester with different slip-angles .....	61
Figure 61: Different load conditions .....	62
Figure 62: Vertical drop test (laser displacement oscillation) – GoodYear tyre.....	64
Figure 63: GoodYear tyre carcass shape.....	65
Figure 64: Michelin tyre carcass shape.....	66
Figure 65: Repeated Illustration of coefficients contained in the ‘Magic Formula’ (Bakker E et al, 1989) .....	68
Figure 66: Microsoft Excel solver interface.....	69
Figure 67: GoodYear Pacejka 89 curve fit.....	70
Figure 68: Michelin Pacejka 89 curve fit.....	71
Figure 69: GoodYear tyre: Lateral load cells data comparison (Pacejka 89, Slip-angle = 4°, load condition: Load 1).....	73
Figure 70: GoodYear tyre: Lateral load cells data comparison (Pacejka 89, Slip-angle = 10°, load condition: load 3).....	74
Figure 71: GoodYear tyre: Side-force versus slip-angle comparison of tyre models and measured data (Load 1).....	75
Figure 72: GoodYear tyre: Side-force versus slip-angle comparison of tyre models and measured data (Load 2).....	76
Figure 73: GoodYear tyre: Side-force versus slip-angle comparison of tyre models and measured data (Load 3).....	76
Figure 74: GoodYear tyre: Root mean squared error comparison of tyre models and measured data.....	77
Figure 75: Michelin tyre: Lateral load cells data comparison (Pacejka 89, Slip-angle = 4°, load condition: Load 1).....	78
Figure 76: Michelin tyre: Lateral load cells data comparison (Pacejka 89, Slip-angle = 10°, load condition: load 3).....	79
Figure 77: Michelin tyre: Side-force versus slip-angle comparison of tyre models and measured data (Load 1).....	80
Figure 78: Michelin tyre: Side-force versus slip-angle comparison of tyre models and measured data (Load 2).....	81
Figure 79: Michelin tyre: Side-force versus slip-angle comparison of tyre models and measured data (Load 3).....	81
Figure 80: Michelin tyre: Root mean squared error comparison of tyre models and measured data .....	82
Figure 81: GoodYear tyre: Pacejka 89 tyre model Curve-fit and Simulated data compared to measured data .....	83

Figure 82: Michelin tyre: Pacejka 89 tyre model Curve-fit and Simulated data compared to measured data .....84

Figure 83: GoodYear tyre: Double lane change data (load condition: load 1).....86

Figure 84: GoodYear tyre: Root mean squared error comparison for double lane change (load 1) .....87

Figure 85: GoodYear tyre: Double lane change data (load condition: load 2).....88

Figure 86: GoodYear tyre: Root mean squared error comparison for double lane change (load 2) .....89

Figure 87: Michelin tyre: Double lane change data (load condition: load 1).....90

Figure 88: Michelin tyre: Root mean squared error comparison for double lane change (load 1).91

Figure 89: Michelin tyre: Double lane change data (load condition: load 2).....92

Figure 90: Michelin tyre: Root mean squared error comparison for double lane change (load 2).93



## List of tables

Table 1: 'Magic Formula' lateral coefficients.....	15
Table 2: GoodYear tyre details .....	28
Table 3: Michelin tyre details .....	29
Table 4: GoodYear tyre: wheel loads (unladen load condition).....	31
Table 5: GoodYear Tyre load conditions.....	32
Table 6: Michelin Tyre load conditions .....	33
Table 7: GoodYear Tyre: Side-force & Slip-angle data.....	37
Table 8: Michelin Tyre: Side-force & Slip-angle data.....	39
Table 9: Fiala CALPHA values .....	67

## List of symbols

### *English letters, symbols and notations (Upper case)*

A	-	Point where the centre of gravity of the Tyre Tester is located
B	-	Stiffness factor in 'Magic Formula'
BCD	-	Slope at zero slip-angle in 'Magic Formula'
C	-	Shape factor in 'Magic Formula'
$C_{\alpha}$	-	Cornering stiffness (UA tyre model)
$C_{\gamma}$	-	Camber stiffness (UA tyre model)
CALPHA	-	Fiala tyre model cornering stiffness
CD	-	Product of C and D as used in 'Magic Formula'
D	-	Peak factor in 'Magic Formula'
E	-	Curvature factor in 'Magic Formula'
F	-	Force value as obtained from the load cell, at a specific lift angle ( $\beta$ ) – used for vertical centre of gravity determination
$F_{\text{Front landing legs}}$	-	Sum total of forces on both the front landing legs of the Tyre Tester
$F_{\text{Lateral\_applied}}$	-	Applied lateral force to the Tyre Tester
$F_{\text{Lateral\_front\_loadcell}}$	-	Force as measured by the front lateral load cell on the Tyre Tester
$F_{\text{Lateral\_rear\_loadcell}}$	-	Force as measured by the rear lateral load cell on the Tyre Tester
$F_{\text{Left-front}}$	-	Force acting on left front landing leg
$F_{\text{Left-rear}}$	-	Force acting on left rear landing leg
$F_{\text{Longitudinal\_applied}}$	-	Applied longitudinal force to the Tyre Tester
$F_{\text{Longitudinal\_front\_loadcell}}$	-	Force as measured by the longitudinal load cell on the Tyre Tester
$F_{\text{Rear landing legs}}$	-	Sum total of forces on both the rear landing legs of the Tyre Tester
$F_{\text{Right-front}}$	-	Force acting on right front landing leg
$F_{\text{Right-rear}}$	-	Force acting on right rear landing leg
$F_{\text{Total weight of tyre tester}}$	-	Total weight of Tyre Tester
$F_{\text{Vert\_applied}}$	-	Applied vertical force to the Tyre Tester
$F_{\text{Vert\_front\_loadcell}}$	-	Force as measured by the front vertical load cell on the Tyre Tester
$F_{\text{Vert\_middle\_loadcell}}$	-	Force as measured by the middle vertical load cell on the Tyre Tester
$F_{\text{Vert\_rear\_loadcell}}$	-	Force as measured by the rear vertical load cell on the Tyre Tester
$F_x$	-	Tyre longitudinal force
$F_y$	-	Tyre lateral force
$F_z$	-	Tyre vertical force
H	-	

$$H = 1 - \left( \frac{CALPHA \cdot |\tan(\alpha)|}{3 \cdot U \cdot |F_z|} \right) \text{ (Fiala tyre model)}$$

**English letters, symbols and notations (Upper case)**

$I_0$	-	Moment of inertia about the axis of rotation
$\bar{I}_{roll}$	-	Roll moment of inertia of the Tyre Tester about its centre of gravity
$I_{body}$	-	Roll moment of inertia
$I_{XX}$	-	Pitch moment of inertia
$I_{YY}$	-	Yaw moment of inertia
$I_{ZZ}$	-	Longitudinal distance of the centre of gravity to the pivot point o
$L_1$	-	Vertical height of the centre of gravity from ground level
$L_2$	-	Distance of the spring from pivot point o
$L_{force}$	-	Measured track data (force) at slip-angle i
$M_i$	-	Roll moment or overturning couple
$M_x$	-	Driving/braking torque and rolling resistance torque
$M_y$	-	Self aligning moment
$M_z$	-	Lateral slip due to slip angle (UA tyre model)
$S_\alpha$	-	Lateral slip due to camber (angle) inclination (UA tyre model)
$S_Y$	-	Horizontal shift in 'Magic Formula'
$S_h$	-	Simulated tyre model data (force) at slip-angle i
$S_i$	-	Longitudinal slip ratio
$S_s$	-	Vertical shift in 'Magic Formula'
$S_v$	-	Current coefficient of friction (Fiala tyre model)
$U$	-	Speed of travel of wheel centre (with x, y components)
$V$	-	Total weight of the Tyre Tester
$W$	-	Composite angle in 'Magic Formula'
$X_1$	-	Longitudinal centre of gravity
$X_{CG}$	-	Lateral centre of gravity
$Y_{CG}$	-	Vertical centre of gravity
$Z_{CG}$	-	

**English letters, symbols and notations (Lower case)**

$a_0 \dots a_{13}$	-	Lateral coefficients in 'Magic Formula'
$c$	-	Damping coefficient
$i$	-	Counter as used in $\Sigma$ operations
$k$	-	Spring stiffness coefficient
$l_n$	-	Contact patch length (UA tyre model)
$m_{\text{body}}$	-	Mass of the Tyre Tester (excluding the tyre and rim)
$o$	-	Pivot point
$p$	-	Longitudinal distance of the centre of gravity to the front landing legs of the Tyre Tester (mm)
$q$	-	Lateral distance of the centre of gravity to the right front landing leg of the Tyre Tester (mm)
$s$	-	Tyre longitudinal slip
$x_1$	-	Longitudinal length of the Tyre Tester from the rear landing legs (pivot point) to the front tow hitch (lifting point)
$x_2$	-	Longitudinal distance of the centre of gravity to the rear landing legs (pivot point)
$z_1$	-	Vertical height of the centre of gravity from the ground (mm)
$z_2$	-	Vertical height from ground to the tow hitch (lifting point)

### ***Greek symbols and notations***

$\sum F_{\text{Lateral\_loadcells}}$	-	Sum of forces of the two lateral load cells on the Tyre Tester
$\sum F_{\text{Longitudinal\_loadcell}}$	-	Sum of forces of the (single) longitudinal load cell on the Tyre Tester
$\sum F_{\text{Vert\_loadcells}}$	-	Sum of forces of the three vertical load cells on the Tyre Tester
$\sum T_o$	-	Sum of moments of the external forces about point o
$\alpha$	-	Tyre slip-angle (degrees)
$\alpha_y$	-	Is defined as the product of the slip-angle and camber angle, taking their signs into consideration (UA tyre model)
$\beta$	-	Lift angle of the Tyre Tester as measured from the ground (horizontal)
$\gamma$	-	Camber angle
$\delta$	-	Logarithmic decrement
$\zeta$	-	Damping ratio
$\theta$	-	Angle (degrees)
$\ddot{\theta}$	-	Angular acceleration
$\mu$	-	Coefficient of friction
$\mu_y$	-	Coefficient of friction in the lateral direction (UA tyre)
$\mu_y^{(m)}$	-	Modified coefficient of friction in the lateral direction (UA tyre)
$T$	-	period (s)
$T_d$	-	Damped period (s)
$\Omega$	-	Wheel speed of revolution
$\omega_n$	-	Natural frequency (rad/s)

### ***Abbreviations***

ADAMS	-	Automatic Dynamic Analysis of Mechanical Systems (Computer software)
GPS	-	Global Positioning System
RMSE	-	Root Mean Squared Error
UA	-	University of Arizona

## Large Tyre Testing and Modelling for Handling

# 1. Large Tyre Testing and Modelling for Handling

This first chapter provides a basic introduction to the research project of large tyre testing and modelling for handling, describing the background to the project, highlighting project objectives and scope as well as the methodology of the study.

### **1.1 Introduction**

Air filled rubber tyres are used in many applications, ranging from bicycles, motorcycles, recreational quad bikes, passenger cars, pick-ups, sport utility vehicles (SUV's), minibuses, busses, trucks, farming tractors, truck-tractor trailer combinations, military vehicles and even on aeroplanes.

When travelling, these vehicles do not always encounter a straight path. They more often than not encounter curved paths; and need to be able to negotiate them. When a tyre negotiates a curved path, it is its lateral characteristics that are currently at 'work'. This study focuses on these lateral characteristics. More specifically, it is the side (lateral) force versus slip-angle characteristic of a tyre that is the focus of this study. The two types of tyres chosen for this study were a truck tyre, and a military vehicle tyre. The truck tyre was an on-road type tyre, whilst the military vehicle tyre was a multipurpose, on and off-road type tyre.

With regards to the side-force versus slip-angle characteristics, data in this form, especially for large tyres, is not openly available. Tyre manufacturers may not have, or do not openly publish this data. In order to obtain this side-force versus slip-angle data, physical tyre tests need to be performed. One of the aims of this study was to physically measure this tyre characteristic (data) for a large truck and a military vehicle tyre.

Tyre testing equipment was available, but the equipment was out of commission for the last 10 years, therefore, there was a low degree of confidence in the equipment, or the data that the equipment could possibly produce. A key objective of this study was to revive the tyre test equipment, and to develop a capability to measure tyre data, and furthermore to develop tyre testing into a commercial business opportunity for Gerotek Test Facilities.

The tyre testing equipment available was a large trailer-type Tyre Tester. This Tyre Tester had the capability of measuring tyre forces, whilst the slip-angle and the vertical tyre load could be varied.

Once the equipment was commissioned and the required confidence in the equipment was developed, side-force versus slip-angle tests for three different vertical load conditions, as well as a double lane change test were performed.

The specific details of the tyres tested are as follows, the first tyre is typically used on trucks and is manufactured by GoodYear. It is the GoodYear Regional 385/65R22.5 tyre. The second tyre is typically used on military vehicles and is manufactured by Michelin. It is the Michelin 16.00 R20 XZL tyre.

Once the side-force versus slip-angle data was obtained, from the above mentioned tests, tyre models were then parameterised. The importance of tyre models is that they are used in vehicle simulations, during development and evaluation, to fine tune aspects such as handling, acceleration, braking and ride comfort.

## Large Tyre Testing and Modelling for Handling

With regards to the verification of the tyre models, an ADAMS model of the Tyre Tester was developed incorporating the measured physical parameters of the actual Tyre Tester, such as the geometry, mass, centre of gravity and the moments of inertia. These tyre models were then simulated with the ADAMS model of the Tyre Tester to establish correlation between simulated results and measured results.

Pacejka 89, Fiala and UA (University of Arizona) tyre models were parameterised and fine-tuned. The results of each tyre model were compared to the measured test data. Conclusions could then be drawn as to which tyre model produced the best correlation with the measured data.

### **1.2 Organisation of the report**

This report contains the following chapters and appendices:

Chapter 1 serves as an introduction to the study of “Large Tyre Testing and Modelling for Handling”.

Chapter 2 contains the technical introduction and the literature study.

Chapter 3 contains details on the Tyre Tester and the verification tests done prior to track testing.

Chapter 4 contains the track testing exercise, and resulting tyre characteristic data.

Chapter 5 contains the characterisation tests conducted on the Tyre Tester to develop the ADAMS dynamic simulation model.

Chapter 6 contains the parameterisation of the tyre models

Chapter 7 contains the correlation between simulated results and the measured track results.

Chapter 8 contains the conclusions and recommendations.

The list of references follows at the end of the report.

The following appendices are also contained within the report.

Appendix A: ADAMS tyre model files.

Appendix B: Load cell calibration certificate.

## Large Tyre Testing and Modelling for Handling

### **2. Technical introduction and literature survey**

The second chapter contains general information about tyres, and then moves on to explain the concepts of side-force and slip-angle. The next section contains details of the various Tyre Testers available internationally which are capable of measuring lateral tyre characteristics. The importance of this is to gauge the capability of what is available internationally, as well as to understand the latest trends. Relevant literature on tyre modelling is highlighted including the tyre models used in this study, and finally large tyres are discussed at the end of this chapter.

#### **2.1 General information about tyres**

“Tyre” versus “Tire”

Reading or browsing through literature on the subject of tyres, one encounters two different spellings of the words tyre, both of equal frequency. According to Tire vs tyre – Grammarist (2013), “Tire” is the preferred spelling in the United States and Canada, whilst “Tyre” is preferred spelling outside North America.

According to Haney (2003), a modern pneumatic tyre is a complicated composite construction of strong, light polymer fibres held together in a matrix of viscoelastomeric polymers – rubbers.

According to Pacejka (2006), the complexity of the structure and behaviour of the tyre are such that no complete and satisfactory theory has yet been propounded.

Both of the above descriptions indicate that the tyre is a complex entity, and is an area that is still to be fully understood. It therefore forms an excellent basis for research and development.

#### **2.2 Slip-angle and side-force explained**

As the focus of this study concerns side-force and slip-angle, a simplistic explanation regarding the above terms follows:

According to Haney (2003), slip-angle occurs when the steering wheel (of a vehicle) is turned from straight ahead and the tyre creates an angle ( $\alpha$ ) between where the tyre is pointed and where the car is actually going. It is the elastic nature of a tyre which makes the slip-angle possible.

The generation of tyre side-force is described as follows by Haney (2003): Following the turning of a tyre and the creation of a slip-angle, each small increment of tread rubber rotating into the contact patch latches onto the road surface a small increment towards the new heading. The tread actually deforms as it rotates through the contact patch. The force needed to deform the tyre is what produces the lateral (side) force needed to change the path of the car.

According to Wong (2001), the relationship between the cornering force and the slip-angle is of fundamental importance to the directional control and stability of road vehicles.

Figure 1 depicts a picture of a vehicle negotiating a corner. The above mentioned side-force and slip-angle are present during this manoeuvre.



## Large Tyre Testing and Modelling for Handling



**Figure 1: Vehicle cornering (“Car of the week” Hotrod Ramblings Part 2 | MyRideisMe.com, 2014)**

A typical side-force versus slip-angle relationship is depicted in Figure 2.

A description is given according to Haney (2003); at low slip-angles the lateral force is proportional to the slip-angle, as depicted in the “elastic” or “linear” region of Figure 2. The slope of the curve in this region represents the cornering stiffness of the tyre. It should be noted that in the “elastic” or “linear” region of the curve, the tyre’s tread is not sliding on the road, at any point in its contact patch.

As the slip-angle increases further, portions of the tyre patch start sliding, and as a result there is less increase in lateral force with an increase in slip-angle. The lateral force also reaches its peak in this region, known as the “transitional” region. Typically race car drivers aim to operate at this point during cornering, as they are thus extracting the maximum lateral force the tyre is capable of producing.

As the slip-angle increases further, more of the contact patch is sliding and the tire is producing less lateral force. At high slip-angles most of the contact patch is sliding, producing a lot of heat and wear. This area is marked as the “frictional” region of Figure 2.

Each tyre will have its own side-force versus slip-angle characteristic curve. Note that changing parameters such as camber, vertical tyre load and tyre pressure will produce different side-force versus slip-angle curves for the same tyre.

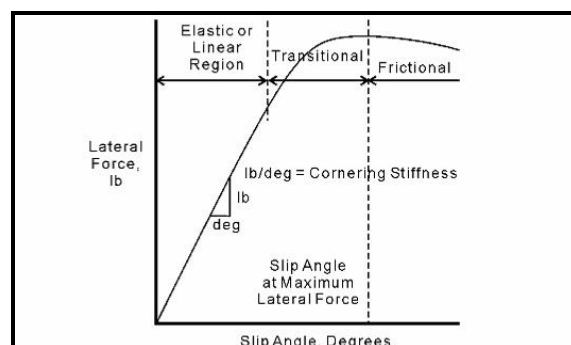


**Figure 2: Typical side-force versus slip-angle characteristic graph (Haney, 2003)**

## Large Tyre Testing and Modelling for Handling

For completeness sake, the full array of forces acting on a tyre may be described as follows:

According to Jazaar (2008), tyres may be considered as a force generator with two major outputs which are longitudinal force ( $F_x$ ) and lateral force ( $F_y$ ). There are also three minor outputs being the self aligning moment ( $M_z$ ), the roll moment or overturning couple ( $M_x$ ) and the driving/braking torque and rolling resistance torque ( $M_y$ ).

The input of the force generator is the tyre vertical load ( $F_z$ ) sideslip ( $\alpha$ ), longitudinal slip ( $s$ ) and camber angle ( $\gamma$ ) Figure 3 shows a graphical illustration of the forces mentioned above.

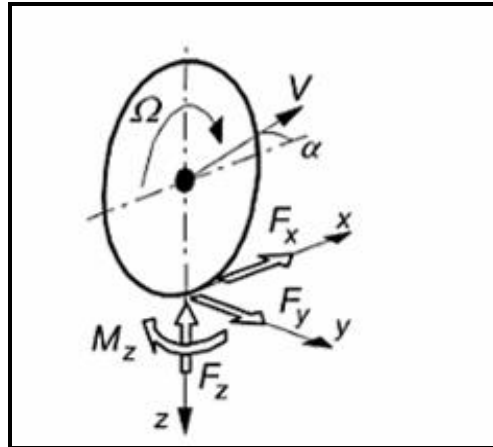


Figure 3: Forces acting on a tyre (Pacejka 2006)

### 2.3 Tyre testers

Tyre testers are used for characterising tyres, in terms of the amount of lateral and longitudinal force they can produce. Tyre characterisation can be performed under various load conditions, tyre pressures, camber and caster angles etc.

There are 2 different types of tyre testers available. The majority of them are the laboratory or indoor type tyre testers, and the minority are the mobile type tyre testers. There are also tyre testers for farm tractor tyres (soft soil tyre tests).

#### **Laboratory type testers – Drum tester**

Figure 4 shows an example of a typical drum type tyre tester (VMI Group | Force and moment testing, 2014). It is manufactured by VMI in Holland. The VMI group manufactures a comprehensive range of machinery for the rubber compound and the tyre manufacturing industry. This includes injection moulding machines and equipment for tyre manufacturing, assembly and testing.

## Large Tyre Testing and Modelling for Handling

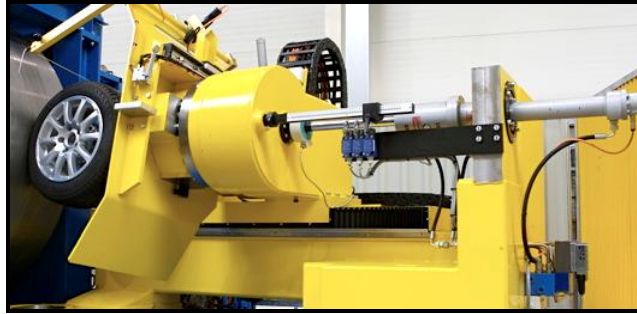


**Figure 4: VMI Tire test machine (VMI Group | Force and moment testing, 2014)**

### ***Laboratory type testers – Belt Tyre Tester***

Figure 5 shows the MTS Flat Trac classic Tyre Tester (Flat-Trac® Tire Test Systems, 2005). MTS is based in the United States of America and specialises in equipment for mechanical testing and simulation. The Flat Trac classic Tyre Tester consists of a stainless steel belt with an abrasive surface coating driven by two drums, powered by DC motors. The spindle pushes the tyre onto the steel belt, applying a vertical load. The spindle is able to rotate, thereby creating a slip-angle, with respect to the steel belt surface. The test rig is capable to handle passenger car and some light truck tyres.

The capability of the MTS Flat Trac classic Tyre Tester is as follows:

It has a slip-angle range of  $-15^{\circ}$  to  $+15^{\circ}$ . The vertical load capability is 24 000 N, and the lateral force capability is 15 000 N.



**Figure 5: MTS Flat Trac classic Tyre Tester (Flat-Trac® Tire Test Systems, 2005)**

## Large Tyre Testing and Modelling for Handling

Figure 6 shows FKA's dynamic tyre test rig ([www.ika.rwth-aachen.de](http://www.ika.rwth-aachen.de), 2007). FKA is based in Germany and specialises in design simulation, prototyping and testing with regards to vehicles. FKA's dynamic tyre test rig consists of a single drum, driven by a DC motor. Its maximum test velocity is 150 km / h. This test rig is limited to testing of car and motorcycle tyres.

The capability of FKA's dynamic tyre test rig is as follows:

It has a slip-angle range of  $-12^\circ$  to  $+12^\circ$ . It has a vertical load capability of 10 000 N.



**Figure 6: FKA's dynamic tyre test rig ([www.ika.rwth-aachen.de](http://www.ika.rwth-aachen.de), 2007)**

Figure 7 shows the MTS Flat-Trac Roadway for Dynamic Road Handling testing on large vehicles (Flat-Trac® Tire Test Systems, 2005). It utilises four Flat-Trac roadways so that the entire vehicle with tyres can be tested. The system is designed to test the performance and durability of large trucks and trailers. The rig can handle vehicles up to 36 tons.

## Large Tyre Testing and Modelling for Handling



**Figure 7: MTS – Flat-Trac Roadway for Dynamic Road Handling testing on large vehicles (Flat-Trac® Tire Test Systems, 2005)**

### ***Mobile type tyre tester***

Figure 8 shows a picture of the TU-Delft Tyre test trailer. Details are courtesy of Pacejka (2006): The trailer has two measuring stations, one for passenger car size tyres, where relatively small camber angles ranges are encountered. The other station is used for motorcycle tyres which can accommodate the large camber angles encountered by motorbikes. The passenger car tyre can be subjected to a fixed or sweeping steer angle ranging from  $-18^\circ$  to  $+18^\circ$ . The camber angle is set mechanically within a range of  $-5^\circ$  to  $30^\circ$ . The motorcycle test station can handle a swept camber from  $-20^\circ$  to  $70^\circ$ , or can be set at a fixed camber angle. The wheels can also be braked up to full wheel lock. Water can also be sprayed at a controlled rate in front of the test tyre.



**Figure 8: The Delft tyre test trailer (Yunus.hacettepe.edu.tr, (n.d.))**

## Large Tyre Testing and Modelling for Handling

One of the main significant differences between mobile and laboratory tyre testers is that mobile tyre testers utilise the actual road surface that the tyres are used on, whereas laboratory tyre testers utilise an artificially created road surface on a drum or on a steel belt.

### ***Tyre testers for farm tractor tyres – soft soil***

Kutzbach et al (2009) conducted a review of various single wheeled field testers for farm tractor tyres. Most of these single wheeled farm tractor tyre testers have been used for special research projects. The focus of these types of tests are the soft soil tyre interaction forces.

These types of tyre testers are either used in indoor applications, such as in soil bins, or in outdoor field tests. The most time consuming aspect in these types of tests is the preparation and the exchange of the soil, and ensuring that the moisture content is correct and consistent.

Figure 9 shows a few illustrations of the tyre testers discussed by Kutzbach et al (2009)



**Figure 9: Farm tractor tyre testers (Kutzbach et al, 2009)**

## Large Tyre Testing and Modelling for Handling

### **2.4 Tyre modelling**

According to Blundell (2004), the function of a tyre model is to establish the forces and moments occurring at the tyre to road contact patch, and resolve these to the wheel centre and hence into the vehicle.

Two popular models are referred to by Blundell (2004), one being the 'Magic Formula' model and the other being the Fiala model, as implemented in MSC.ADAMS.

The 'Magic Formula' model is summarised by Pacejka (2006), as being a widely used semi-empirical tyre model, used to calculate steady state force and moment characteristics for use in vehicle dynamic studies. The paper by Bakker et al (1989) describes the equations as well as the various parameters used in the equations. The parameters in the 'Magic Formula' model have physical significance, and are relatable to a characteristic of the tyre.

According to Blundell (2004), the Fiala model is probably most well-known to MSC.ADAMS users, as it is provided as a standard feature of the program. He goes on to mention that although the Fiala model is limited in capability, this model has the advantage of requiring only a few input parameters to create the model. The Fiala model ignores the influence of camber angle, and the model cannot represent combined cornering and braking, or cornering and driving. The variation in cornering stiffness at zero slip-angle with tyre load is also not considered.

#### ***Virtual tyre rig model***

Blundell (2006) refers to a functional model of the Flat Bed Tyre Test machine at Coventry University which has been developed in MSC.ADAMS. He states that the test rig is useful when data has been used to develop mathematical model parameters. These mathematical models can be simulated on the MSC.ADAMS test rig model, and the simulated data obtained can be compared to the actual data. This is a way of confirming the mathematical models are accurate and represent the actual tyre. Blundell also recommends it as "good practice" to validate tyre models with measured test data, before incorporating tyre models into a full vehicle simulation.

#### ***Comparison between tyre models***

Blundell (2004) has conducted a comparison between the 'Magic Formula' and the Fiala tyre model, whilst using an Interpolation model as the benchmark. This was done for a 195/65R15 passenger car tyre. He has conducted the test with four vertical wheel loads of 200, 400, 600 and 800kg. The conclusion was that the 'Magic Formula' produces a much better match than the simpler Fiala model. The Fiala model underestimates lateral force where higher slip-angles coincide with higher wheel loads.

### **2.5 Tyre models used in this study**

The MSC.ADAMS documentation contains a table (see Figure 10) which shows all the tyre models available and their applicability to different events/manoeuvres (ADAMS View HELP, 2012). For this study we have adopted the approach of first considering the simplest or easiest to configure tyre model, and then progressing onto more complex models. The tyre models chosen for this study were:

- Fiala tyre model
- UA (University of Arizona) tyre model
- Pacejka 89 tyre model

## Large Tyre Testing and Modelling for Handling

MD Adams	Event / Maneuver	ADAMS/ Handling Tire						
		PAC2002	PAC-TIME	PAC89	PAC94	FIALA	5.2.1.	UA Tire
Handling	Stand still and start	+	o/+	o/+	o/+	o/+	o/+	o/+
	Parking (standing steering effort)	+	-	-	-	-	-	-
	Standing on tilt table	+	+	+	+	+	+	+
	Steady state cornering	+	+	o/+	+	o	o	o/+
	Lane change	+	+	o/+	+	o	o	o/+
	ABS braking distance	+	o/+	o/+	o/+	o	o	o/+
	Braking/power-off in a turn	+	+	o	o	o	o	o
	Vehicle Roll-over	+	o	o	o	o	o	o
Ride	On-line scaling tire properties	+	-	-	-	-	-	-
	Cornering on uneven roads <sup>1</sup>	o/+	o	o	o	o	o	o
	Braking on uneven roads <sup>1</sup>	o/+	o	o	o	o	o	o
	Crossing cleats / obstacles	-	-	-	-	-	-	-
	Driving over uneven road	-	-	-	-	-	-	-
Chassis Control	4 post rig (A/Ride)	+	o/+	o/+	o/+	o/+	o/+	o/+
	ABS braking control	o/+	o	o	o	o	o	o
	Shimmy <sup>2</sup>	o/+	o	o	o	o	o	o
	Steering system vibrations	o/+	o	o	o	o	o	o
	Real-time	+	-	-	-	-	-	-
Dura-bility	Chassis control systems > 8 Hz	o/+	-	-	-	-	-	-
	Chassis control with ride	-	-	-	-	-	-	-
	Driving over curb	-	-	-	-	-	o	o
	Driving over curb with rim impact	o	-	-	-	-	o	o
Misc	Passing pothole	-	-	-	-	-	o	o
	Load cases	-	-	-	-	-	o	o
	Design of Experiments	-	-	-	-	-	-	-
	SMP parallel	+	+	+	+	+	+	+

-	Not possible/Not realistic	<sup>1</sup> wavelength road obstacles > tire diameter
o	Possible	<sup>2</sup> wheel yawing vibration due to
o/+	Better	supension flexibility and tire dynamic response
+	Best to use	tire models assumed to be used in transient and combined slip mode

**Figure 10: ADAMS Tyre model table (ADAMS View HELP, 2012)**

The focus of this study is the tyre side-force versus slip-angle characteristic, as well as a double lane change manoeuvre, therefore the equivalent events/manoeuvres applicable from the table are thus the 'steady state cornering' and the 'lane change'. All three tyre models chosen can be used for the types of tests conducted; with the Fiala model showing a 'possible' categorisation, and the UA and Pacejka 89 model showing a 'better' categorisation according the table (Figure 10).

A discussion of each tyre model that was chosen follows:

### ***Fiala tyre model***

The description and implementation of the Fiala tyre model that follows is taken from ADAMS View HELP (2012). The Fiala tyre model is a physics-based tyre model. The carcass is modelled as a beam on an elastic foundation in the lateral direction. Elastic brush elements provide the contact between the carcass and the road. Analytical assumptions are derived for the steady state slip characteristics; these form the basis for the longitudinal and lateral forces in ADAMS. The Fiala tyre model has the following features/limitations:

- Rectangular contact patch or footprint
- Pressure distribution uniform across the contact patch
- No tyre relaxation effects are considered
- Camber angle has no effect on tyre forces



## Large Tyre Testing and Modelling for Handling

As the focus of this study is on tyre models for handling, we will discuss the lateral force generation of the Fiala tyre model in ADAMS.

Firstly, the Fiala tyre model defines the critical lateral slip as:

$$\alpha_{critical} = \arctan\left(\frac{3 \times U \times |F_z|}{CALPHA}\right)$$

Where U is the current coefficient of friction defined as:

$$U = U_{max} - (U_{max} - U_{min}) \times S_s \alpha$$

With  $S_s \alpha$  being defined as the comprehensive slip:

$$S_s \alpha = \sqrt{(S_s^2 + \tan^2(\alpha))}$$

Where

$S_s$  being the longitudinal slip ratio

$F_z$  being the tyre vertical force and

CALPHA being the partial derivative of lateral force ( $F_y$ ) with respect to slip-angle ( $\alpha$ ) at zero slip-angle, commonly known as cornering stiffness.

The lateral force peaks at a value of  $U \times |F_z|$  when the slip-angle ( $\alpha$ ) equals the critical slip-angle ( $\alpha_{critical}$ )

The Fiala model considers two cases when calculating the lateral force ( $F_y$ ):

Case 1: Elastic deformation  $|\alpha| < \alpha_{critical}$

The lateral force is defined as:

$$F_y = -U \times |F_z| \times (1 - H^3) \times \text{sign}(\alpha)$$

where

$$H = 1 - \left( \frac{CALPHA \cdot |\tan(\alpha)|}{3 \cdot U \cdot |F_z|} \right)$$

Case 2: Elastic deformation  $|\alpha| > \alpha_{critical}$

The lateral force is defined as:

$$F_y = -U \times |F_z| \times \text{sign}(\alpha)$$

Therefore, in totality, the calculation of the lateral force ( $F_y$ ) in the Fiala tyre model considers the following parameters:

- Current coefficient of friction
- Vertical wheel load ( $F_z$ )
- Slip-angle ( $\alpha$ )
- Cornering stiffness (CALPHA)
- Comprehensive slip (i.e. the effect of combined longitudinal slip and lateral slip)

## Large Tyre Testing and Modelling for Handling

### **UA tyre model**

The description and implementation of the UA tyre model that follows is taken from ADAMS View HELP (2012). The University of Arizona (UA) tyre model was originally developed by Drs P.E. Nikravesh and G. Grim. The UA tyre model includes relaxation effects, both in the longitudinal and lateral direction. The UA Tyre model calculates the forces at the ground contact point as a function of the tire kinematic states. The tyre deflection and deflection velocity are determined using either a point follower or a durability contact model.

Similarly as are focussing on tyre models for handling, we will discuss the lateral force ( $F_y$ ) calculation of the UA tyre model:

For the UA tyre model, the lateral force is generated dependent on the precise operating conditions:

Operating condition 1:  $\alpha_y < 0$

Operating condition 2:  $\alpha_y \geq 0$  and  $C_\alpha S_\alpha \geq C_\gamma S_\gamma$

Operating condition 3:  $\alpha_y \geq 0$  and  $C_\alpha S_\alpha < C_\gamma S_\gamma$

where

$\alpha_y$  is the product of the slip-angle and camber angle, taking their signs into consideration

$C_\alpha$  is the cornering stiffness

$S_\alpha$  is the lateral slip due to slip-angle

$C_\gamma$  is the camber stiffness

$S_\gamma$  is the lateral slip ratio due to camber (angle) inclination

For each operating condition, there is a lateral force calculation done for:

- The elastic deformation state
- The complete sliding state

The calculation of the lateral force for operating condition 1 and operating condition 2, elastic deformation state is as follows:

$$F_y = C_\alpha S_s l_n^2 + \mu_y^{(m)} F_z (1 - 3l_n^2 + 2l_n^3) + C_\gamma S_\gamma$$

where

$S_s$  is the longitudinal slip ratio

$l_n$  is the contact patch length

$\mu_y^{(m)}$  is the modified coefficient of friction in the lateral direction

$F_z$  is the vertical wheel load

The calculation of the lateral force for operating condition 3, elastic deformation state is as follows:

$$F_y = C_\gamma S_\gamma (3l_n^2 + 2l_n^3) - C_\alpha S_\alpha l_n^2 + \mu_y F_z (1 - 3l_n^2 + 2l_n^3)$$

where

$\mu_y$  is the coefficient of friction in the lateral direction

The calculation of the lateral force for operating condition 1, 2 and 3, completely sliding is as follows:

$$F_y = \mu_y F_z$$

Therefore, in totality, the calculation of the lateral force ( $F_y$ ) for the UA tyre model considers the following parameters:

## Large Tyre Testing and Modelling for Handling

- Cornering stiffness (CALPHA)
- Lateral slip due to camber (angle) inclination
- Lateral slip due to slip-angle
- Camber stiffness
- Longitudinal slip ratio
- Coefficient of friction in the lateral direction
- Vertical wheel load
- The contact patch length

### **Pacejka 89 tyre model**

The description and implementation of the Pacejka 89 tyre model that follows is taken from ADAMS View HELP (2012). The Pacejka 89 tyre model as implemented in ADAMS is based on the Magic-Formula Tyre model, as described by Bakker E, et al (1989). It is an empirical tyre model that describes measured tyre characteristics by means of formulas and interpolation schemes for which the parameters are determined by curve-fitting to experimental data.

Similarly as are focussing on tyre models for handling, we will discuss the lateral force calculation of the Pacejka 89 tyre model. It is based on the following formula, also commonly referred to as the 'Magic Formula'. The lateral force is defined as:

$$F_y = D \sin \left[ C \arctan \left\{ BX_1 - E \left( BX_1 - \arctan \left( BX_1 \right) \right) \right\} \right] + S_v$$

An illustration of the curve and the various coefficients are given in Figure 11:

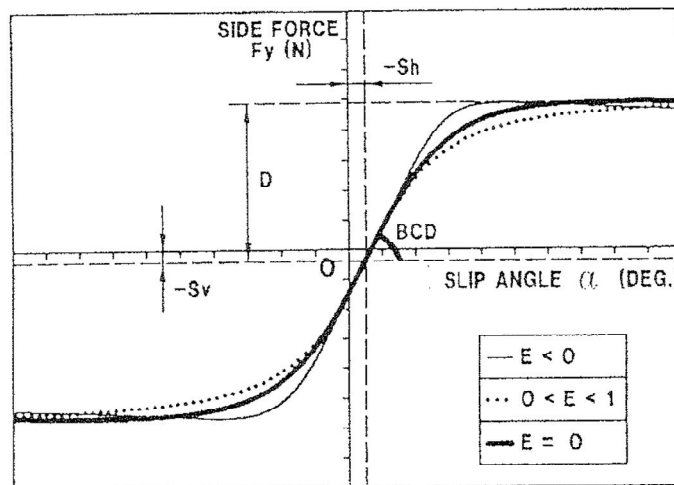


**Figure 11: Illustration of coefficients contained in the 'Magic Formula' (Bakker E et al, 1989)**

The various coefficients are defined as follows:

$F_y$  is the Lateral force generated by the tyre, and  $\alpha$  is the slip-angle.

$D$  is the peak value of the lateral force

$$D = \mu F_z$$

$$\text{With: } \mu = a_1 F_z + a_2$$

## Large Tyre Testing and Modelling for Handling

C is the shape factor

$$C = a_0 = 1.30 \text{ – for side-force}$$

BCD is the slope at zero slip-angle

$$BCD = a_3 \sin(2 \arctan(F_z / a_4))(1 - a_5|\gamma|)$$

B is the stiffness factor

$$B = BCD / CD$$

E is the curvature factor

$$E = a_6 F_z + a_7$$

The horizontal shift is defined as

$$S_h = a_9 F_z + a_{10} + a_8 \gamma$$

The vertical shift is defined as

$$S_v = a_{11} F_z \gamma + a_{12} F_z + a_{13}$$

Composite

$$X_1 = (\alpha + S_h)$$

Table 1 shows of summary of the Pacejka 89 'Magic Formula' lateral coefficients and their descriptions.

<b>Table 1: 'Magic Formula' lateral coefficients</b>	
<b>Coefficient</b>	<b>Description</b>
$a_0$	Shape factor
$a_1, a_2$	Peak factor
$a_3, a_4, a_5$	BCD calculation
$a_6, a_7$	Curvature factor
$a_8, a_9, a_{10}$	Horizontal shift
$a_{11}, a_{12}, a_{13}$	Vertical shift

A curve-fitting exercise (parameterisation) is required to generate the coefficients of the 'Magic Formula'. See Chapter 6 for details of the implementation.

Therefore the calculation of the lateral force ( $F_y$ ) for the Pacejka 89 tyre model considers the following parameters:

- Peak lateral force
- Camber stiffness (does take into account the effect of different vertical loads)
- Slip-angle
- Horizontal and vertical shifts (includes the effect of camber on lateral force)
- Vertical wheel load
- Camber angle

## Large Tyre Testing and Modelling for Handling

### **2.6 Large tyres**

Literature and data on large tyres are scarce, in comparison to the literature available for passenger car tyres.

In differentiating large tyres from passenger tyres, Ervin (1976) has concluded that the cornering stiffness sensitivity to vertical load is perhaps the most significant lateral traction characteristic distinguishing the truck tyre from the passenger tyre. In particular a truck tyre exhibits a steep slope in its cornering stiffness versus vertical load relationship in the vicinity of its rated load.

Ervin (1976) has also found that the sensitivity of lateral traction to velocity has been observed to be virtually insignificant for his particular set of tyres examined.

On curve fitting, Pacejka (2006) has conducted a 'Magic Formula' curve fit comparison on measured tyre data of a truck tyre, 315/80R22.5. He has shown good agreement with the curve fit, particularly on the side-force versus slip-angle curve fit.

### **2.7 Summary of Technical introduction and literature survey**

This chapter has discussed general information regarding tyres, highlighted the complexity of tyres, thereby proving it to be a prospective area for research. The next section in this chapter discussed concepts which this study focuses on, namely side-force and slip-angle. Tyre test equipment available internationally was then discussed, commenting that the major difference between mobile tyre testers and laboratory tyre testers is the road surface on which the tests are conducted. Tyre modelling was then discussed citing popular tyre models used in the industry by well-known authors. The three tyre models selected for this study were then discussed in detail. Lastly brief information on large tyres was highlighted quoting the conclusions of work done with regards to large tyres.

## Large Tyre Testing and Modelling for Handling

### 3. The Tyre Tester

The previous chapter, based on the technical introduction and literature survey, focussed on the tyre lateral force, slip-angle, tyre modelling and the equipment (laboratory and mobile type) available to characterise tyres. Our overall object is to characterise a tyre's lateral characteristic, by utilising equipment available, thereafter parameterising a tyre model, and validating the simulated data with the measured data. Chapter 3 concentrates on the Tyre Tester used in this study. It starts with a brief introduction to the Tyre Tester, describing the functionality and the features. The next step was to develop confidence in the equipment. This was done by verifying or calibrating the load cells. Once this was done satisfactorily, the next step was to apply a known force to wheel hub of the Tyre Tester and to verify whether the load cells measure these known applied forces. At the end of this chapter a confidence level in the Tyre Tester could be established, in order to perform track tests.

#### ***3.1 Description of the Tyre Tester***

The Tyre Tester as depicted in Figure 12 is a large rigid “trailer” with 2 tyres mounted on adjustable hubs. In this configuration, its unladen mass is approximately 4 800kg. It requires a heavy tow vehicle to pull it over the relevant test surface. Figure 13 shows a CAD model of the Tyre Tester. Figure 14, Figure 15 and Figure 16 show the overall dimensions of the Tyre tester. It provides an overall idea of its size, being 4 648 mm in length, 3 052mm in width and 2 387mm in height.



**Figure 12: Tyre Tester**

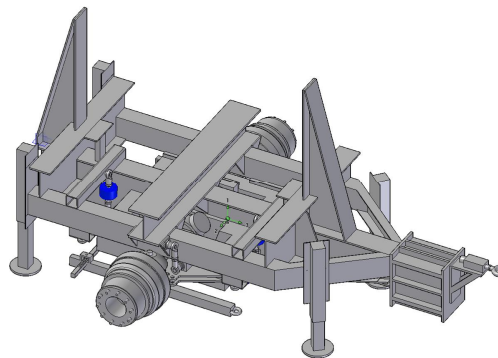


**Figure 13: CAD Model of Tyre Tester**

## Large Tyre Testing and Modelling for Handling

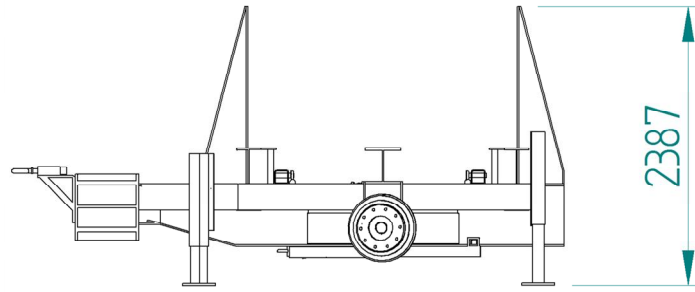


Figure 14: Side view of Tyre Tester (dimensions in mm)

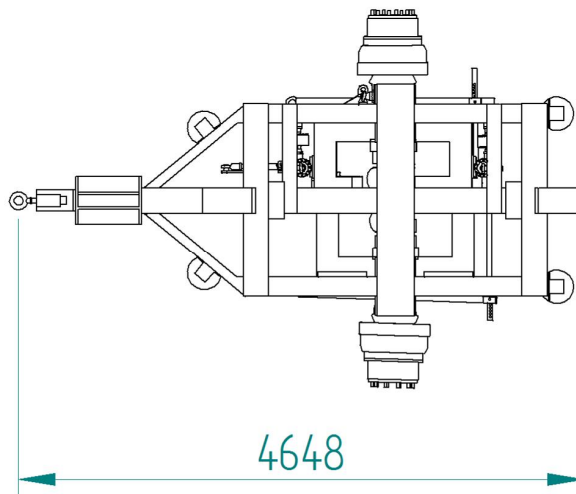


Figure 15: Top view of Tyre Tester (dimensions in mm)

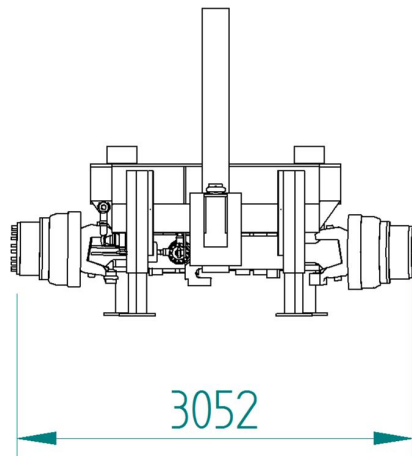


Figure 16: Front view of Tyre Tester (dimensions in mm)

## Large Tyre Testing and Modelling for Handling

The slip-angle of each wheel can be adjusted manually in fixed increments of approximately 2 degrees. The total range of adjustment is  $-2^{\circ}$  to  $+10^{\circ}$ . The following slip-angles could thus be tested:  $-2^{\circ}$ ,  $0^{\circ}$ ,  $2^{\circ}$ ,  $4^{\circ}$ ,  $6^{\circ}$ ,  $8^{\circ}$  and  $10^{\circ}$ . The camber of the tyre is fixed and is non-adjustable.

The right-hand side hub is mounted on a subframe. The mainframe and subframe are interconnected via the six load cells. The six load cells thus measure the forces on the right tyre. The forces are transmitted from the tyre via the of the wheel rim, wheel hub, subframe, then onto the load cells. The load cells measure tension-compression only and are mounted in spherical bearings (rod-ends) to eliminate bending loads.

Figure 17 shows the CAD model with the load cells (highlighted in dark blue) mounted between the sub-frame (highlighted in orange) and the main-frame (highlighted in grey) of the structure of the Tyre Tester. The load cells are used to measure lateral, vertical and longitudinal forces on the right hand side tyre.

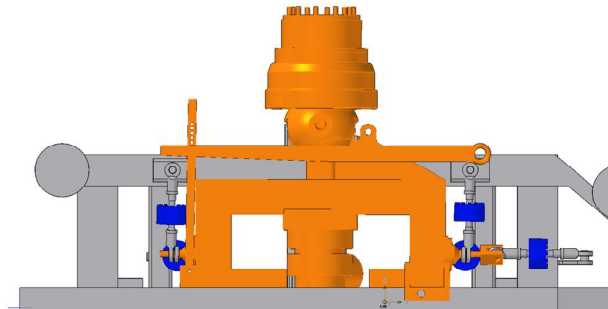


**Figure 17: CAD model with load cells**

Figure 18 shows a view of some of the physical load cells, as installed on the Tyre Tester.



**Figure 18: Tyre Tester load cells**



## Large Tyre Testing and Modelling for Handling

The Tyre Tester is capable of being loaded with steel ballast plates, therefore allowing the static vertical load on the tyre to be varied as required.

The Tyre Tester was last utilised more than 10 years ago. Therefore the approach to using the equipment was first to ensure that it was in working order. This was done by removing all the load cells and visually inspecting them for damage, and then verifying that they produced the correct outputs.

### **3.2 Load cell verification exercise**

The load cells from the large Tyre Tester needed to be verified against a known standard. This was to ensure that whatever measurements we obtain, are trustworthy, and traceable, to an international calibration standard. The large Tyre Tester initially had three load cells (10 000 kg capacity each). These were used to measure the lateral force (two load cells), and the longitudinal force (one load cell).

Two additional load cells (also 10 000 kg capacity) were procured and installed, and another custom sized load cell was fabricated and installed. These three load cells will be used to measure the vertical force on the tyre.

All of these load cells were verified in tension (10 000 kg) and compression (10 000 kg).

#### ***Tension verification exercise:***

Mass pieces at Gerotek Test Facilities were utilised for this exercise. The following masses were used:

- 500kg
- 1 000kg
- 2 000kg
- 5 000kg
- 10 000kg

One of the existing load cells was verified by a SANAS (South African National Accreditation System) accredited calibration laboratory. See Appendix B for the details of calibration certificate. This load cell was used as the reference load cell, and the values of the other load cells were compared to this reference load cell.

The load cell (reference) was attached to a crane, and each of the mass pieces was lifted, and their values noted. Refer to Figure 19 for a depiction of the setup. The Somat e-DAQ data acquisition system was used to record the load cells output (values).

The above exercise was done for all load cells. The output value of each load cell was compared to the reference load cell and the deviation (if any) in percentage form was noted.

#### ***Compression verification exercise:***

A bench press was utilised for this exercise. The reference load cell and each of the other load cells was placed on the bench press, in series. See Figure 20 for a depiction of the set-up. Both load cells were 'zeroed'. A load was applied (compression load) and the values on each load cells were noted. The load was increased gradually up to 10 000 kg.

The output values of the reference load cell and each other load cell were compared, and the deviation (if any) in percentage form was be noted.

## Large Tyre Testing and Modelling for Handling

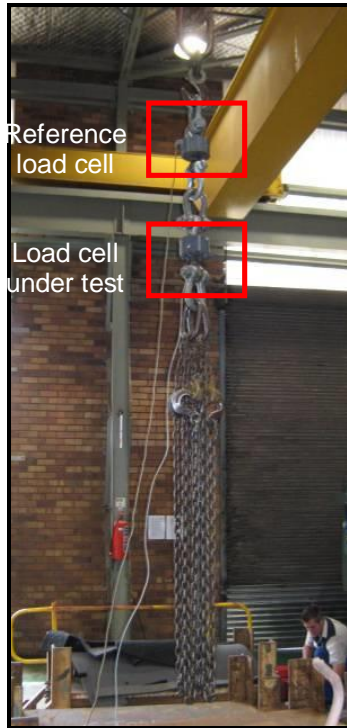


Figure 19: Tension verification setup

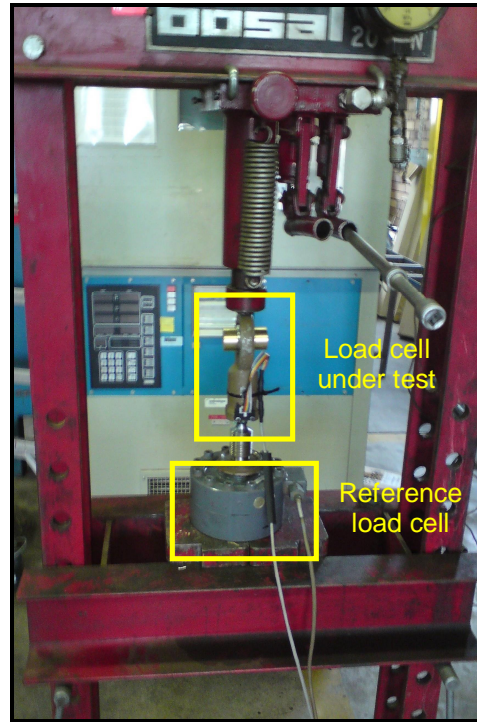
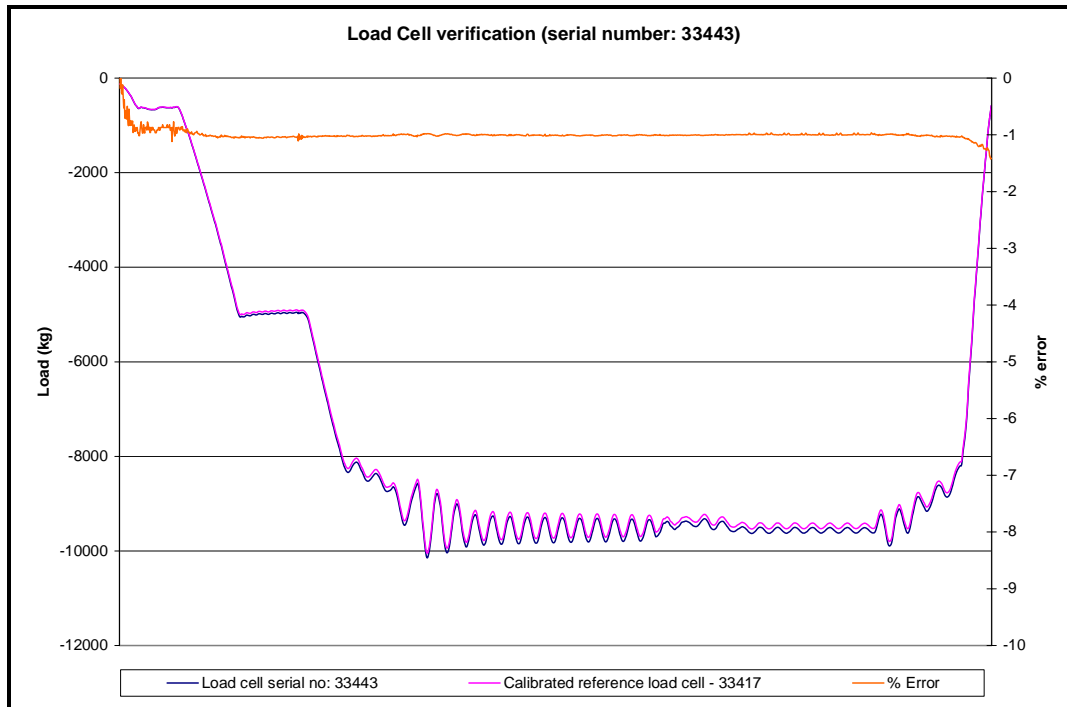


Figure 20: Compression verification setup

A sample of the verification data is shown in Figure 21. The specific test conducted was a tension test. The tensile load was applied and then removed. The deviation of the load cell under test from the calibrated reference load cell was minimal. The mean percentage deviation was 1 %.

## Large Tyre Testing and Modelling for Handling



**Figure 21: Load cell verification - serial number: 33443 (Tension test)**

### **Conclusion to the load cell verification exercise:**

All the other load cells exhibited a similar behaviour, i.e. showing a similar percentage deviation as per the above sample i.e. approximately 1%. Therefore, one can conclude that all the load cells are in good working order, i.e. they are within 1% of a calibrated and traceable load cell.

### **3.3 Applying forces to the Tyre Tester**

After verifying that the load cells were in working order and their outputs verified against a calibrated standard, they were installed back in to the Tyre Tester. The next step was to ensure that the readings obtained from the load cells *in situ* represented the actual tyre forces. Therefore the Tyre Tester was mounted onto a rigid immovable base, and controlled forces were applied to the wheel hub. Lateral, vertical and longitudinal forces were individually applied to the Tyre Tester. This method also ensures that the geometry and equations used to relate the six load cell forces to the Tyre Tester are correct.

This exercise was performed at the University of Pretoria, Heavy Machine Labs. The Tyre Tester was mounted to the rigid floor in the lab, and the forces were applied by means of a hydraulic jack. The forces were applied to the wheel hub edge, which is the part that the wheel rim is mounted to the Tyre Tester. Note, the forces from the tyre are transferred via the rim and the wheel hub and eventually to the load cells.

Figure 22 shows a lateral force being applied to the bottom edge of the wheel hub. A load cell was used between the hydraulic jack and the vertical support to measure the applied lateral force.

## Large Tyre Testing and Modelling for Handling

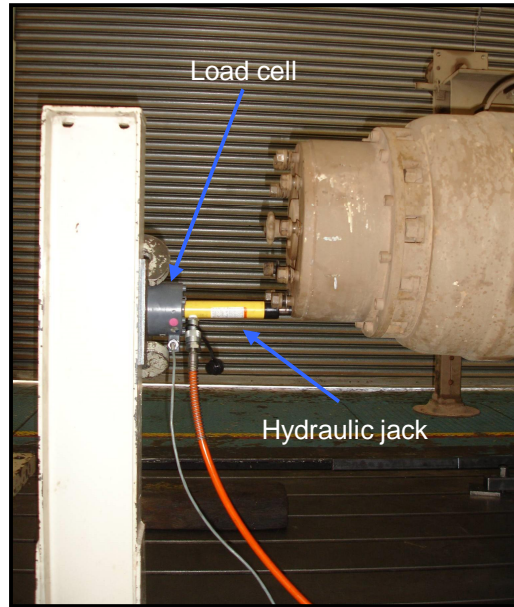


**Figure 22: Lateral force applied perpendicular to wheel hub in the Y direction**

The force balance for the above lateral force can be described as:

$$F_{Lateral\_applied} = \sum F_{Lateral\_loadcells} = F_{Lateral\_front\_loadcell} + F_{Lateral\_rear\_loadcell}$$

Figure 23 (top left graph) shows the lateral force versus time graph. It illustrates two 'cycles' of the force being applied then released. Figure 23 (top right graph) shows an overlay of the applied lateral force, and the sum of the lateral load cells. It should be noted that the difference between the applied lateral force and the sum of the lateral load cells was less than 2.5% (see Figure 23 (bottom right graph)). This is possibly due to the structure flexing and the lost 2.5% of the lateral force was taken up by the other four load cells. Also, the load cells are not perfectly orthogonal, and there is a small amount of uncertainty regarding the exact force application point.

## Large Tyre Testing and Modelling for Handling

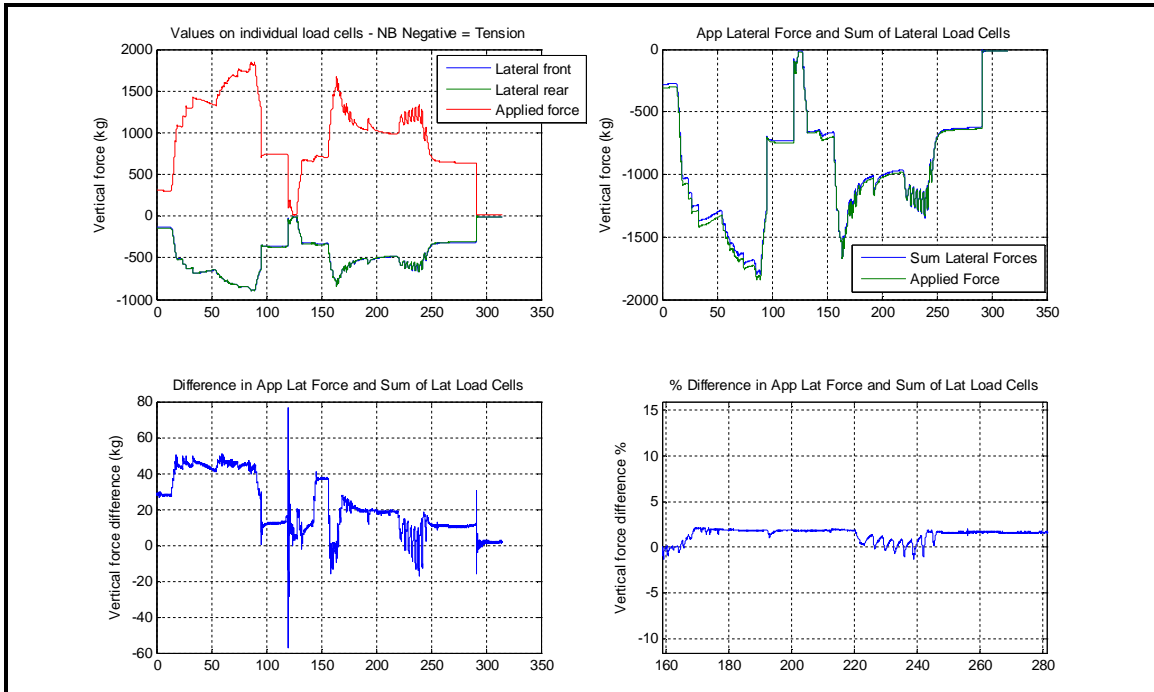


**Figure 23: Analysis of applied lateral force**

Similarly a vertical force was applied. Note it was not possible to apply a large vertical force at the hub edge, as application surface area was small, and there was a risk of the jack jumping out. Therefore the force was applied away from the hub edge, but still on the hub, and in a vertical direction. Figure 24 shows the exact setup.

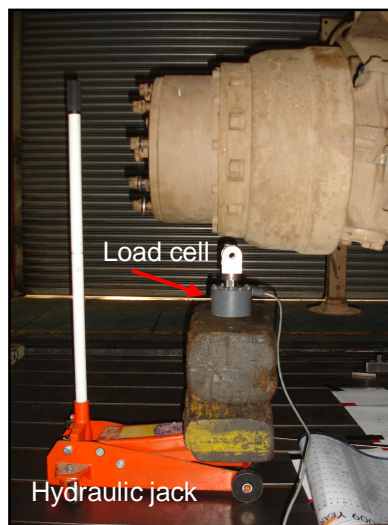


**Figure 24: Vertical force applied perpendicular to wheel hub in the Z direction**

## Large Tyre Testing and Modelling for Handling

The force balance for the vertical applied force can be described as follows:

$$F_{Vert\_applied} = \sum F_{Vert\_loadcells} = F_{Vert\_front\_loadcell} + F_{Vert\_middle\_loadcell} + F_{Vert\_rear\_loadcell}$$

Similarly Figure 25 (top left graph) shows the vertical force versus time graph. It illustrates how the applied force increases in steps as the hydraulic jack is pumped. Figure 25 (top right graph) shows an overlay of the applied vertical force, and the sum of the vertical load cells.

Again, it should be noted that the difference between the applied vertical force and the sum of the vertical load cells was less than 4%. This is possibly due to the structure flexing and the lost 4% of the vertical force was taken up the other three load cells.

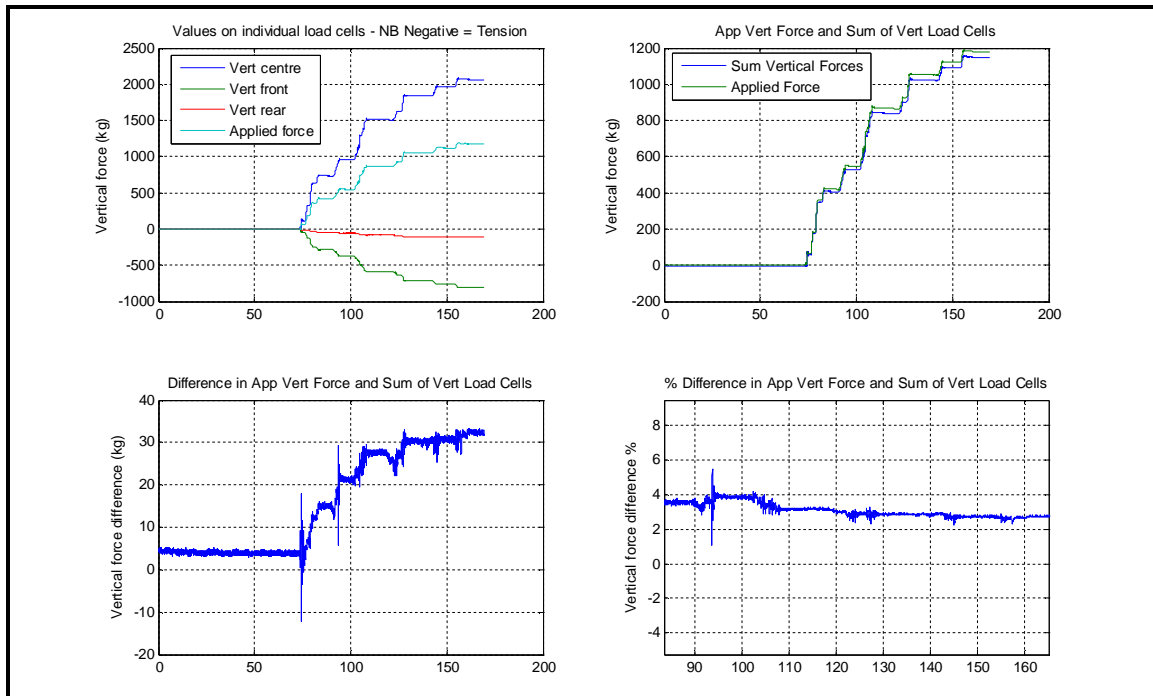


**Figure 25: Vertical applied force analysis**

Similarly a longitudinal force was applied. Figure 26 shows the exact setup.

## Large Tyre Testing and Modelling for Handling

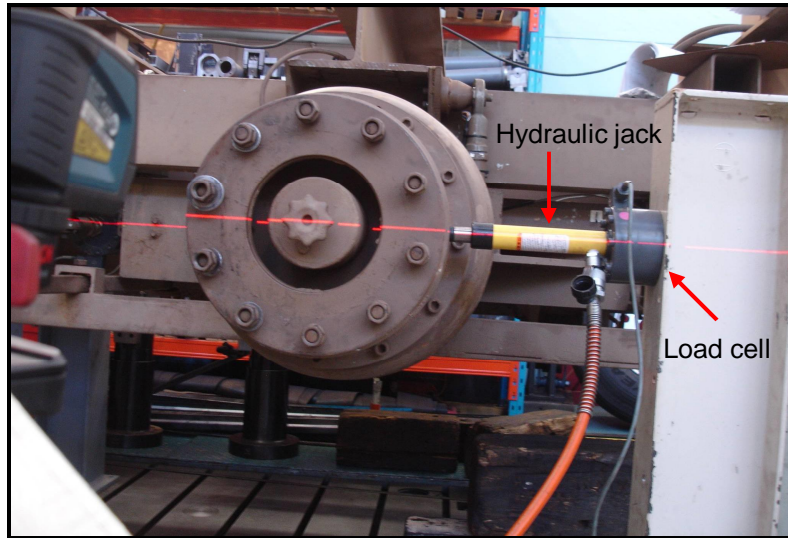


**Figure 26: Longitudinal force applied parallel to wheel hub in the X direction**

The force balance for the longitudinal applied force can be described as follows:

$$F_{Longitudinal\_applied} = \sum F_{Longitudinal\_loadcell} = F_{Longitudinal\_front\_loadcell}$$

Similarly Figure 27 (top left graph) shows the longitudinal force versus time graph. It illustrates two 'cycles' of the force being applied then released. Figure 27 (top right graph) shows an overlay of the applied longitudinal force together with the force as measured on the longitudinal load cell.

Again, it should be noted that the difference between the applied longitudinal force and the value of the only longitudinal load cell was less than 5%. This is possibly due to the structure flexing and the lost 5% of the longitudinal force was taken up the other five load cells.

## Large Tyre Testing and Modelling for Handling

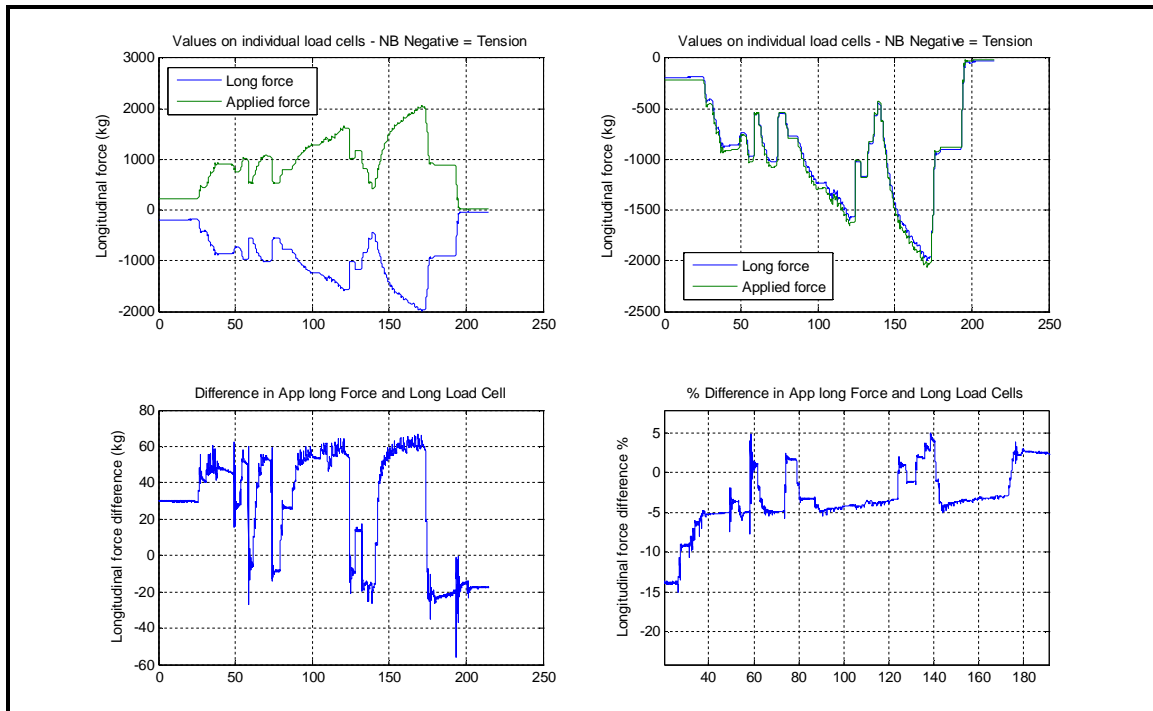


**Figure 27: Longitudinal force analysis**

### ***Discussion on forces applied to the Tyre Tester:***

The lateral force has the smallest deviation error (2.5%) compared to the vertical (4%) and longitudinal force (5%). It should be noted that these errors are due more to the non-ideal test setup with associated uncertainties than to the accuracy of the load cells. The focus of this study is primarily on lateral forces produced by the tyre, seeing that the lateral verification tests produced the smallest deviation; the Tyre Tester was thus a suitable platform to perform the proposed tests.

### ***3.4 Summary of the Tyre Tester***

This chapter provided an overview of the Tyre Tester together with its functionality, capability and features. The load cell verification exercise was then discussed concluding that the load cells of the Tyre Tester have a 1% variation from a calibrated reference load cell. The applications of forces to the Tyre Tester, in the lateral, longitudinal and vertical directions were then discussed. The conclusion is that the Tyre Tester is a suitable platform to perform the proposed lateral characterisation tests.



## Large Tyre Testing and Modelling for Handling

### 4. Track testing


The previous chapter focussed on verifying the load cells, and applying forces to the Tyre Tester to confirm that the applied forces are similar to the load cell forces. Once that exercise was completed, the Tyre Tester was ready to perform track tests. This chapter focuses on the track tests and the side-force versus slip-angle results obtained from the tests.

#### 4.1 Tyres

This study focussed on two truck tyres with very different construction.

Table 2 supplies details of the GoodYear Regional RHT tyre. This tyre is typically used on trucks and trailers operating on regional roads. It has a tread pattern designed mainly for straight-line running on good roads. It is normally not used on steered axles.

Table 3 supplies the details of the Michelin XZL tyre, designed for general purpose off-road conditions in the military and earth moving industries. It has a coarse tread pattern to enable traction under off-road conditions.

<b>Table 2: GoodYear tyre details</b>	
<b>Tyre manufacturer</b>	GoodYear
<b>Tyre series</b>	Regional RHT
<b>Tyre size</b>	385/65R22.5
<b>Tyre pressure (as tested)</b>	740kPa
<b>Speed symbol</b>	K (110 km/h)
<b>Load index</b>	160 (4500 kg)
<b>Tread pattern</b>	

## Large Tyre Testing and Modelling for Handling

<b>Table 3: Michelin tyre details</b>	
<b>Tyre manufacturer</b>	Michelin
<b>Tyre series</b>	XZL
<b>Tyre size</b>	16.00 R20
<b>Tyre pressure (as tested)</b>	300kPa
<b>Speed rating</b>	55 mph = 88.5 km/h
<b>Load range</b>	M (14540 lbs = 6595 kg)
<b>Tread pattern</b>	

Note should be taken of the difference in tread pattern between the two tyres. The GoodYear tyre has an on-road type tread pattern, whereas the Michelin tyre has more off-road type tread pattern, though also suitable for on-road use as well. The “knobs” on the Michelin tyre assist in vertical climbing of off-road obstacles. Such obstacles are often encountered in rocky off-road terrain.

### **4.2 Track testing at Gerotek Test Facilities**

Tests were performed at Gerotek Test Facilities. Gerotek is a test facility consisting of vehicle test tracks, situated west of Pretoria in South Africa. The tyre tests were performed on Gerotek’s Straight Track. The Straight track has a brushed concrete test surface. It is one kilometre in length, and is level in the lateral and longitudinal direction (Gerotek, 2013). Figure 28 and Figure 29 depict the view of the Gerotek’s Straight Track and a close up view of the surface respectively.

Two sets of tyre tests were performed:

- Lateral tyre characterisation test: For this test, the side-force at specific slip-angles was measured. The specific slip-angles tested were: -2°, 0°, 2°, 4°, 6°, 8° and 10°. The end result would be a side-force versus slip-angle graph.
- Dynamic test - A double lane change test was performed. During this test the dynamic change of side-force and slip-angle could be captured with respect to time.

## Large Tyre Testing and Modelling for Handling



**Figure 28: Gerotek's Straight Track**



**Figure 29: Close-up view of the surface of Gerotek's Straight Track**

The tow vehicle utilised was a heavy three axle vehicle with a mass of 15 740kg. The mass of the towing vehicle was much larger than the mass of the Tyre Tester. In this configuration, dynamic inputs from the Tyre Tester were 'absorbed' by the towing vehicle due to its mass. This results in a very stable Tyre Tester which consequently results in less unwanted inputs (or noise) in the measured data. Figure 30 shows the depiction of the tow vehicle and the Tyre Tester.



**Figure 30: Tow vehicle and Tyre Tester**

## Large Tyre Testing and Modelling for Handling

### **4.3 Instrumentation on the Tyre Tester:**

The Tyre Tester was equipped with the following instrumentation for the track tests:

- Six permanently installed load cells (See Chapter 3 for full description) which had the following functionality:
  - 2 lateral load cells – these are used to measure the lateral force on the tyre.
  - 3 vertical load cells – these are used to measure the vertical input to the tyre.
  - 1 longitudinal load cell - this is used to determine the longitudinal force on the tyre.
- A Gyroscope to measure Roll, Pitch and Yaw angular velocity.
- Accelerometers measuring in the vertical and lateral directions, at specific points on the Tyre Tester.
- A Corsys Datron Correvit® S-HR optical sensor. The sensor's following two outputs were utilised:
  - Slip-angle
  - Longitudinal speed
- Differential GPS for speed and accurate position

All of the above inputs were connected up to a Somat e-DAQ data acquisition system, sampling at 1 000 Hz.

#### **Description of the Corsys Datron Correvit® S-HR optical sensor (Correvit® S-HR Sensors, 2012)**

As the slip-angle measurement was central to the results obtained in these tests, a description of the sensor and its key features are presented below:

The Corsys Datron Correvit® S-HR optical sensor is a non-contact high resolution sensor used to measure slip-angle with high dynamics, and exceptionally high accuracy. It is capable of slip-angle measurements ranging from  $-40^{\circ}$  to  $+40^{\circ}$ . It has a High Resolution slip-angle measurement option, which was selected for these tests. The High Resolution slip-angle measurement range is from  $-15^{\circ}$  to  $+15^{\circ}$ , which is sufficient, as the Tyre Testers slip-angle capability is from  $-2^{\circ}$  to  $+10^{\circ}$ .

The specification on the Angle Resolution for the sensor is  $< 0.01^{\circ}$ , and the Angle Accuracy is  $< \pm 0.1^{\circ}$ . The sensor is capable of High Resolution slip-angle measurement within the speed range of 10km/h to 250 km/h. The measurement frequency of the sensor is 250Hz.

After the Tyre Tester was instrumented, and the first set of tyres were fitted (GoodYear) the Tyre Tester was then weighed on the Gerotek Weigh Bridge. The results of the weighing exercise are presented in Table 4 below:

<b>Table 4: GoodYear tyre: wheel loads (unladen load condition)</b>		
<b>Left wheel (kg)</b>	<b>Right wheel (kg)</b>	<b>Total (kg)</b>
2 200	2 255	4 455

The mass of the unladen Tyre Tester was 4 455 kg, with the left vertical wheel load being 2 200 kg and the right vertical wheel load being 2 255 kg. Note, this the minimum vertical wheel load that can be tested on the Tyre Tester, as this is the mass of the empty Tyre Tester with no mass pieces added on. It should be noted that the load cells are connected to the right wheel, and the right wheel's data is used for analysis.

## Large Tyre Testing and Modelling for Handling

### **4.4 Side-force slip-angle testing**

The tow vehicle and Tyre Tester was then driven to the Gerotek Straight Track and positioned at the start of the track. The procedure for testing was as follows:

- The slip-angle was set at  $-2^\circ$
- The data acquisition system was activated.
- The tow vehicle was then driven in a straight line.
  - The vehicle accelerated from rest until a constant speed of 12 km/h was obtained. Pacejka (2006) has shown, for large truck tyres, the side-force versus slip-angle curve is not significantly influenced by the speed of the test, in dry conditions. Therefore a constant maintainable speed of 12km/h was chosen for all tests. This was achieved by selecting a low gear, and using maximum throttle, until the speed stabilised against the diesel engines speed governor.
- The run continued for approximately 20 seconds which allowed for sufficient steady state data to be captured.
- The slip-angle was then manually incremented and the above process was repeated.
- Slip-angle tests were conducted at the following intervals:  $-2^\circ$ ,  $0^\circ$ ,  $2^\circ$ ,  $4^\circ$ ,  $6^\circ$ ,  $8^\circ$  and  $10^\circ$ .

It should be noted that two runs were conducted per slip-angle. By confirming each runs data with the repeated run, the possibility of erroneous and outlying data is reduced. Multiple runs also increase the confidence in the data. Too many runs can however not be performed due to extensive wear and heat generation of the tyres, especially at the large slip-angles.

The load condition was then changed by adding steel ballast plates and the testing was conducted as per the process above.

A summary of the vertical tyre loads with the GoodYear tyre for the three different load conditions are given in Table 5 below:

<b>Table 5: GoodYear Tyre load conditions</b>			
<b>Load condition</b>	<b>Left wheel (kg)</b>	<b>Right wheel (kg)</b>	<b>Total (kg)</b>
<b>Load 1 (unladen)</b>	2 200	2 255	4 455
<b>Load 2</b>	3 705	3 835	7 540
<b>Load 3</b>	5 015	5 235	10 250

Note, as mentioned previously, the right tyre load is the important load to take note of, as the side-force measurement is conducted on this tyre of the Tyre Tester.

Similarly testing was conducted, as per the above method, with the Michelin tyre. A summary of the vertical wheel loads for the three different load conditions are given in Table 6. The base load (load 1) on the Michelin tyre is slightly higher because the Michelin tyre is heavier than the GoodYear tyre.

## Large Tyre Testing and Modelling for Handling

<b>Table 6: Michelin Tyre load conditions</b>			
<b>Load condition</b>	<b>Left wheel (kg)</b>	<b>Right wheel (kg)</b>	<b>Total (kg)</b>
<b>Load 1 (unladen)</b>	2 335	2 385	4 720
<b>Load 2</b>	3 845	3 940	7 785
<b>Load 3</b>	5 150	5 390	10 540

Figure 31 shows a depiction of the Tyre Tester (top view) with specific slip-angle being set. Figure 32 shows a depiction of the tow vehicle towing the Tyre Tester, whilst the side-force versus slip-angle test was being performed. Figure 33 shows the tyre scrub marks on the concrete surface, due to the slip-angle of the tyre. Figure 34 shows the tyre friction wear (marks) on the tread, as a result of the slip-angle tests.



**Figure 31: View from top of wheel set at a specific slip-angle (GoodYear tyre)**



**Figure 32: Tow vehicle with Tyre Tester performing slip-angle tests (Michelin tyre)**



**Figure 33: Tyre scrub marks (Michelin tyre)**



**Figure 34: Tyre scrub wear (Michelin tyre)**

## Large Tyre Testing and Modelling for Handling

### **4.5 Characteristic tyre data – side-force slip-angle**

The objectives for performing the above tests were to generate side-force slip-angle characteristic data for the GoodYear and the Michelin tyres.

Figure 35 shows typical raw data, from a single test run with the slip-angle of set to 2°. The graphs depict the following data in order from top to bottom:

- Values on individual loads cells - 3 vertical load cells.
- Values on individual loads cell - 1 longitudinal load cell.
- Values on individual loads cells – 2 lateral load cells.
- Longitudinal speed of the tyre test rig.
- Slip-angle of the test tyre, as obtained from the slip-angle sensor.

## Large Tyre Testing and Modelling for Handling

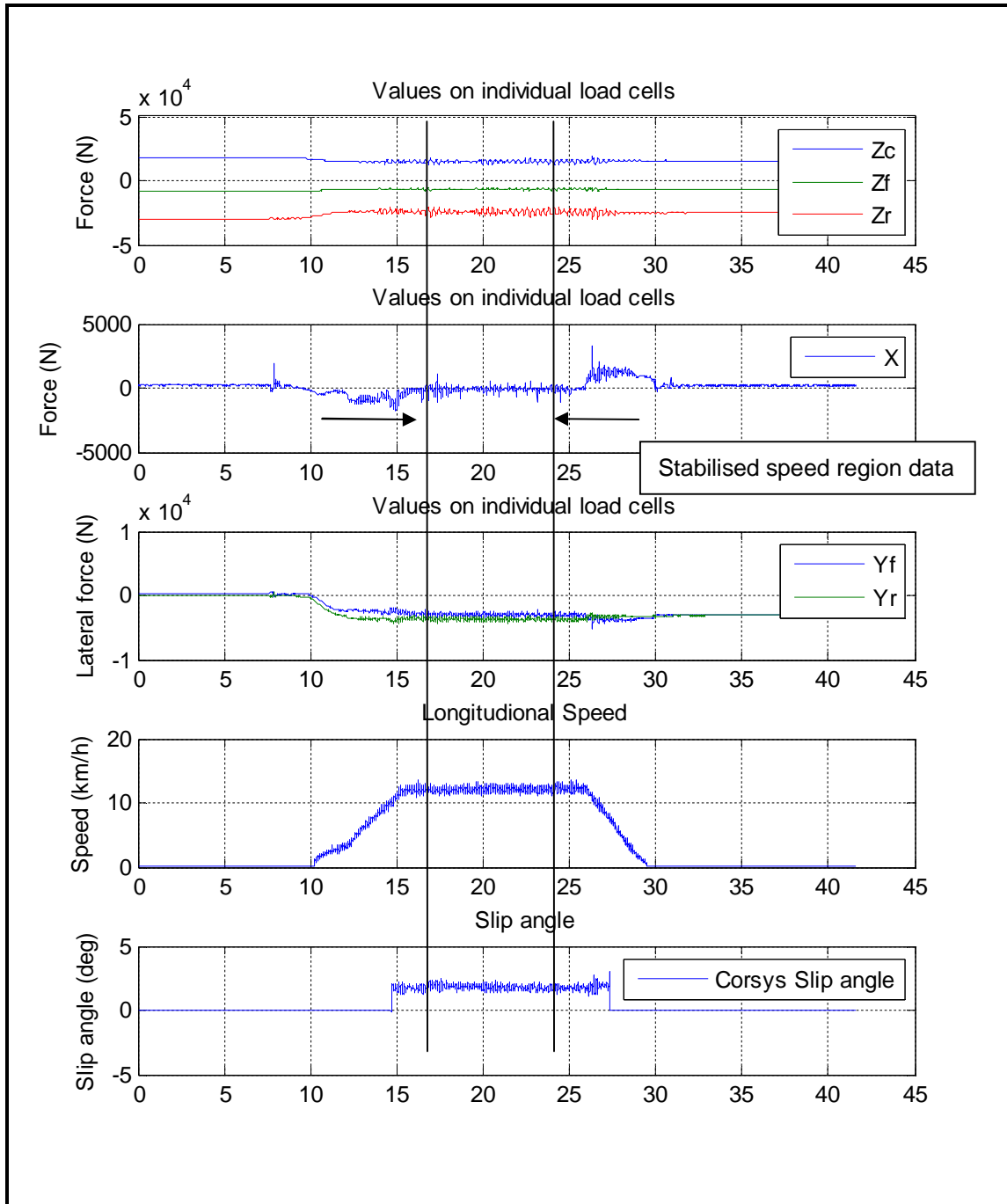


**Figure 35: Data showing individual values on load cells, speed and slip-angle**

The data was visually checked to note any abnormalities in the stabilised speed region. If there were no abnormalities in the data, the data was then processed. Figure 36 shows the relevant data for just the side-force slip-angle characteristics:

- The two lateral load cells summed together, to produce the total lateral force.
- The slip-angle was obtained from the slip-angle sensor.
- The longitudinal speed of the test rig.



## Large Tyre Testing and Modelling for Handling

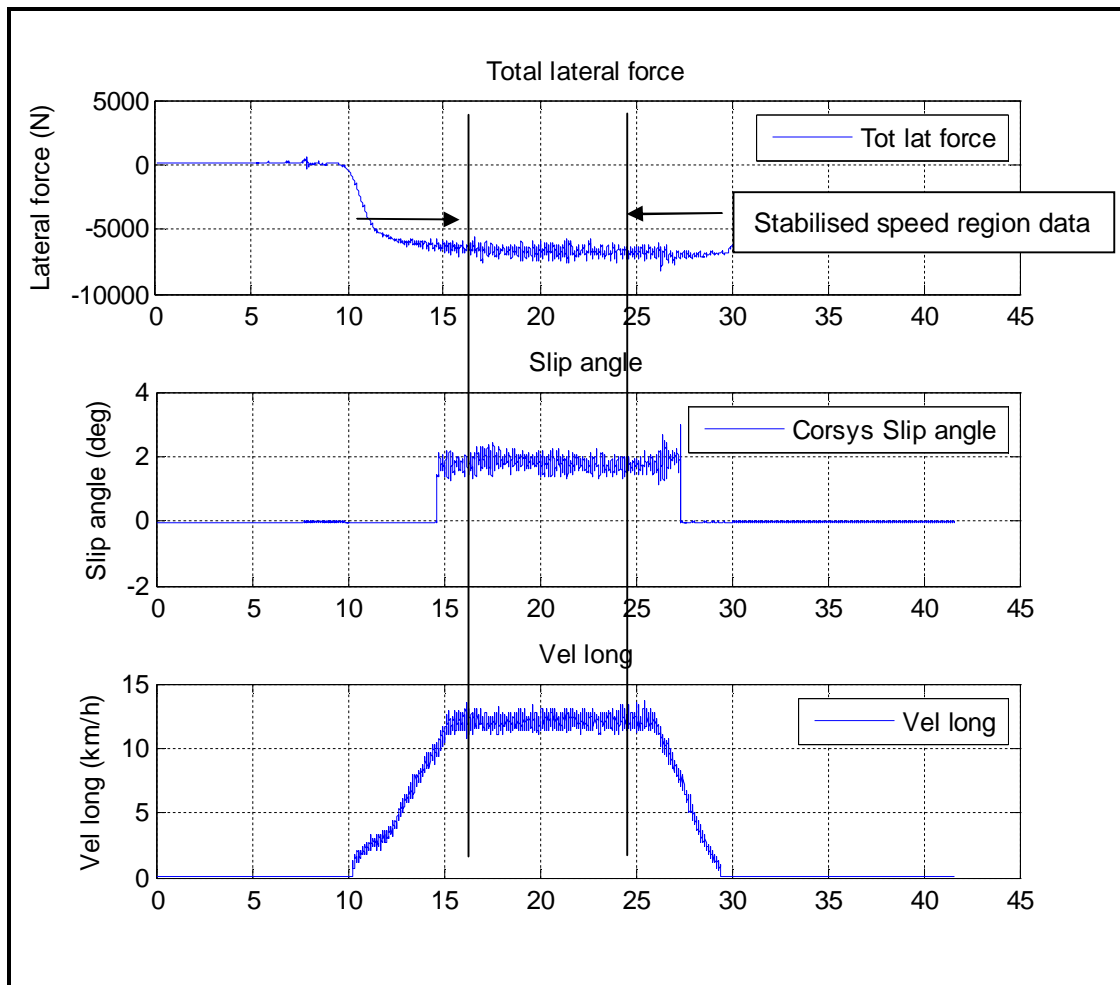


**Figure 36: Data of total lateral force, slip-angle and speed**

An average value was taken over the stabilized speed region of total lateral force and the slip-angle. These values contribute points on the side-force slip-angle characteristic curve. Also slip-angle values are not exactly the set values because the two tyres are not identical and the vertical loads show a small difference as well.

### ***Correction of side-force data:***

When the slip-angle is at zero degrees i.e. when the tyre is running parallel to the direction of travel, the side-force exerted on the tyre is simply the sum of the values of the lateral load cells. Note: The load cells are then perpendicular to the tyre.

When a slip-angle is present the load cells are not perpendicular to the tyre, hence the actual side-force is a component of the force.

Therefore the side-force on the tyre is:

$$F_{\text{Tyre}} = F_{\text{lateral load cells}} \times \text{Cos (slip-angle)}$$

## Large Tyre Testing and Modelling for Handling

### **4.6 GoodYear tyre testing data**

Table 7 shows a summary of the side-force slip-angle data for the GoodYear tyre. For each load, the first column shows the average slip-angle (of two runs) whilst the second column shows the average (of two runs) of the cosine corrected side-force.

<b>Table 7: GoodYear Tyre: Side-force &amp; Slip-angle data</b>					
<b>Load 1</b>		<b>Load 2</b>		<b>Load 3</b>	
<b>Slip-angle (°)</b>	<b>Side-force (N)</b>	<b>Slip-angle (°)</b>	<b>Side-force (N)</b>	<b>Slip-angle (°)</b>	<b>Side-force (N)</b>
-2.6	-5 918	-2.5	-10 087	-2.4	-8 523
-0.6	-274	-0.5	-1 087	-0.5	-190
1.8	6 825	1.8	11 191	1.8	12 174
3.9	11 824	3.9	20 360	3.9	25 944
6.0	15 439	6.0	26 435	5.9	33 857
8.1	17 603	7.9	29 279	7.7	37 605
9.9	18 771	9.6	30 596	9.4	38 771

Summary of peak forces and slip-angles:

For load 1, the peak lateral force measured was 18 771 N, at a slip-angle of 9.9°.

For load 2, the peak lateral force measured was 30 596 N, at a slip-angle of 9.6°.

For load 3, the peak lateral force measured was 38 771 N, at a slip-angle of 9.4°.

The data for each load condition was plotted and Figure 37 shows the side-force slip-angle characteristic curve for the GoodYear tyre, at 740 kPa tyre pressure and for the three vertical load conditions:

## Large Tyre Testing and Modelling for Handling

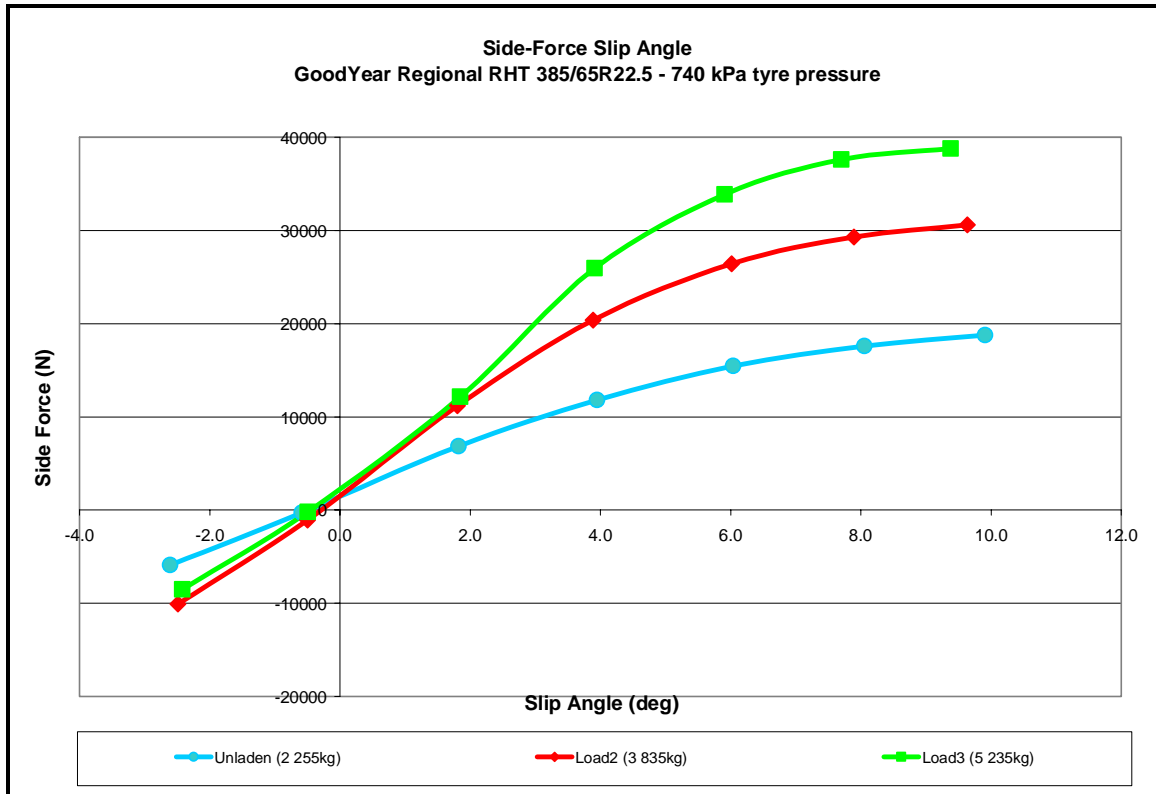


Figure 37: Side-force slip-angle characteristic curve: GoodYear Tyre

### Discussion of results – Side-force versus slip-angle data – GoodYear tyre

From Figure 37 the following is noted:

- The overall 'shape' of the curves is typical of the expected side-force slip-angle characteristic curves of a tyre.
- It is observed that the cornering stiffness (gradient at zero slip-angle) does not increase going from load 2 to load 3.
- The curves do not pass through the origin; this can be attributed to the camber offset. The camber offset was measured as  $-0.3^\circ$ . Furthermore tyres often do not generate zero lateral force at zero slip-angle due to the conicity and ply steer effects.
- The maximum  $10^\circ$  slip-angle allowed by the Tyre Tester is not large enough to properly identify the peaks.

### 4.7 Michelin tyre testing data

Similarly the data was processed for the Michelin tyre and the results are presented in the following tables:

## Large Tyre Testing and Modelling for Handling

Table 8: Michelin Tyre: Side-force & Slip-angle data					
Load 1		Load 2		Load 3	
Slip-angle (°)	Side-force (N)	Slip-angle (°)	Side-force (N)	Slip-angle (°)	Side-force (N)
-2.4	-7 884	-2.3	-10 829	-2.4	-5 125
-0.7	-1 099	-0.7	-1 129	-0.7	959
1.6	9 810	1.6	12 903	1.5	12 398
3.5	15 989	3.5	22 744	3.4	25 385
5.1	18 434	5.2	26 419	5.1	31 066
6.6	19 283	6.7	27 914	6.5	33 196
7.3	19 460	8.0	28 405	7.8	34 154

Summary of peak forces and slip-angles:

For load 1, the peak lateral force measured was 19 460 N, at a slip-angle of 7.3°.

For load 2, the peak lateral force measured was 28 405 N, at a slip-angle of 8.0°.

For load 3, the peak lateral force measured was 34 154 N, at a slip-angle of 7.8°.

The data for each load condition was plotted and Figure 38 shows the side-force slip-angle characteristic curve for the Michelin tyre at 300 kPa tyre pressure, for 3 vertical load conditions:

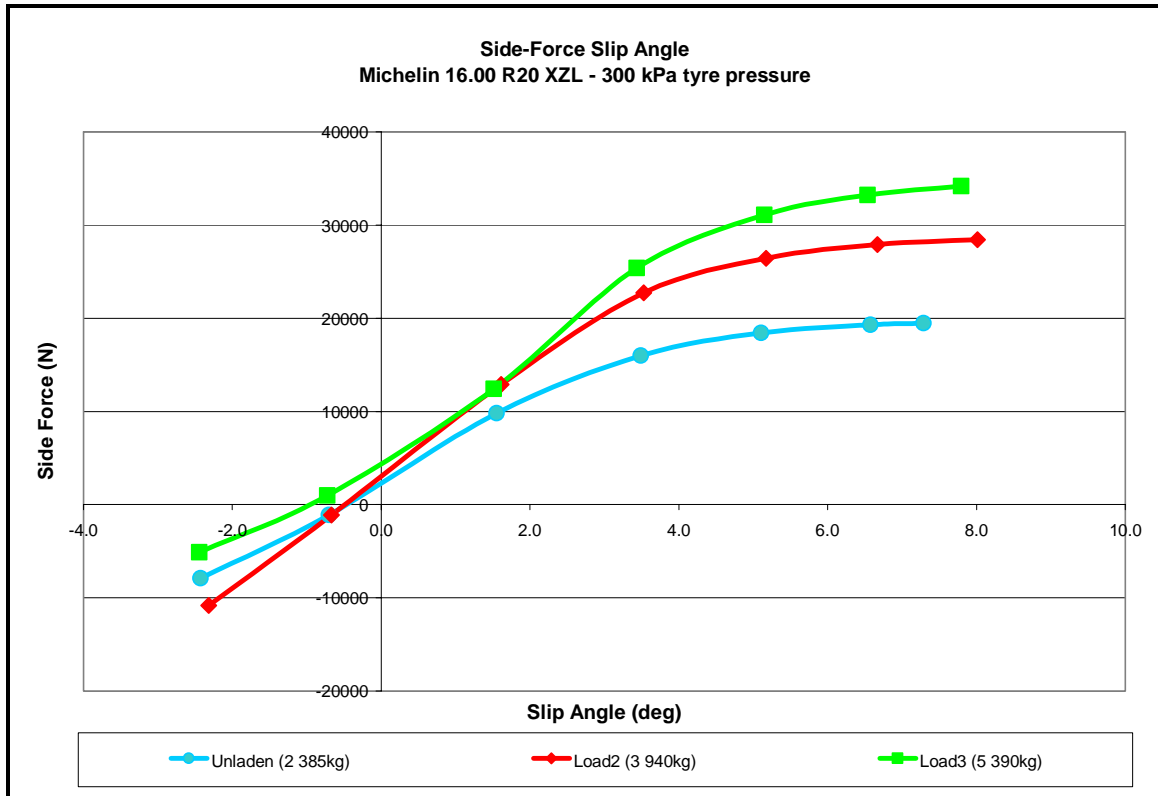


**Figure 38: Side-force slip-angle characteristic curve: Michelin Tyre**

## Large Tyre Testing and Modelling for Handling

### **Discussion of results – Side-force versus slip-angle data –Michelin tyre**

From the figure above the following is noted:

- The overall 'shape' of the curves is typical of the expected side-force slip-angle characteristic curves of a tyre.
- It is observed that the cornering stiffness (gradient at zero slip-angle) does not increase going from load 2 to load 3.
- The curves do not pass through the origin; this can be attributed to the camber offset. The camber offset was measured as  $-0.3^\circ$ . Furthermore tyres often do not generate zero lateral force at zero slip-angle due to the conicity and ply steer effects.
- The maximum  $10^\circ$  slip-angle allowed by the Tyre Tester is not large enough to properly identify the peaks.

### **General discussion of results for the side-force versus slip-angle tests**

It has been shown that the methodology followed of verifying the load cells, and then applying forces to the Tyre Tester, and then performing track tests, has resulted in good repeatable and reliable data for side-force versus slip-angle tests. This exercise has shown that results can be produced with a high confidence level, and the possibility of extending this test to a commercial testing opportunity is becoming more of a reality.

#### **4.8 Double lane change test**

A double lane change track was set-up on Gerotek's Straight Track. The objective of performing the double lane change was to measure dynamic data, such as the changing slip-angle and side-force as the Tyre Tester negotiates the double lane change. Note that the slip-angle of the Tyre Tester was set to zero degrees for the double lane change tests. This data will later be used for a dynamic simulation comparison i.e. we would be able to compare the track test data of the double lane change to the simulated ADAMS Tyre Tester model data of the double lane change.

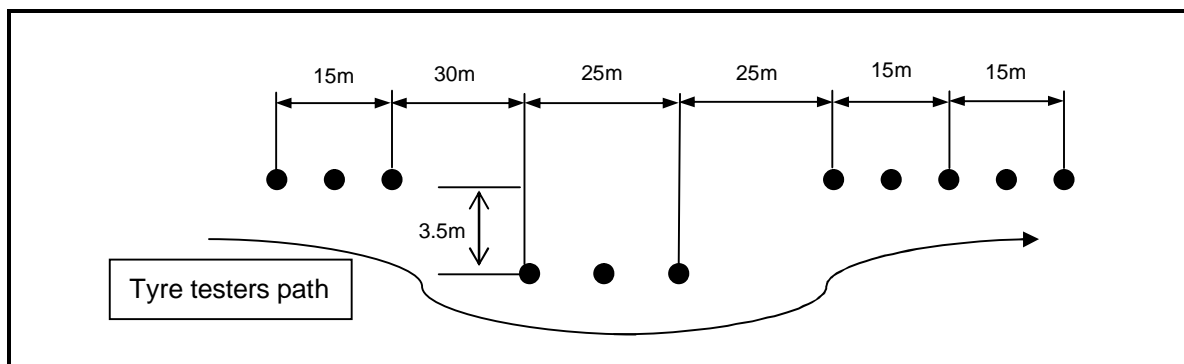


**Figure 39: Double lane change track**

## Large Tyre Testing and Modelling for Handling

The tow vehicle with the Tyre Tester was driven through the double lane change track at speeds up to 45 km/h. The data will be shown later in Chapter 7 together with the simulation comparison.



**Figure 40: Double lane change test being performed**

### ***4.9 Summary of Track Testing***

This chapter focussed on the track testing conducted at Gerotek Test Facilities. Gerotek's Straight Track was used to conduct these tests. Side-force versus slip-angle tests were conducted for three vertical wheel loads for both tyres. The characteristic side-force versus slip-angle curves were the output of these tests. A dynamic double lane change was also conducted on the Straight Track at Gerotek Test Facilities. This data will be used for dynamic correlation with the tyre models later on.

### **5. Tyre Tester characterisation and modelling**

The previous chapter focussed on the track testing conducted with the Tyre Tester, and the tyre results obtained thereof. Moving from the track tests, our next objective was to measure the physical characteristics of the Tyre Tester, which were used to develop the ADAMS dynamic simulation model of the Tyre Tester. The physical characteristics measured were:

- The outer dimensions of the Tyre Tester
- Measurement of the major mass components of the Tyre Tester (i.e. the mainframe and the subframe parts)
- Determination of centre of gravity
- Determination of the moments of inertia

All of the above characteristics were required for the ADAMS model. By accurately determining these characteristics and using them into the model, the dynamic behaviour of the model is improved. I.e. The simulation results of the ADAMS model will correlate more closely with the measured track results.

This chapter will focus on measurements of these physical characteristics, and concludes with the generation of the ADAMS model.

#### ***5.1 CAD model dimensions***

The first step was to verify the dimensions of the CAD model which was already started by a previous student. The Tyre Tester was moved into a laboratory and disassembled into its two main significant parts

- The mainframe (See Figure 41)
  - The mainframe consists of the major frame of the Tyre Tester which includes the main 'backbone' structure, the left wheel hub, the towing hitch, and the landing legs.
- The subframe (See Figure 42)
  - The subframe comprises of the subframe "base", the right wheel hub and the mounting interfaces for the load cells.

The mainframe and subframe are inter-connected via the six load cells. The six load cells thus measure the forces on the right tyre. The forces are transmitted from the tyre via the of the wheel rim, wheel hub, subframe, then onto the load cells.

## Large Tyre Testing and Modelling for Handling



**Figure 41: Mainframe of Tyre Tester**

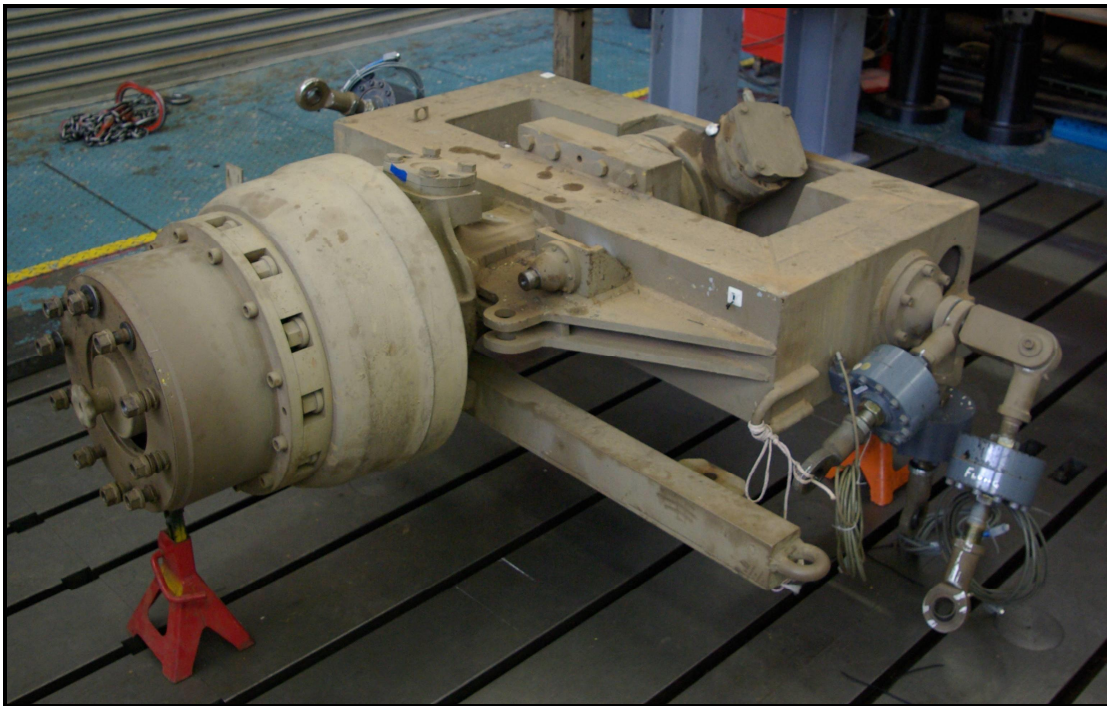


**Figure 42: Subframe of Tyre Tester**



## Large Tyre Testing and Modelling for Handling

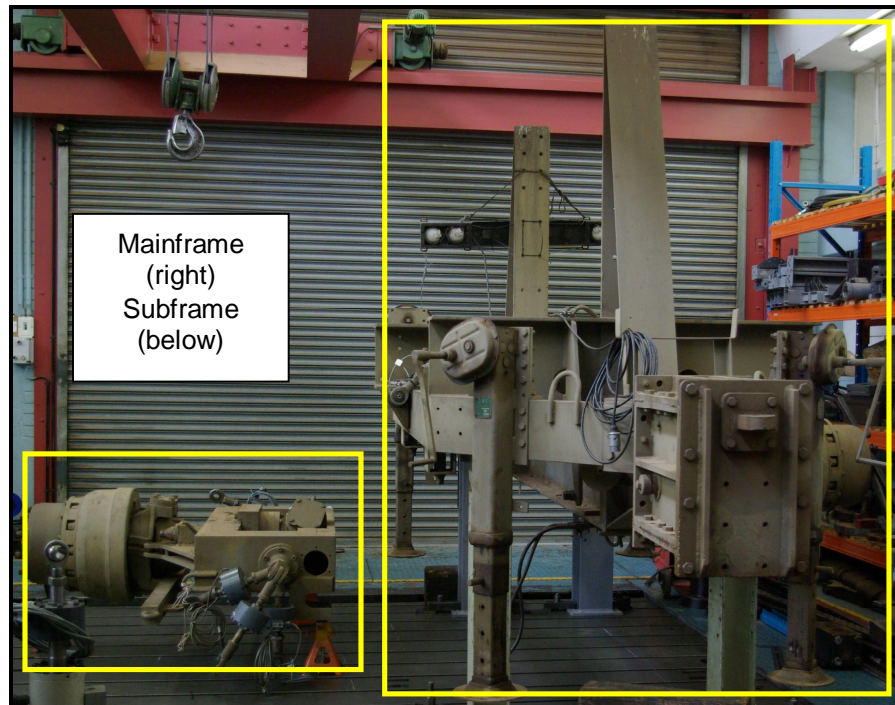


**Figure 43: Mainframe and subframe detached from each other**

The outer dimensions were measured and the various parts of the CAD model were updated. Most importantly the co-ordinates (x,y,z) of the mounting points of the load cells were documented, for use in the ADAMS model. Figure 44 shows a graphic of the assembled CAD model of the Tyre Tester.

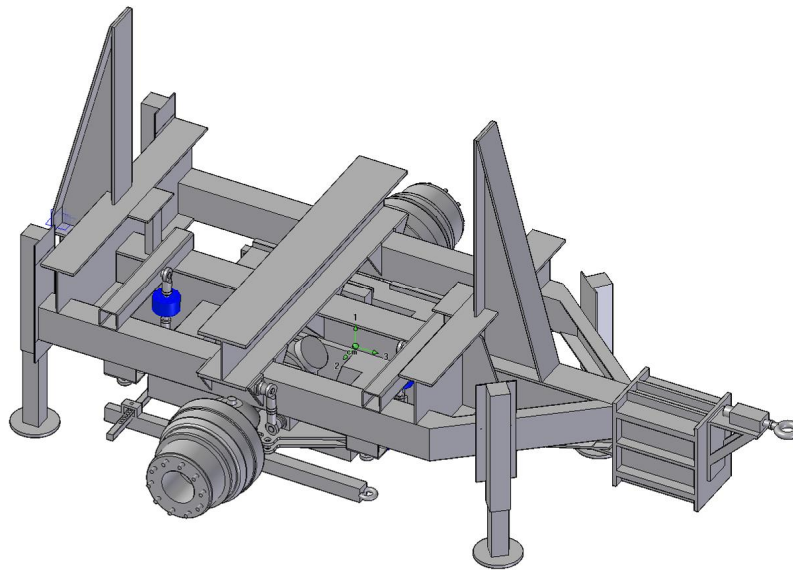


**Figure 44: CAD model of assembled Tyre Tester**

## Large Tyre Testing and Modelling for Handling

### **5.2 Mass of Tyre Tester**

The mass of the Tyre Tester was a property required for the ADAMS dynamic simulation model. The Tyre Tester consisted of two major parts i.e. the mainframe and the subframe. The ADAMS model was configured with those two major parts as well. Therefore, it was important to determine the mass of these two major parts. In order to determine the masses of these individual parts, the subframe was detached from the mainframe. Smaller load cells of 2 000kg capacity each was used to weigh the subframe first. The subframe's mass was 1 208.5 kg. The mainframe's mass was 3 496.5 kg. The total mass of the Tyre Tester was 4 705 kg. Figure 45 shows the depiction of the weighing exercise of the Tyre Tester with the load cells under the landing legs.

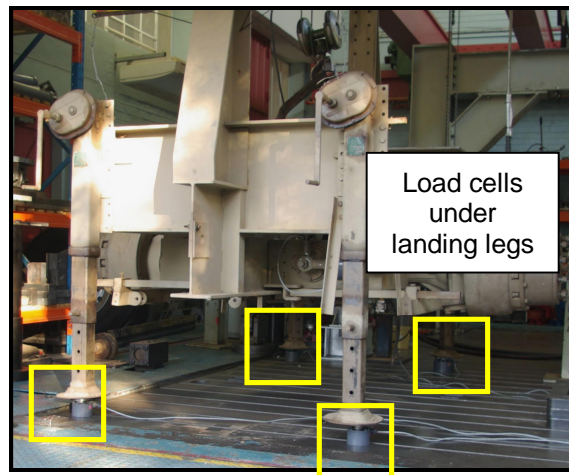


**Figure 45: Tyre Tester with load cells (highlighted) under landing legs**

## Large Tyre Testing and Modelling for Handling

### 5.3 Centre of gravity

Another property required for the ADAMS model was the location of the centre of gravity. The centre of gravity is a virtual point where the entire mass of the body is concentrated. The centre of gravity consists of co-ordinates in the lateral, longitudinal and vertical directions.

#### Longitudinal centre of gravity

The longitudinal centre of gravity was determined from the weighing exercise, which utilised four load cells placed under the landing legs of the Tyre Tester. The longitudinal centre of gravity ( $X_{CG}$ ) was determined by taking a sum of moments around a point in the force diagram. The details are as follows:

The force diagram in the longitudinal plane of the Tyre Tester is shown in Figure 46 below:

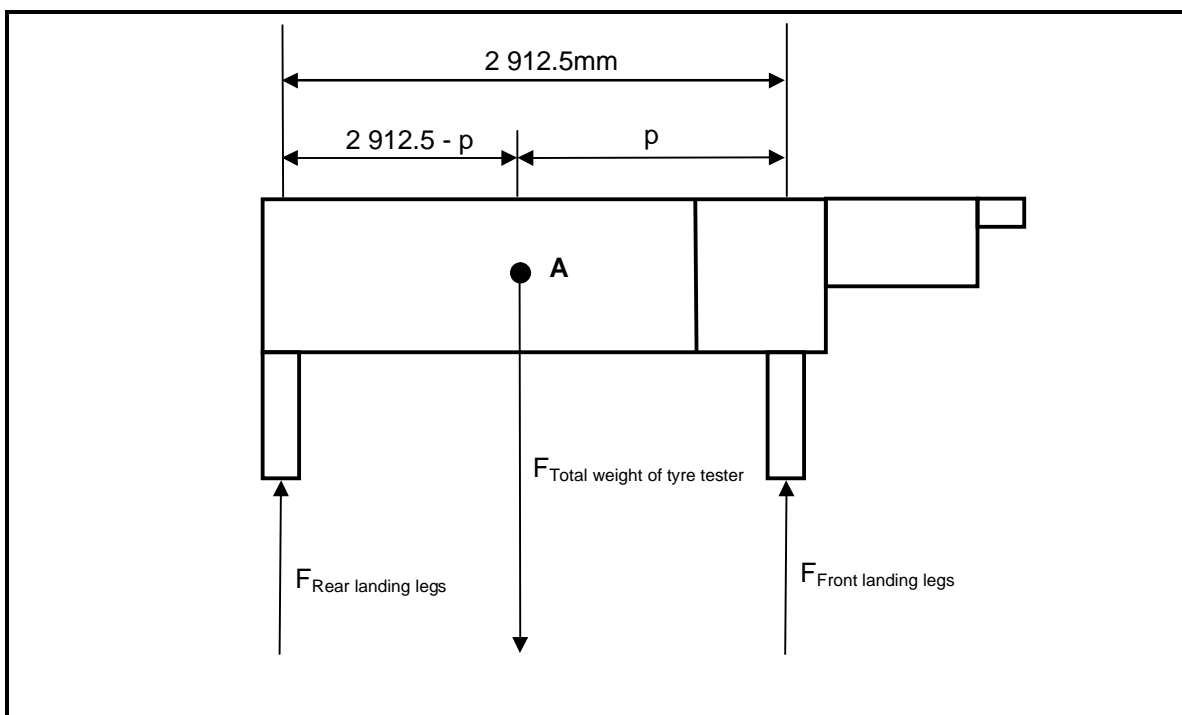


Figure 46: Force diagram in longitudinal plane of Tyre Tester

Where:

$F_{Rear\ landing\ legs}$  = sum total of forces on both the rear landing legs of the Tyre Tester. Note: both the rear landing legs lie in the same lateral plane.

$F_{Front\ landing\ legs}$  = sum total of forces on both the front landing legs of the Tyre Tester. Note: both the front landing legs lie in the same lateral plane.

$F_{Total\ weight\ of\ tyre\ tester}$  = total weight of Tyre Tester, acting on the centre of gravity at point A, at a distance  $p$  away from the front landing legs.

## Large Tyre Testing and Modelling for Handling

The body is in equilibrium; hence forces in the vertical direction are in balance. Therefore the sum of moments around point A is equal to unity, and is represented mathematically as follows:

$$\Sigma M_A = 0$$

Therefore:

$$[(2\,015 \times 9.81) \times (2.912\,5 - p)] - [(2.690 \times 9.81) \times p] = 0$$

Solving for  $p$  results in:

$$p = 1\,247\text{ mm}$$

In order to better understand this calculated value, a visual representation of the centre of gravity is provided in the CAD model (side view), shown in Figure 47.

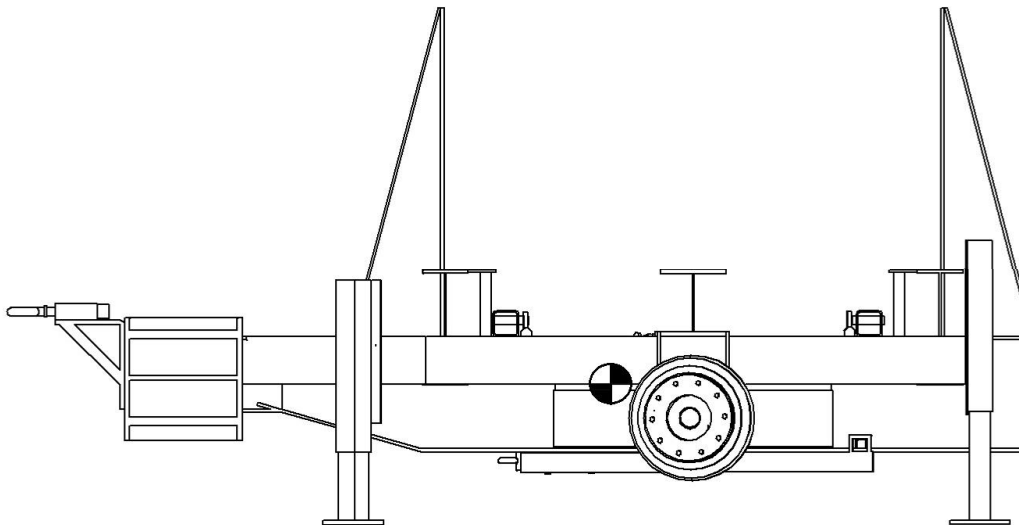


**Figure 47: Side view of Tyre Tester highlighting the Centre of Gravity position**

The longitudinal centre of gravity lies at a distance of 1 247 mm rearwards of the front landing legs. This was then converted to global co-ordinates for use in the ADAMS model. The longitudinal centre of gravity lies slightly forward of the midpoint between the front and rear landing legs. This makes sense as there is more mass ahead of the front landing legs, also resulting in the front landing legs having a higher combined mass as compared to the rear. Furthermore this puts a small vertical downforce on the tow hitch, which assists in the stability of Tyre Tester whilst being towed.

## Large Tyre Testing and Modelling for Handling

### Lateral centre of gravity

Similarly the lateral centre of gravity ( $Y_{CG}$ ) was required for the ADAMS model. It was also similarly determined from the masses of the four landing legs, and the sum of moments.

The force diagram in the lateral plane of the Tyre Tester is showing in Figure 48 below:

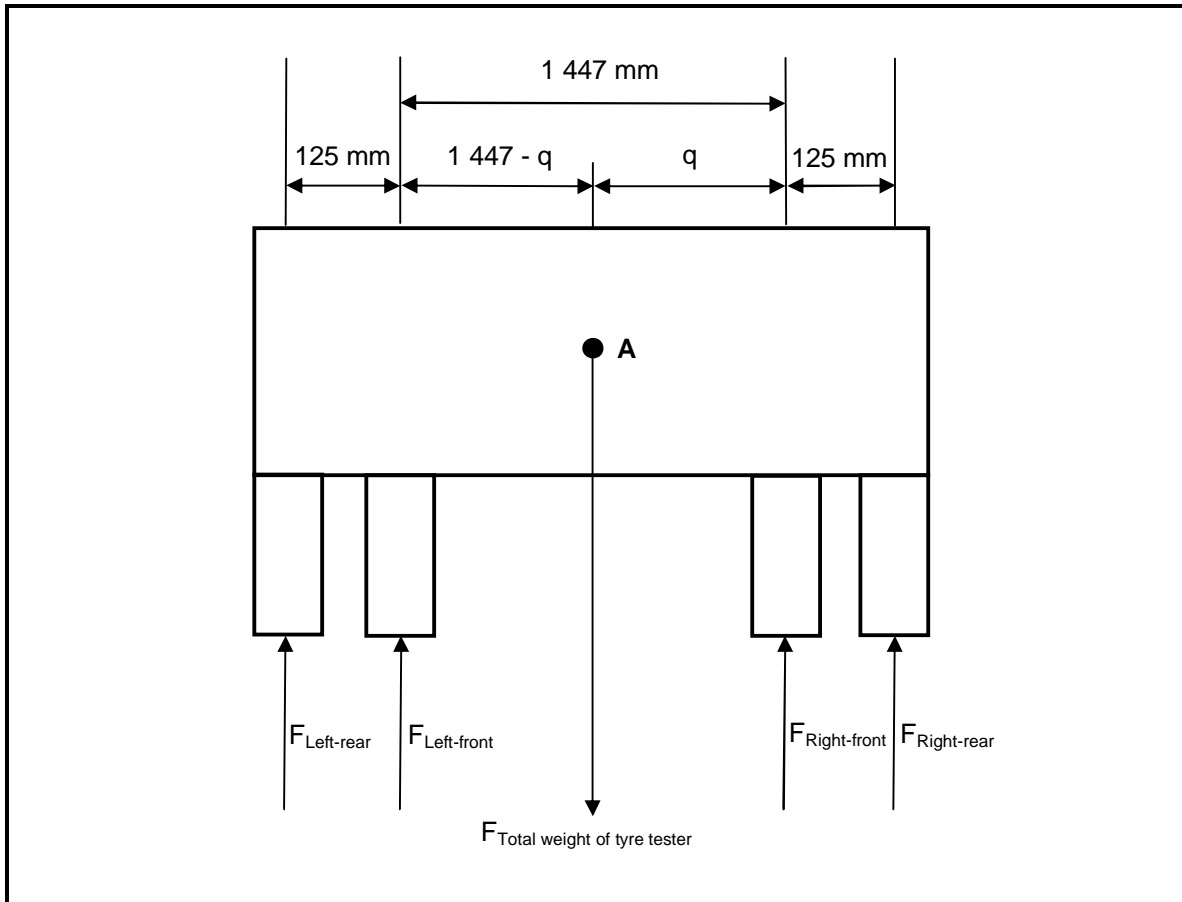


**Figure 48: Force diagram in lateral plane of Tyre Tester**

$F_{Left-rear}$  = force acting on left rear landing leg.

$F_{Left-front}$  = force acting on left front landing leg.

$F_{Right-front}$  = force acting on right front landing leg.

$F_{Right-rear}$  = force acting on right rear landing leg.

$F_{Total\ weight\ of\ tyre\ tester}$  = total weight of Tyre Tester, acting at the centre of gravity at point A, at a distance  $q$  away from the right-front landing leg.

The body is in equilibrium; hence forces in the vertical direction are in balance. Therefore the sum of moments around point A is equal to unity, and is represented mathematically as follows:

## Large Tyre Testing and Modelling for Handling

$$\Sigma M_A = 0$$

The above summation was computed resulting in:

$$q = 605 \text{ mm}$$

In order to better understand this calculated value, a visual representation of the centre of gravity is provided in the CAD model (top view), shown in Figure 49.

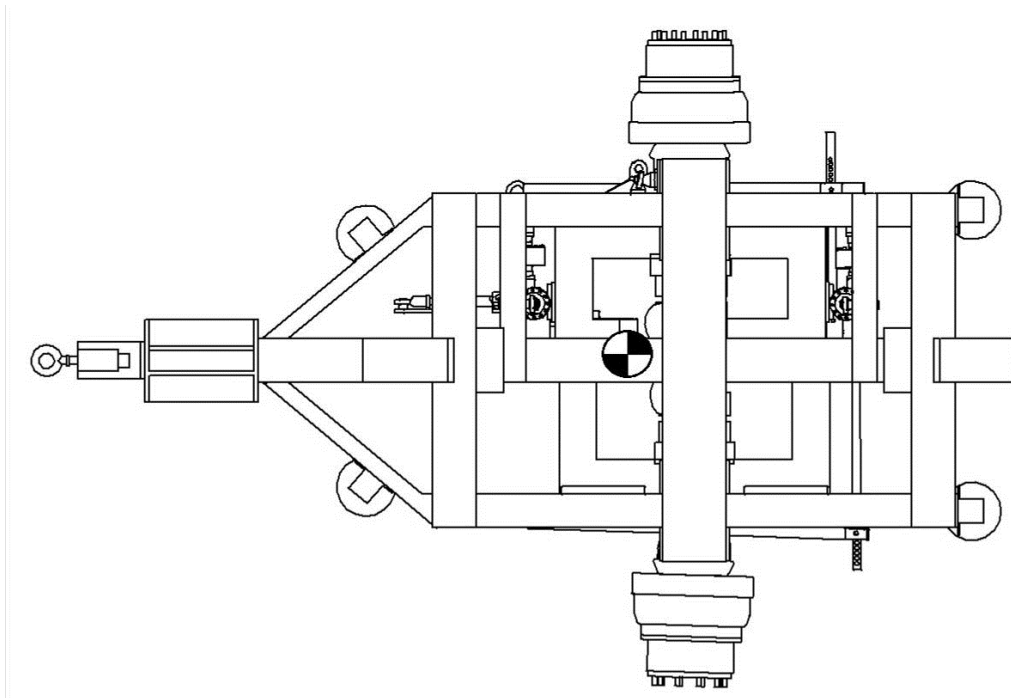


**Figure 49: Top view of Tyre Tester highlighting the Centre of Gravity position**

The lateral centre of gravity lies at a distance of 605 mm left of the right-front landing leg. This was then converted to global co-ordinates for use in the ADAMS model. The lateral centre of gravity lies to the right of the lateral midpoint of the Tyre Tester. This makes sense as the right side of the Tyre Tester contains the load cells and the subframe structure making it heavier than the left side.

## Large Tyre Testing and Modelling for Handling

### ***Vertical centre of gravity***

The vertical position of the centre of gravity ( $Z_{CG}$ ) was determined by adopting the *ISO 10392:2011(E): Road vehicles – Determination of centre of gravity* (International organisation for standardisation, 2011) specification. Specifically the lift method was utilised. This test was conducted by lifting the Tyre Tester by its towing hitch, and allowing it to pivot at the rear landing legs. By lifting the Tyre Tester at the towing hitch, this results in a mass transfer to the rear landing legs. A load cell is connected at the tow hitch point where the Tyre Tester is lifted. The load cell reading and the corresponding lift angle (measured with an inclinometer) was recorded. The values were recorded on the upwards lift, as well as the descending exercise. Figure 50 below shows a graphic of the lift method being performed. The Tyre Tester is depicted at the highest lift angle of 25.6° (limited by the overhead crane).



**Figure 50: Lift method to determine vertical position of the centre of gravity**

## Large Tyre Testing and Modelling for Handling

The force balance diagram for the vertical lift of the Tyre Tester is depicted in Figure 51:

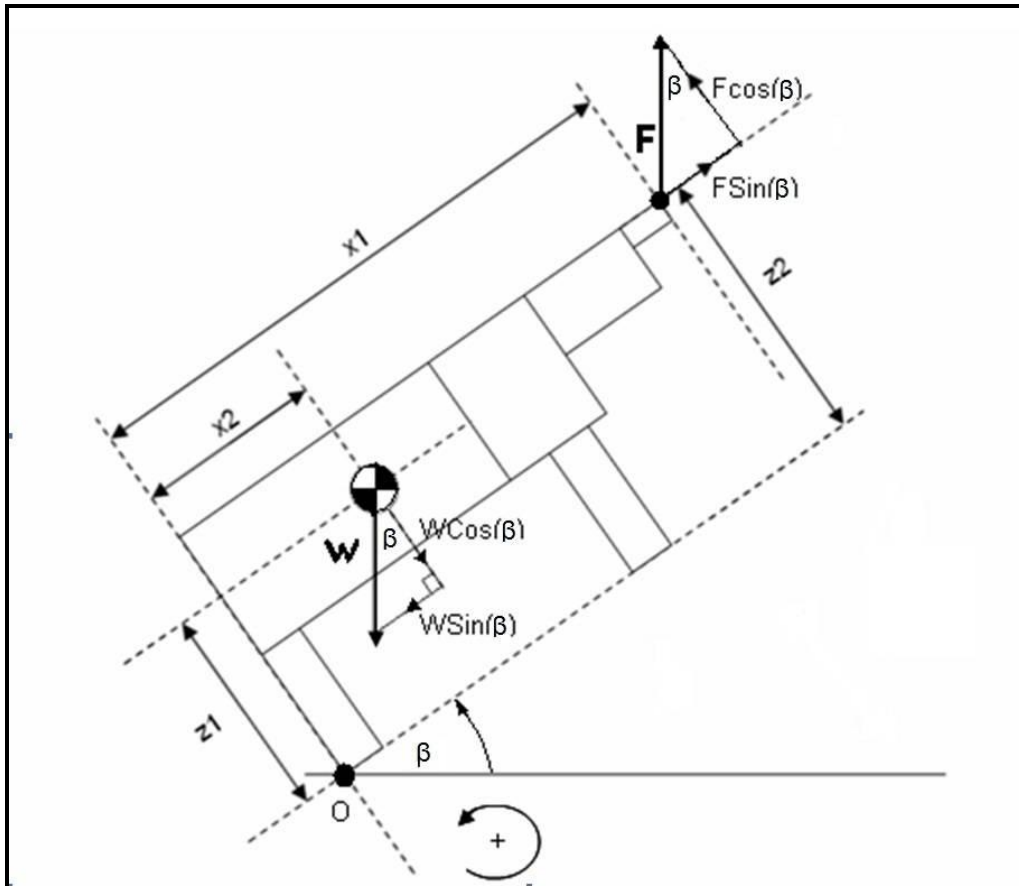


Figure 51: Force diagram used to determine vertical position of the centre of gravity

Where:

$W$  = total weight of Tyre Tester, acting at the centre of gravity, at a distance  $x_2$  forward from the rear landing legs pivot point. Note distance  $x_2$  is known, as this is the longitudinal centre of gravity distance from the rear landing legs pivot point.

$\beta$  = the lift angle of the Tyre Tester, as measured from the ground (horizontal)

$F$  = the value as obtained from the load cell, at a specific lift angle ( $\beta$ )



## Large Tyre Testing and Modelling for Handling

The forces  $F$  and  $W$  are in balance (at each specific lift angle  $[\beta]$ ) hence, the sum of moments around point  $O$  is equal to unity, and is represented mathematically as follows:

$$\Sigma M_O = 0$$

Therefore:

$$-(W \cos \beta \times x_2) + (F \cos \beta \times x_1) + (W \sin \beta \times z_1) - (F \sin \beta \times z_2) = 0$$

$$z_1 = \frac{(W \cos \beta \times x_2) - (F \cos \beta \times x_1) + (F \sin \beta \times z_2)}{W \sin \beta}$$

$$z_1 = \frac{x_2}{\tan \beta} - \frac{F \times x_1}{W \tan \beta} + \frac{F \times z_2}{W}$$

$z_1$  is calculated at each lift angle. Figure 52 depicts the results obtained for different lift angles. It was noticed, also by Uys et al. (2006), that as the lift angle increased, accuracy of the method improves, and the height of the centre of gravity stabilises.

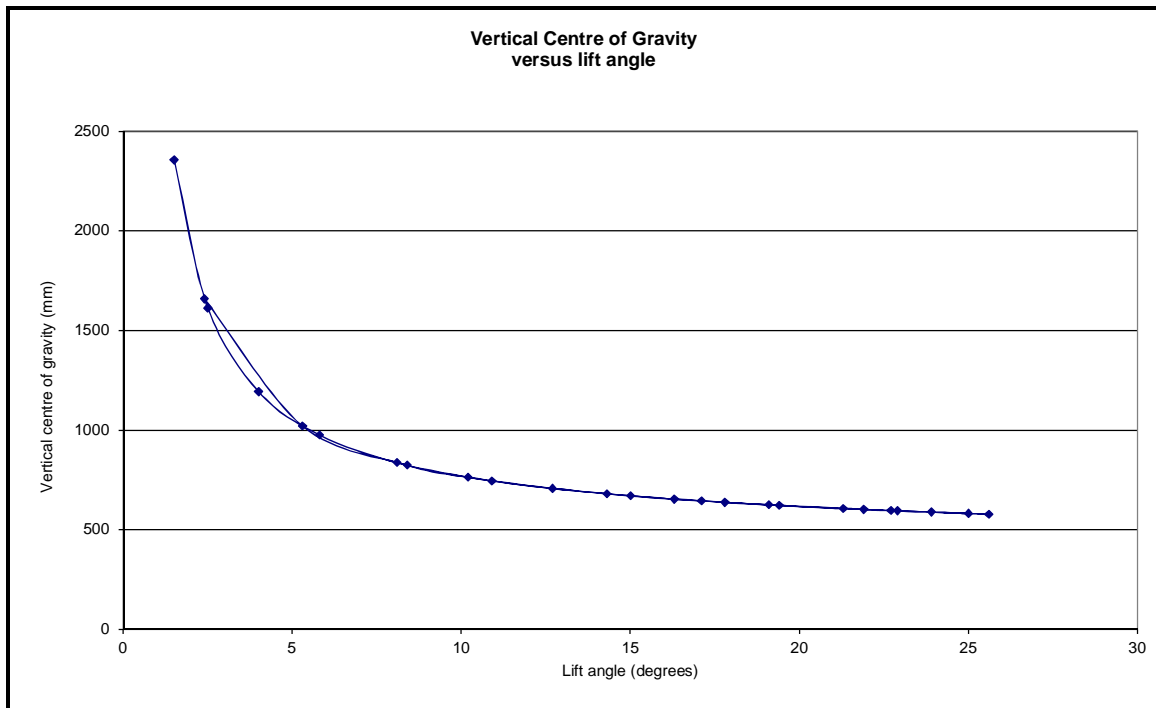


Figure 52: Vertical centre of gravity versus lift angle

The vertical centre of gravity was calculated (by averaging  $z_1$  at higher lift angles) to be 610mm above ground. In order to better understand this calculated value, refer back to Figure 47, which depicts the side view Centre of Gravity position.

This was then converted to global co-ordinates for use in the ADAMS model.

## Large Tyre Testing and Modelling for Handling

### 5.4 Moments of Inertia

The moments of inertia parameters were required for the ADAMS dynamic simulation model. The roll ( $I_{xx}$ ), pitch ( $I_{yy}$ ) and yaw ( $I_{zz}$ ) moments of inertia parameters provide the ADAMS simulation model with a more accurate real world representation of the Tyre Tester. As a result, the simulation outputs for dynamic manoeuvres such as lane changes will be more representative of real world results.

The method used to determine the moments of inertia is based on a paper published by Uys et al, (2006) – *Experimental determination of moments of inertia for an off-road vehicle in a regular engineering laboratory*. The paper describes a procedure of determining the moments of inertia using basic equipment found in a university laboratory, in a cost effective way. The basic concept involves a rigid body oscillating about a pivot point, with a spring providing the restoring force. The moment of inertia is then calculated using two methods. The first is by using the period of oscillation calculation method, and the second is by calculating the gradient of the torque-angular acceleration curves. It was found by Uys et al, (2006) that the period of oscillation calculation method produced more accurate results, as the friction moment induced by the oscillation at the pivot point was taken into account which is not the case with the gradient-torque calculation method.

The theory of the moment of inertia calculations applied are presented below, as described in Uys et al (2006)

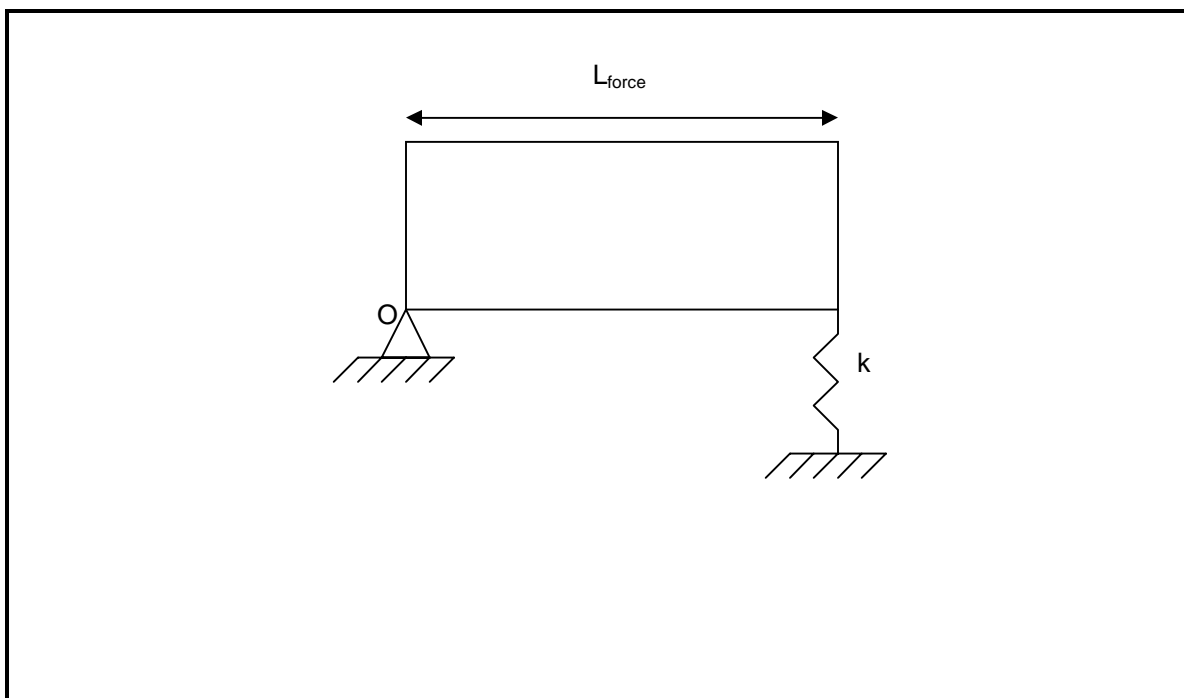


Figure 53: Schematic presentation of the rotational vibration of a rigid body

The basic idea is to apply the equations of motion to a rigid body oscillating about a pivot point, as shown in Figure 53. The body is supported by a spring of stiffness coefficient  $k$ , and is allowed to oscillate at the pivot point O, and only in the vertical plane. Applying Newton's second law of motion we get:

## Large Tyre Testing and Modelling for Handling

$$\sum T_0 = I_o \ddot{\theta} \dots (5.1)$$

Where:

$\ddot{\theta}$  is the angular acceleration,

$\sum T_0$  is the sum of the moments of the external forces about O,

$I_o$  is the moment of inertia about the axis of rotation.

Once the body starts to oscillate, the body forms an angle  $\theta$ , with the horizontal and the spring displacement is thus  $L_{force} \sin(\theta)$ . The spring force which equals  $kx$  can be written as  $kL_{force} \sin(\theta)$ . The restoring moment at point O is  $kL_{force}^2 \sin(\theta) \cos(\theta)$ .

For small angles of  $\theta$ ,  $\sin(\theta)$  can be approximated to equal  $\theta$ , and  $\cos(\theta)$  can be approximated to equal 1. Taking this into consideration the restoring moment can be simplified into:

$$\sum T_0 = -kL_{force}^2 \theta \dots (5.2)$$

Substituting (5.2) into (5.1) we get:

$$\ddot{\theta} + \frac{kL_{force}^2}{I_o} \theta = 0 \dots (5.3)$$

Where the displacement from the equilibrium position is considered and

$$\omega_n = \sqrt{\frac{kL_{force}^2}{I_o}} \text{ (in rad/s) } \dots (5.4)$$

is the undamped natural frequency of the system. The period of free vibration is thus given by:

$$\tau = 2\pi \sqrt{\left(\frac{I_o}{kL_{force}^2}\right)} \dots (5.5)$$

by measuring the period of oscillation, the moment of inertia can be calculated as follows:

$$I_o = \frac{\tau^2 kL_{force}^2}{(2\pi)^2} \dots (5.6)$$

### ***Determination of the roll moment of inertia ( $I_{xx}$ )***

In order to determine the roll moment of inertia ( $I_{xx}$ ) the Tyre Tester was allowed to pivot along its longitudinal (x) axis. A spring was mounted between the floor and right wheel hub to provide the restoring moment. The total equipment for the test consisted of:

- 'Knife' edges mounted underneath the Tyre Tester in the longitudinal direction.
- Jack stands with angle 90° angle iron attached to provide the support for the knife edges
- A spring supporting the wheel hub.
- A load cell to measure the force on the spring.
- A displacement transducer to measure spring travel.
- Accelerometer at base of spring

The setup is shown in Figure 54:

## Large Tyre Testing and Modelling for Handling

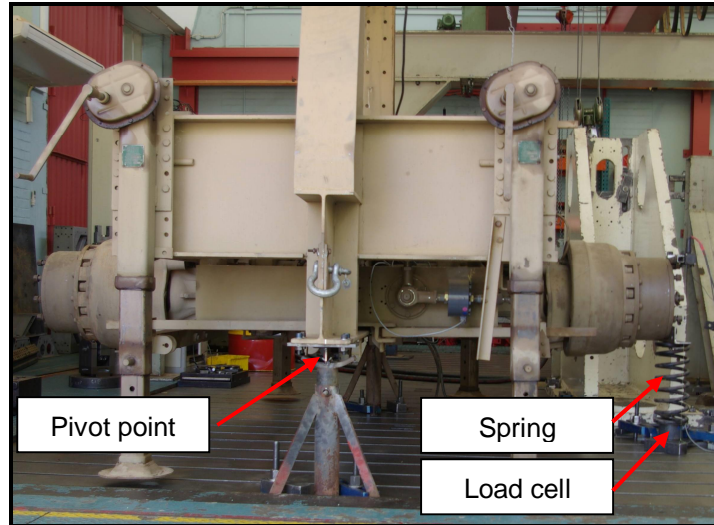


**Figure 54: Roll moment of inertia setup**

The body was pushed vertically down at the wheel hub to initiate the oscillation. The spring displacement and force was measured, together with the acceleration experienced at the spring base. The oscillation experienced by the spring is shown in Figure 55 below:

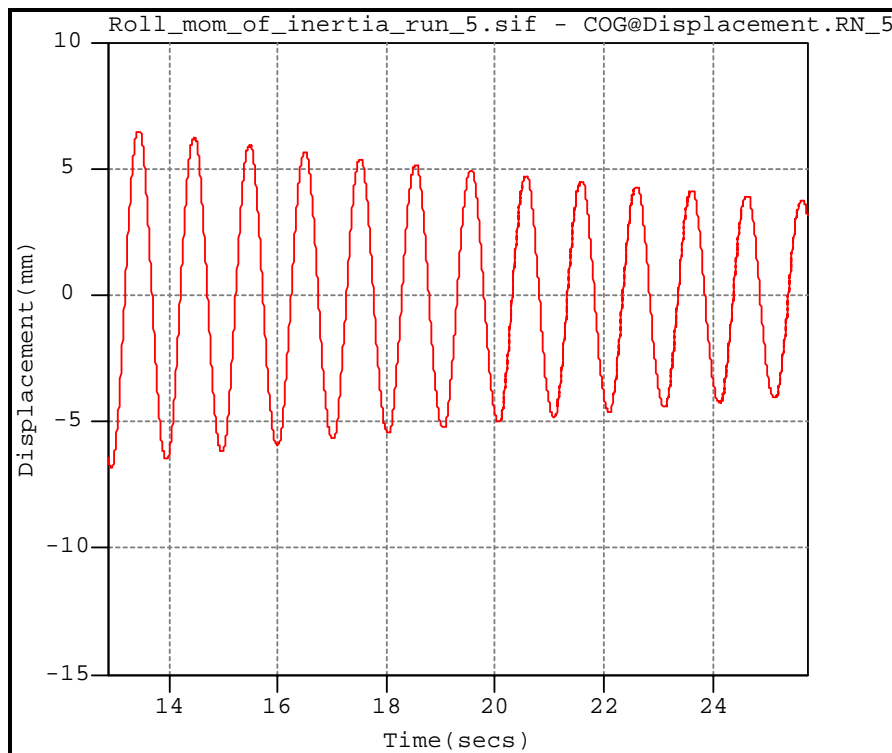


**Figure 55: Spring displacement as measured during roll moment of inertia determination**

## Large Tyre Testing and Modelling for Handling

Figure 55 depicts the damped oscillatory spring displacement. The period as required in equation (5.6) is the natural period, hence the derivation to compute the natural period follows:

We first compute the logarithmic decrement ( $\delta$ ). This is computed by taking the natural logarithm of the amplitude ratio of two successive peaks:

$$\delta = \ln \frac{x_1}{x_2} \dots (5.7)$$

The damping ratio can then be calculated as follows:

$$\zeta = \frac{\delta}{\sqrt{\delta^2 + (2\pi)^2}} \dots (5.8)$$

The natural period can then be calculated using the observed damped period  $\tau_d$  from Figure 55 above

$$\tau = \sqrt{1 - \zeta^2} \tau_d \dots (5.9)$$

It is also observed, as commented by Uys et al, that there are negligible differences between the natural and damped periods.

Now, all of the parameters of the moment of inertia ( $I_0$ ), equation (5.6) could thus be determined.

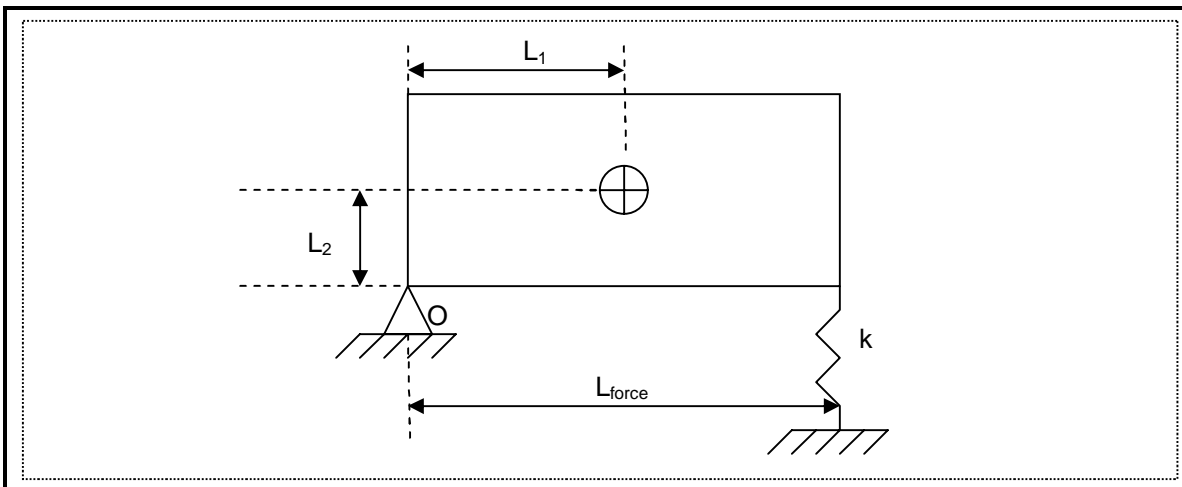


**Figure 56: Determining the moment of inertia at the centre of gravity**

Determining the moment of inertia at the centre of gravity is calculated as follows:

$$\bar{I}_{body}^{roll} = I_0 - m_{body} (L_1^2 + L_2^2) \dots (5.10)$$

Multiple runs were recorded with the roll moment of inertia setup. In the calculation of  $I_0$ , for each run, six successive oscillations from the data were used, and an average of the six was computed. Multiple oscillations were chosen to check for consistency in the calculation and method. This approach also results in more confidence in the data.

This was done for each run conducted, and then finally an average of the 3 runs was taken to get to the final value of  $I_0$ .

This resulted in the roll moment of inertia ( $I_{xx}$ ) finally being calculated as 3 776.0 kgm<sup>2</sup>

## Large Tyre Testing and Modelling for Handling

### ***Determination of the Pitch Moment of Inertia ( $I_{YY}$ )***

A similar approach was followed to determine the pitch moment of inertia ( $I_{YY}$ ). The Tyre Tester's axle was used as a pivot point, and a spring was placed, in a vertical orientation, under the front tow hitch of the Tyre Tester.

A depiction of the setup is shown in Figure 57.

The instrumentation used was the same as for the roll moment of inertia conducted previously.

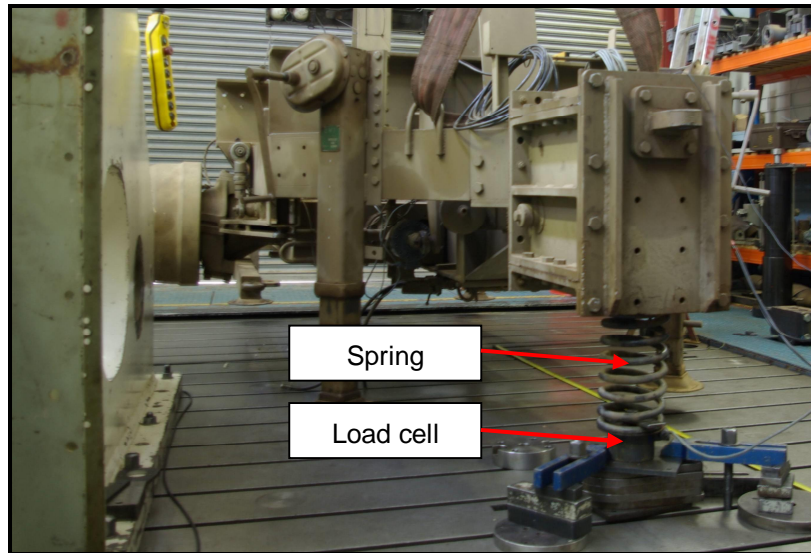


**Figure 57: Pitch moment of inertia setup**

Again multiples runs were conducted. The same data processing and averaging was conducted and the end result was a pitch moment of inertia of 5 859.6  $\text{kgm}^2$ .

## Large Tyre Testing and Modelling for Handling

### ***Determination of the Yaw Moment of Inertia ( $I_{zz}$ )***

The setup to determine the yaw moment of inertia was as follows:

- A revolute joint was attached to the tow hitch of the Tyre Tester, this allowed rotation around the vertical (z) axis of the Tyre Tester.
- A wheel hub was mounted at the rear of the Tyre Tester. The objective here was to get the Tyre Tester to rotate about the front tow hitch (i.e. around its vertical (z) axis). Oil was applied to the surface where this rear mounted hub made contact with, to lower the coefficient of friction. The end result was the Tyre Tester was allowed to rotate about the front tow hitch, with as little friction as possible.
- The spring was mounted laterally against a pillar, which provided the restoring moment for the oscillation.
- The exact same instrumentation as used for the roll and pitch moments of inertia test were used.

A depiction of the setup is showing in Figure 58:

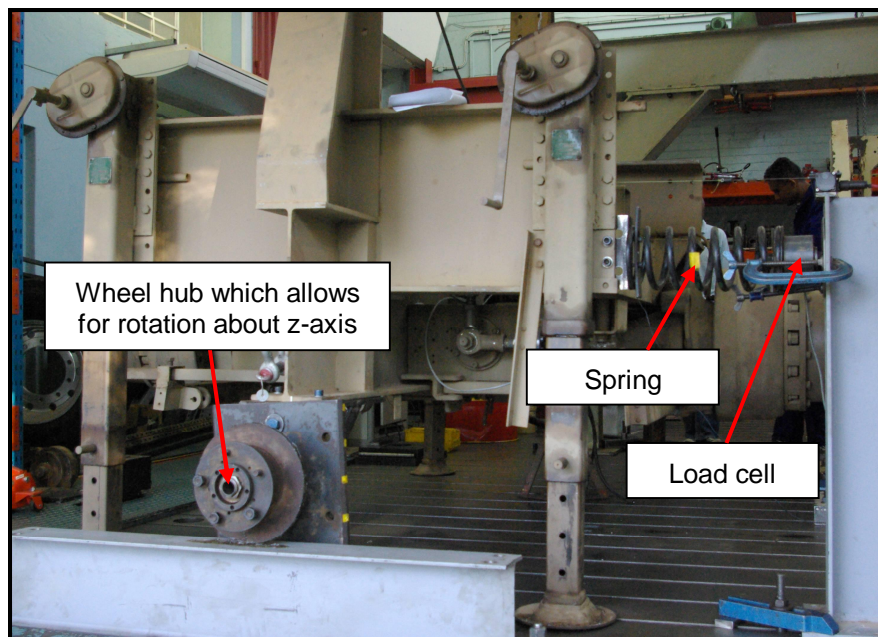


**Figure 58: Depiction of yaw moment of inertia setup**

Again multiples runs were conducted. The same data processing and averaging was conducted and the end result was a yaw moment of inertia of  $10\,456.2\text{ kgm}^2$ .

## Large Tyre Testing and Modelling for Handling

### **5.5 ADAMS simulation model creation**

Following the completion of the above important characterisation exercises i.e. the mass determination, the centre of gravity determination, and the moments of inertia determination, the ADAMS model could be created with all of these valuable characteristics being incorporated into the model.

The basis for the ADAMS model was the CAD model, which was thoroughly verified in terms of its dimensions and integration of the various parts. The importation into ADAMS was then done, with the help of Adam Rehnberg of KTH, in Sweden. Figure 59 shows a graphic of the ADAMS model.

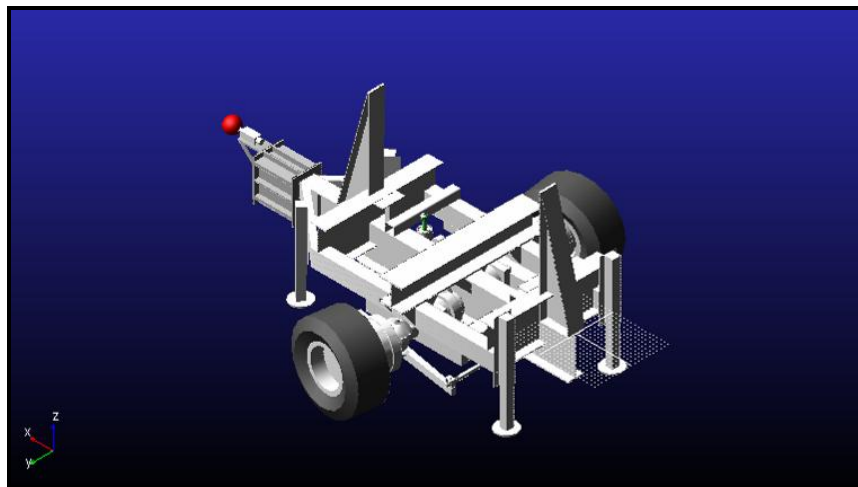


**Figure 59: Graphic of the Tyre Tester ADAMS model**

The model consists of the following rigid bodies:

- Mainframe
- Subframe
- Right wheel hub
- Left wheel hub
- Load cells (12 parts, two parts per load cell)
- Tow hitch
- Tyres

The mass and moments of inertia, of the major parts, as determined in the previous tests, were incorporated into the model.



## Large Tyre Testing and Modelling for Handling

### ***Implementation of load cells:***

Each load cell is implemented as two rigid parts, held together by a translational joint. The joint is locked in place by a MOTION. A MEASURE is applied to the MOTION to measure the force between the parts. As a result, the force experienced by the load cell is measured. This approach was found to be easier to implement and much faster to solve than modelling each load cell as a spring with very high stiffness.

The Tyre Tester ADAMS model has the following major functional features:

- Ability to add on different tyre models.
- Ability to change the slip-angle in fixed increments.
- Ability to drive the model in a straight line, at a user defined speed. (For side-force versus slip-angle tests)
- Ability to add mass plates onto the Tyre Tester, to change the tyre vertical load.
- Ability to execute a double lane change, using the GPS path (splines) of the actual lane change performed to move the tow hitch of the Tyre Tester.

Based on the instrumentation as installed for the track tests (documented in section 4.3), the following measured outputs were configured in the ADAMS model:

- Forces on the load cells:
  - The two lateral load cells.
  - The three vertical load cells.
  - The longitudinal load cell.
- Slip-angle of the right tyre.
- Roll, Pitch, and Yaw measurements of the test rig.
- Accelerations (vertical and lateral) as measured by the accelerometers (precise locations modelled) during track testing.
- Speed of the test rig.

## Large Tyre Testing and Modelling for Handling

Figure 60 shows an illustration of the different discrete slip-angles that can be configured on the Tyre Tester ADAMS model.

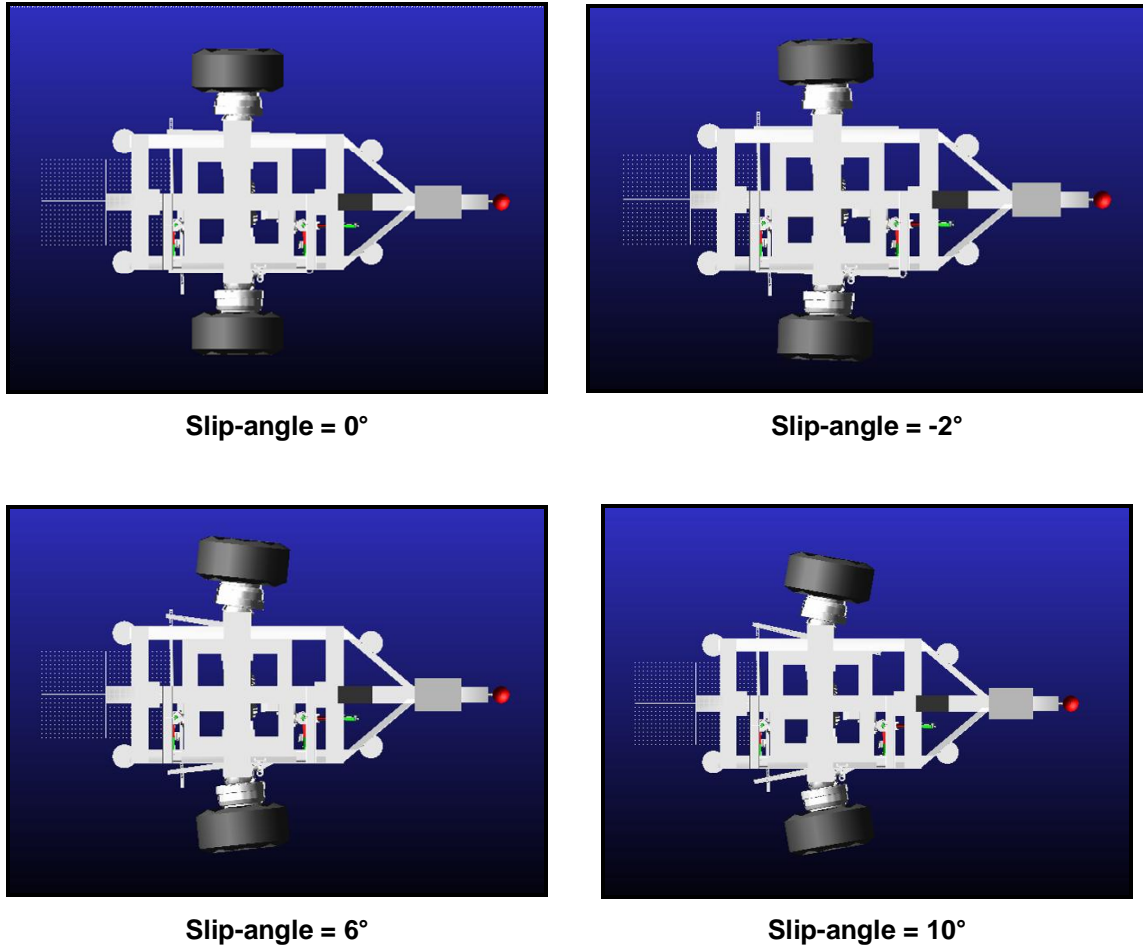


**Figure 60: Illustration of Tyre Tester with different slip-angles**

Different vertical wheel load conditions could be configured. Figure 61 shows the ADAMS model with mass plates (highlighted in orange and brown). The three load conditions tested could thus be modelled.

## Large Tyre Testing and Modelling for Handling

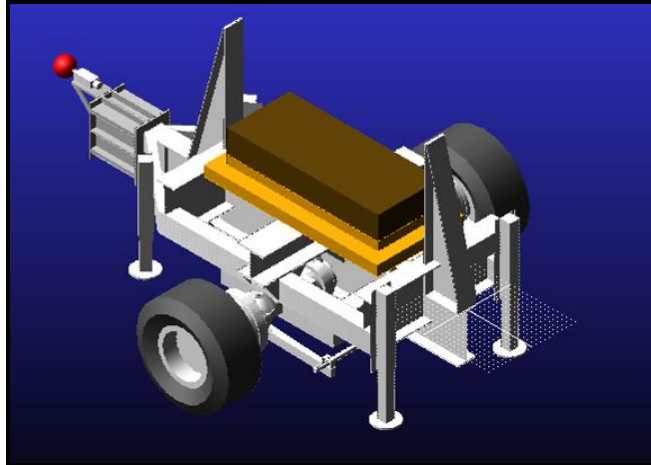


**Figure 61: Different load conditions**

### ***5.6 Summary of Tyre Tester characterisation and modelling***

In summary, this chapter focussed on the characterisation tests that were performed on the Tyre Tester:

- CAD model dimension verification
- Mass determination of mainframe and subframe parts
- Centre of gravity determination
- Moments of inertia determination

The ADAMS model was then created, with the functionality and measurement outputs similar to the actual Tyre Tester. The characteristic results obtained from the above tests were input into the ADAMS model, thereby increasing its static and dynamic accuracy.

## Large Tyre Testing and Modelling for Handling

### 6. Parameterisation of ADAMS tyre models

The previous chapter focussed on development of the ADAMS Tyre Tester model, together with the determination of the important characteristic parameters of the Tyre Tester (i.e. mass determination, centre of gravity determination, moments of inertia determination). Now that the ADAMS model is in place, this chapter focuses on the parameterisation of three frequently used handling tyre models in ADAMS, using the experimental data from Chapter 4.

The approach was to start off with the simplest model, the Fiala tyre model, and then move onto the UA tyre model, then finally onto a more complex model, the Pacejka 89 model. All three of these tyre models were parameterised for both the GoodYear and Michelin tyres.

#### **6.1 Determination of general tyre parameters for tyre models**

The focus of this study is side-force versus slip-angle characteristics of the tyre. Therefore only the parameters relevant for the lateral characteristics of a tyre were calculated in the parameterisation of the tyre models. There are a number of tyre models in the ADAMS simulation package, and it was noted that there are a few parameters that are common across the specific tyre models chosen for this study. These parameters are the following:

- Vertical tyre stiffness
- Vertical tyre damping
- Lateral tyre stiffness
- Tyre shape
- Rolling resistance

The following sections will detail how the values for these parameters were calculated.

#### **Vertical tyre stiffness:**

The vertical tyre stiffness essentially describes the vertical tyre force as a function of the vertical displacement.

The non-rolling static stiffness of the tyres were determined experimentally in the laboratory by means of an actuator applying a force perpendicular to the tyre contact patch via a flat plate. This essentially simulates a vertical tyre load on a smooth flat road. The displacement and load was measured. The resulting vertical stiffness was calculated from an average of three runs.

The vertical stiffness of the GoodYear tyre was 1 025.6 N/mm at an inflation pressure of 740 kPa. For the Michelin tyre the value was 707.0 N/mm at an inflation pressure of 300 kPa.

#### **Vertical tyre damping:**

In order to determine the vertical tyre damping, a vertical drop test was conducted. This test was conducted in the vehicle workshop at Gerotek Test Facilities. The Tyre Tester was jacked up at the rear end while the tow hook remained connected to the test vehicle. It was raised to the point where both the tyres just cleared the ground. A quick (drop) release mechanism was then put in place of the jack. The quick release mechanism was activated which allowed the Tyre Tester to 'fall' to the ground, while oscillating around the tow hitch (pivot point).

The vertical drop test was conducted for each of the three load conditions. Two runs were conducted per load. Figure 62 shows the resulting displacement (oscillating signal) as measured by the laser displacement transducer.

## Large Tyre Testing and Modelling for Handling

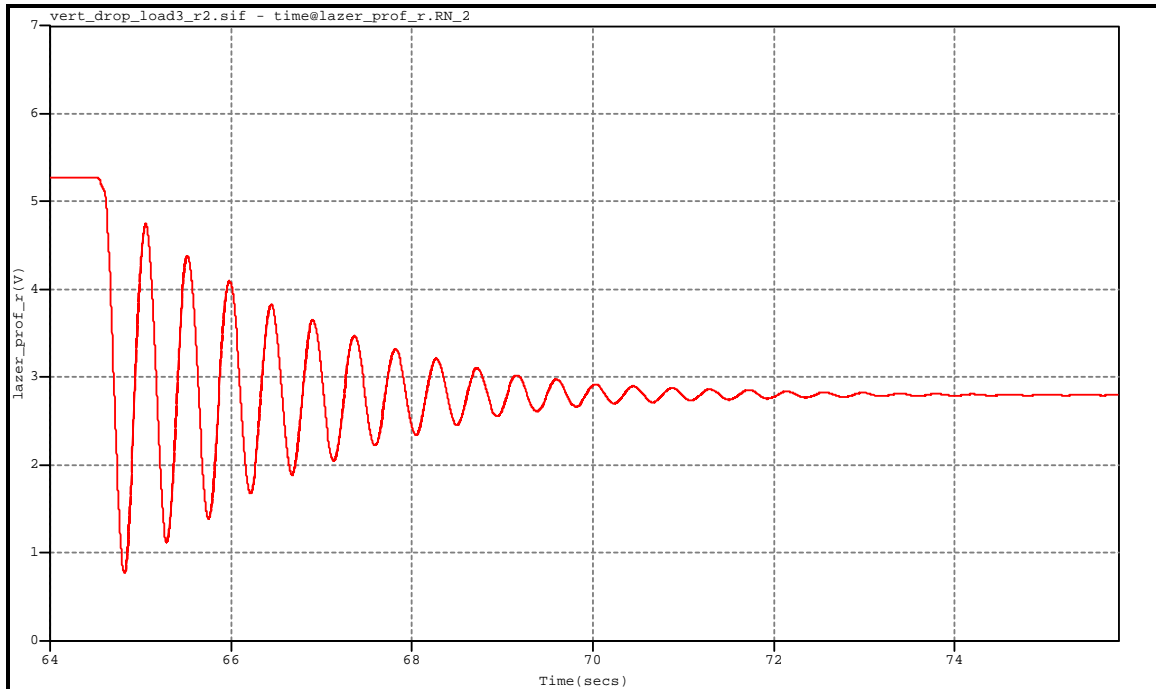


**Figure 62: Vertical drop test (laser displacement oscillation) – GoodYear tyre**

The resulting oscillation of the tyre ‘bouncing’ off the ground was analysed. The analysis was based on a logarithmic decrement method as highlighted by Stallmann (2014), which calculated the tyre damping coefficient. The tyre damping coefficient was thus computed to be 2.6877 Ns/mm (GoodYear tyre) and 2.5869 Ns/mm (Michelin tyre)

### ***Lateral tyre stiffness***

The lateral tyre stiffness essentially describes the stiffness of the sidewall of the tyre, in the lateral direction only. It can also be described as the amount of lateral deflection the sidewall of a tyre experiences; when a when a force is applied to the tyre in the lateral direction. To determine this parameter a test was conducted as follows:

The Tyre Tester was parked adjacent to an anchor point, which was in the form of a pillar. A ratchet was used to pull the Tyre Tester laterally towards the pillar, which causes the tyres to deflect laterally. The ratchet was tensioned to the point, where the wheel did not slide laterally, but was under significant lateral tension. The lateral deflection was measured by a laser, and the lateral force was measured by the lateral load cells on the Tyre Tester. From this data the lateral stiffness was calculated. Two runs were conducted for each of the 3 vertical load conditions. An average was taken over the 3 load conditions, which reflects the average tyre lateral stiffness under the load conditions tested. The results are as follows:

The lateral stiffness of the GoodYear tyre was 407.76 N/mm at an inflation pressure of 740 kPa. For the Michelin tyre the value was 223.09 N/mm at an inflation pressure of 300 kPa.

## Large Tyre Testing and Modelling for Handling

### ***Tyre shape:***

The ADAMS tyre file contains a section where the tyre carcass cross sectional shape can be described. It is strictly required for “ride” modelling and not “handling” modelling. However it was included as it will help with future modelling projects with these tyres. The number of co-ordinates that can be used to describe the cross sectional shape is limited to 9 in ADAMS. Due to the limited co-ordinates, it was decided to model just the outer edge of the tyre in detail. Each tyre’s outer edge shape was measured, and then the best utilisation of 9 co-ordinates was made to describe the tyre shape.

The shapes of the tyres as input into the tyre file are represented graphically in Figure 63 and Figure 64:

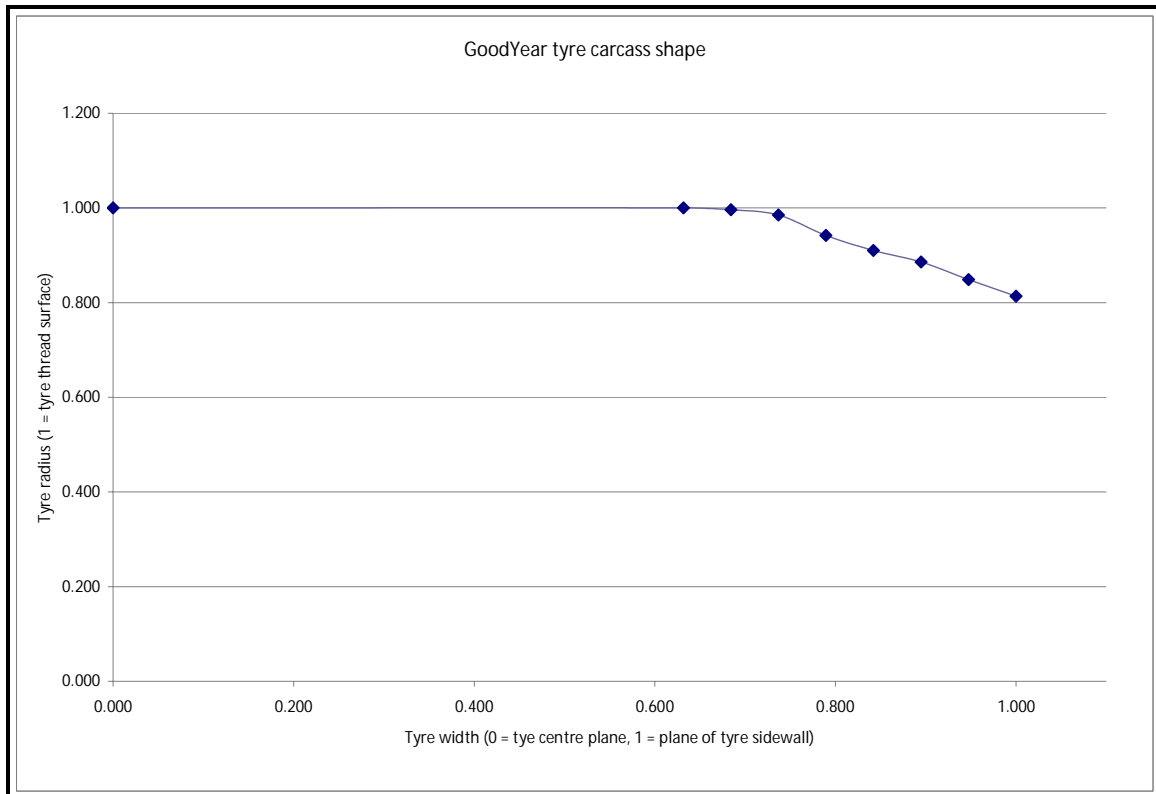


**Figure 63: GoodYear tyre carcass shape**

## Large Tyre Testing and Modelling for Handling

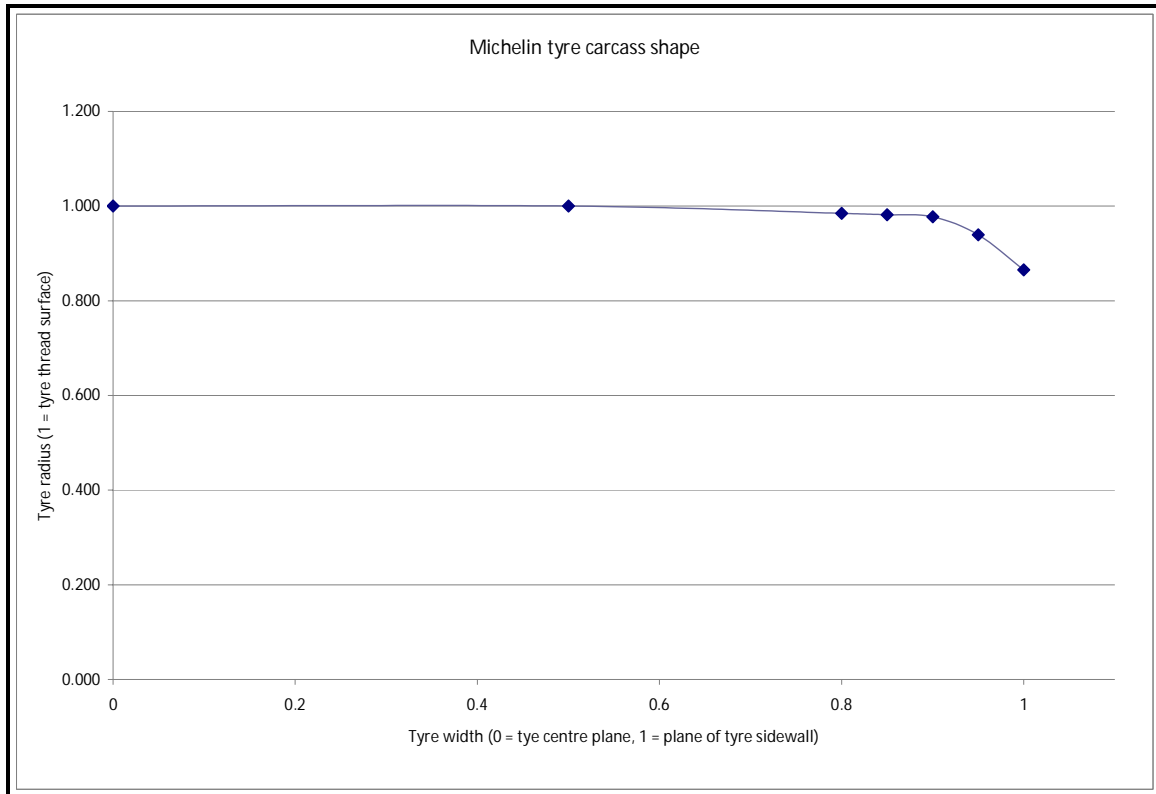


**Figure 64: Michelin tyre carcass shape**

It can be seen from the above figures that the tyre contact edge shape of the GoodYear tyre tapers off more significantly as compared to the Michelin tyre.

### ***Rolling resistance:***

The rolling resistance parameter (not important for handling simulation, but was included for possible future projects) was set to 0.015 (Bosch, 1986).

### ***6.2 Fiala tyre model***

As mentioned in Chapter 2, the Fiala tyre model (ADAMS View HELP, 2012) is a physics-based tyre model. The carcass is modelled as a beam on an elastic foundation in the lateral direction. Elastic brush elements provide the contact between the carcass and the road. Analytical assumptions are derived for the steady state slip characteristics; these form the basis for the longitudinal and lateral forces in ADAMS.

In addition to the general tyre parameters calculated in section 6.1, there are a few additional parameters that are specific to the Fiala tyre model. These will be discussed in detail below:

### ***CALPHA parameter Fiala tyre model***

CALPHA is defined as the partial derivative of lateral force ( $F_y$ ) with respect to slip-angle ( $\alpha$ ) at zero slip-angle, commonly known as the cornering stiffness.

From the side-force slip-angle data obtained from track testing, the gradient around zero slip-angle was evaluated, for each of the three load conditions:

## Large Tyre Testing and Modelling for Handling

$$\text{i.e. } CALPHA = \left. \frac{dF_y}{d\alpha} \right|_{\alpha=0}$$

Table 9 shows the calculated CALPHA values for the Goodyear and Michelin tyres.

<b>Table 9: Fiala CALPHA values</b>			
<b>Goodyear Tyre</b>		<b>Michelin Tyre</b>	
<b>Load (kg)</b>	<b>CALPHA (N/°)</b>	<b>Load (kg)</b>	<b>CALPHA (N/°)</b>
2 255	2 896.1	2 385	4 423.5
3 835	4 948.4	3 940	6 085.1
5 235	4 927.9	5 390	4 493.1
<b>Average</b>	<b>4 257.5</b>	<b>Average</b>	<b>5 000.6</b>

It was noted by Blundell (2004) that the Fiala model only contains a single value for cornering stiffness. Whereas in reality there are different cornering stiffness' for different vertical wheel loads. Blundell (2004) therefore used an average value, so that tyre model comparisons could be conducted. Hence an average CALPHA parameter was computed for the Fiala tyre model.

See Appendix A for ADAMS tyre model files.

### **6.3 UA tyre model**

As mentioned in Chapter 2, the University of Arizona (UA) tyre model (ADAMS View HELP, 2012) was originally developed by Drs P.E. Nikravesh and G. Grim. The UA Tyre model calculates the forces at the ground contact point as a function of the tire kinematic states.

#### **CALPHA parameter UA tyre model**

Similar to the Fiala tyre model, the UA tyre model uses the CALPHA parameter as well. The only difference is the units for CALPHA are Newton per radian (N/rad) for the UA tyre model, as opposed to Newton per degree (N/°) for the Fiala tyre model. Here also the average CALPHA value was used.

See Appendix A for ADAMS tyre model files.

### **6.4 Pacejka 89 ('Magic Formula') tyre model**

As mentioned in Chapter 2, the Pacejka 89 tyre model as implemented in ADAMS (ADAMS View HELP, 2012) is based on the Magic-Formula Tyre model, as described by Bakker E, et al (1989). It is an empirical tyre model that describes measured tyre characteristics by means of formulas and interpolation schemes for which the parameters are determined by curve-fitting to experimental data.

It is based on the following formula, also commonly referred to as the 'Magic Formula'. The lateral force is defined as:

$$F_y = D \sin \left[ C \arctan \left\{ B X_1 - E \left( B X_1 - \arctan \left( B X_1 \right) \right) \right\} \right] + S_v \dots \quad (6.1)$$

An illustration of the curve and the various coefficients are given in Figure 65:



## Large Tyre Testing and Modelling for Handling

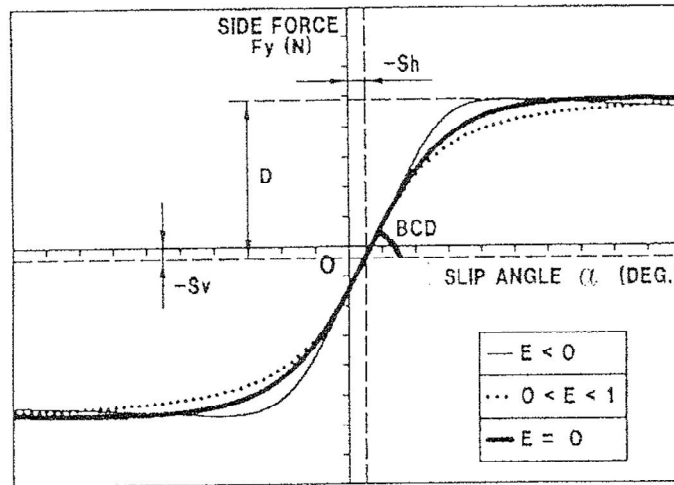


**Figure 65: Repeated Illustration of coefficients contained in the 'Magic Formula' (Bakker E et al, 1989)**

The various coefficients are defined as follows:

$F_y$  is the Lateral force generated by the tyre, and  $\alpha$  is the slip-angle.

D is the peak value of the lateral force

$$D = \mu F_z \dots (6.2)$$

$$\text{With: } \mu = a_1 F_z + a_2 \dots (6.3)$$

C is the shape factor

$$C = a_0 = 1.30 \dots (6.4) \text{ – for side-force}$$

BCD is the slope at zero slip-angle

$$BCD = a_3 \sin(2 \arctan(F_z / a_4)) (1 - a_5 |\gamma|) \dots (6.5)$$

B is the stiffness factor

$$B = BCD / CD \dots (6.6)$$

E is the curvature factor

$$E = a_6 F_z + a_7 \dots (6.7)$$

The horizontal shift is defined as

$$S_h = a_9 F_z + a_{10} + a_8 \gamma$$

The vertical shift is defined as

$$S_v = a_{11} F_z \gamma + a_{12} F_z + a_{13}$$

Composite

$$X_1 = (\alpha + S_h)$$

## Large Tyre Testing and Modelling for Handling

### **Units for Pacejka 89 ‘Magic Formula’**

The Pacejka 89 ‘Magic Formula’ literature does not clearly indicate the units of measure for the above terms. It is not a consistent set of units. e.g. Vertical tyre force is measured in kilo-Newton (kN), whereas Lateral tyre force is measure in Newton (N). It is an area of confusion, especially for an individual exposed to the Pacejka 89 ‘Magic Formula’ for the first time. It took some experimentation with the units, before success with the ‘Magic Formula’ could be achieved. The following is a summary of the units utilised by the critical terms in the Pacejka 89 ‘Magic Formula’:

- D must be in Newton (N)
- BCD must be in Newton per degree (N/deg)
- $F_z$  must be in kilo-Newton (kN)

### **Calculation of Pacejka 89 specific tyre file parameters**

The process followed to calculate the coefficients was as follows:

Firstly, the value of C for lateral force curves is fixed at 1.30. For all three load conditions the peak value D, can be read off the side-force versus slip-angle curves. We thus have three values for D (i.e. one for each load condition). D, which is termed the Peak Factor, is associated with coefficients  $a_1$  and  $a_2$ , according to equations 6.2 and 6.3. In order to solve for  $a_1$  and  $a_2$  use was made of the *solver* algorithm in Microsoft Excel. An example of the Microsoft Excel solver interface is shown in Figure 66

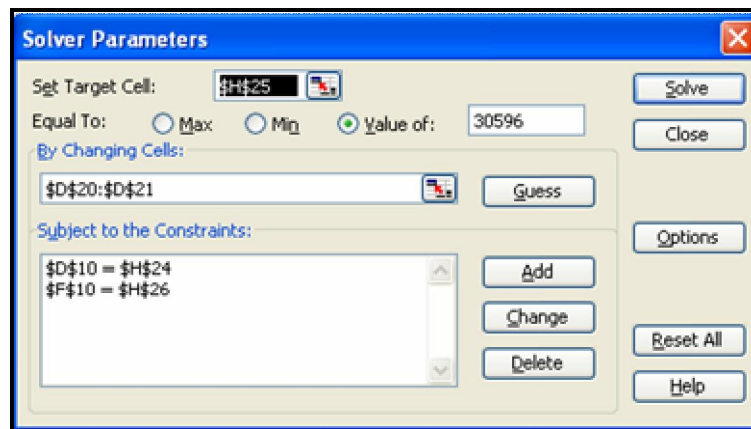


**Figure 66: Microsoft Excel solver interface**

So basically the equations for D (6.2 and 6.3 combined) are input in Microsoft Excel cells. *Solver* works by setting Target cells (equations for D) equal to Fixed Values (measured values of D) by manipulating the coefficients ( $a_1$  and  $a_2$ ), subject to constraints. The optimisers used by *solver* employ the simplex, generalised reduced gradient, and branch and bound methods to find an optimal solution (Fylstra et al., 1998)

Similarly the slope at the origin (BCD) can also be determined for all three load conditions. The coefficients  $a_3$ ,  $a_4$  and  $a_5$  are similarly solved for (via equations 6.5) with the use of Microsoft Excel *Solver*. Coefficients  $a_6$  and  $a_7$  are similarly calculated via equation 6.7. All the coefficients are then entered into the ADAMS Pacejka 89 tyre file. See Appendix A for ADAMS tyre files.

As parameter fitting is a curve fitting exercise, tweaking was done by manipulating the E value until the best fit for the measured data could be obtained. Better results may be obtainable using

## Large Tyre Testing and Modelling for Handling

some kind of optimisation to tweak all parameters for the best parameter fit, though the fit obtained by tweaking just the E parameter was adequate. Figure 67 shows the resulting curve-fit for the GoodYear tyre. It should be noted that the Pacejka 89 'Magic Formula' tries to perform a best curve-fit to all the data points, and for all three load conditions, and therefore some variance in the curve-fit can be expected. For the specific tyre under test, this variance can be seen at negative slip-angles in the data.

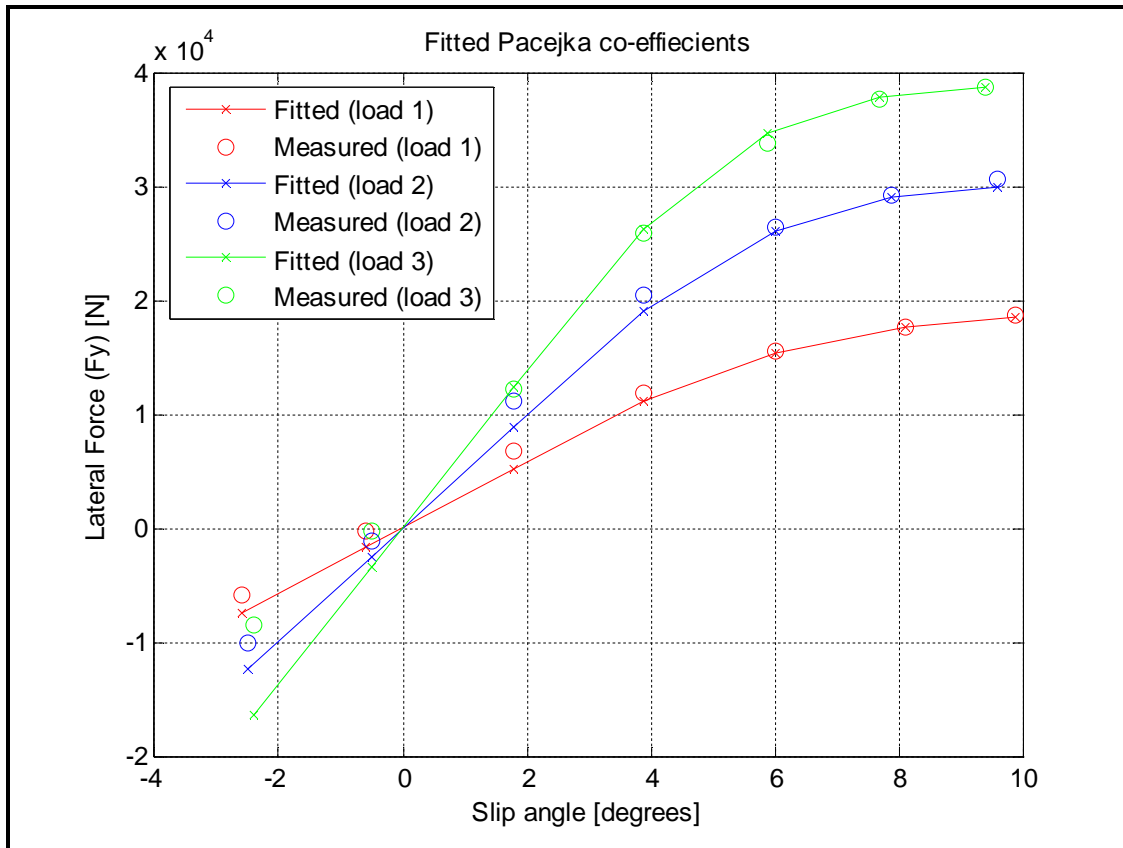


Figure 67: GoodYear Pacejka 89 curve fit

As the focus of this study is on handling specifically, tests were conducted to parameterise the handling (lateral) coefficients only. The longitudinal force ( $F_x$ ) and aligning moment ( $M_z$ ) coefficients were thus set to zero in the Pacejka 89 tyre model file. However it was discovered that the horizontal ( $S_h$ ) and vertical shift ( $S_v$ ) coefficients ( $a_8..a_{13}$ ) were not sensitive (i.e. changing these coefficients had no effect on the tyre forces produced). Through experimentation it was found that the longitudinal coefficients ( $b_0..b_4$ ) need to be parameterised (non-zero) for the lateral force horizontal and vertical shift to be sensitive. This seems to be something unique in the ADAMS View implementation of the Pacejka 89 tyre model, and does not tie up with the ADAMS View help documentation. The horizontal and vertical shift was minimal for the tyre data measured; therefore not implementing a horizontal and vertical shift did not significantly impact the fitted data.

In a similar manner the coefficients and tweaking was conducted for the Michelin tyre. The resulting curve-fit is shown in Figure 68. Similarly, it should be noted that the Pacejka 89 'Magic Formula' tries to perform a best curve-fit to all the data points, and for all three load conditions,

## Large Tyre Testing and Modelling for Handling

and therefore some variance in the curve-fit can be expected. Again, for the specific tyre under test, this variance can be seen at negative slip-angles in the data.

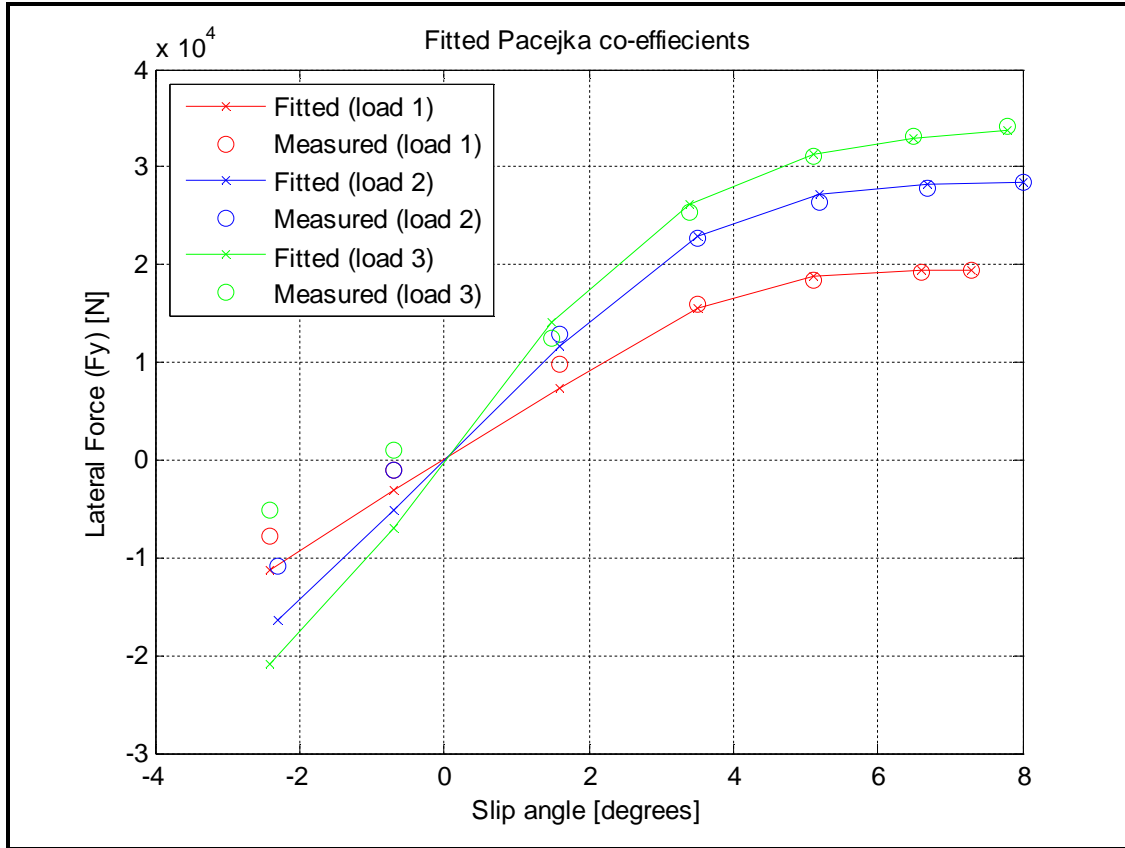


Figure 68: Michelin Pacejka 89 curve fit

Refer to Appendix A which contains the ADAMS tyre model files, which show the coefficients calculated for both GoodYear and Michelin tyres.

### 6.5 Summary of parameterisation of ADAMS tyre models

This chapter detailed the generation of tyre model parameters (relevant to lateral characteristics) for the following tyre models

- Fiala
- UA (University of Arizona)
- Pacejka 89

Tyre models were created for both GoodYear and Michelin tyres. Refer to Appendix A for tyre model (text) files.

## Large Tyre Testing and Modelling for Handling

### 7. Simulation results and correlation

The previous chapter focussed on the parameterisation of ADAMS tyre models. This chapter will focus on simulating the tyre models with the ADAMS model of the Tyre Tester, and finally comparing the simulation data with the actual measured track data.

Side-force slip-angle simulation was first conducted for each tyre model. Side-force versus slip-angle plots were then generated from the simulated data, for each tyre model. Each tyre models side-force versus slip-angle curve was compared to the actual track measured curves. A root mean squared error (RMSE) analysis was done to determine which tyre model produces the closest fit to the measured data. A RMSE analysis was also conducted on the Pacejka 89 'Simulated' data and 'Curve-fit' data compared to the measured (reference) data.

Double lane change simulation was then conducted with each tyre model, and similarly the results of each tyre model were compared with the track testing data.

#### ***ADAMS simulation of side-force versus slip-angle tests***

Once each tyre model file was parameterised, it was tested with the ADAMS Tyre Tester simulation model. The approach was to test as follows:

- The tyre file was loaded into the Tyre Tester simulation model. E.g. Fiala tyre model file
- The load condition was set by specifying the loaded mass on the Tyre Tester.
- The slip-angle was set to the first test condition (e.g.  $-2^\circ$ )
- The simulation was run at 1000 samples per second, for 10 to 12 seconds. This was the same sample rate as used during the track testing.
- The data was then analysed
- The slip-angle was changed until all slip-angles were done ( $-2^\circ$ ,  $0^\circ$ ,  $2^\circ$ ,  $4^\circ$ ,  $6^\circ$ ,  $8^\circ$  and  $10^\circ$ )
- The load condition was changed to load 2 as per the track testing
- All the slip-angles were simulated.
- The load condition was changed to load 3 as per the track testing
- All the slip-angles were simulated.
- This was conducted for all three tyre models
  - Fiala tyre model
  - UA tyre model
  - Pacejka 89 tyre model.

#### ***7.1 Simulation results: GoodYear tyre – Side-force versus slip-angle tests:***

Figure 69 depicts the channel comparisons of load cells, showing their correlation between measured test data and simulated data. There are two cases shown for illustration:

- Unladen (Load 1) load condition, Pacejka 89 tyre model and slip-angle of  $4^\circ$ .
- Load 3 (5 235kg) Pacejka 89 tyre model slip-angle of  $10^\circ$ .

Figure 69 and Figure 70 show the lateral load cell values of the Tyre Tester and that of the ADAMS model. The results for the front and rear lateral load cells are shown, as well as the sum of the front and rear lateral load cells, which is the total lateral force, experienced generated by the tyre. The data is oscillatory, but the magnitude of the oscillation is small compared to the magnitude of the value measured. This can possibly be attributed to the lack of a Lateral Damping parameter in the ADAMS Pacejka 89 tyre model. Furthermore the vertical damping is

## Large Tyre Testing and Modelling for Handling

low and tyre damping is the only damping in the system. Therefore the oscillations are basically the wheel hop characteristic that is lightly damped. It can be seen that there is generally good correlation in terms of magnitude of force of measured on the Tyre Tester data and the simulated data.

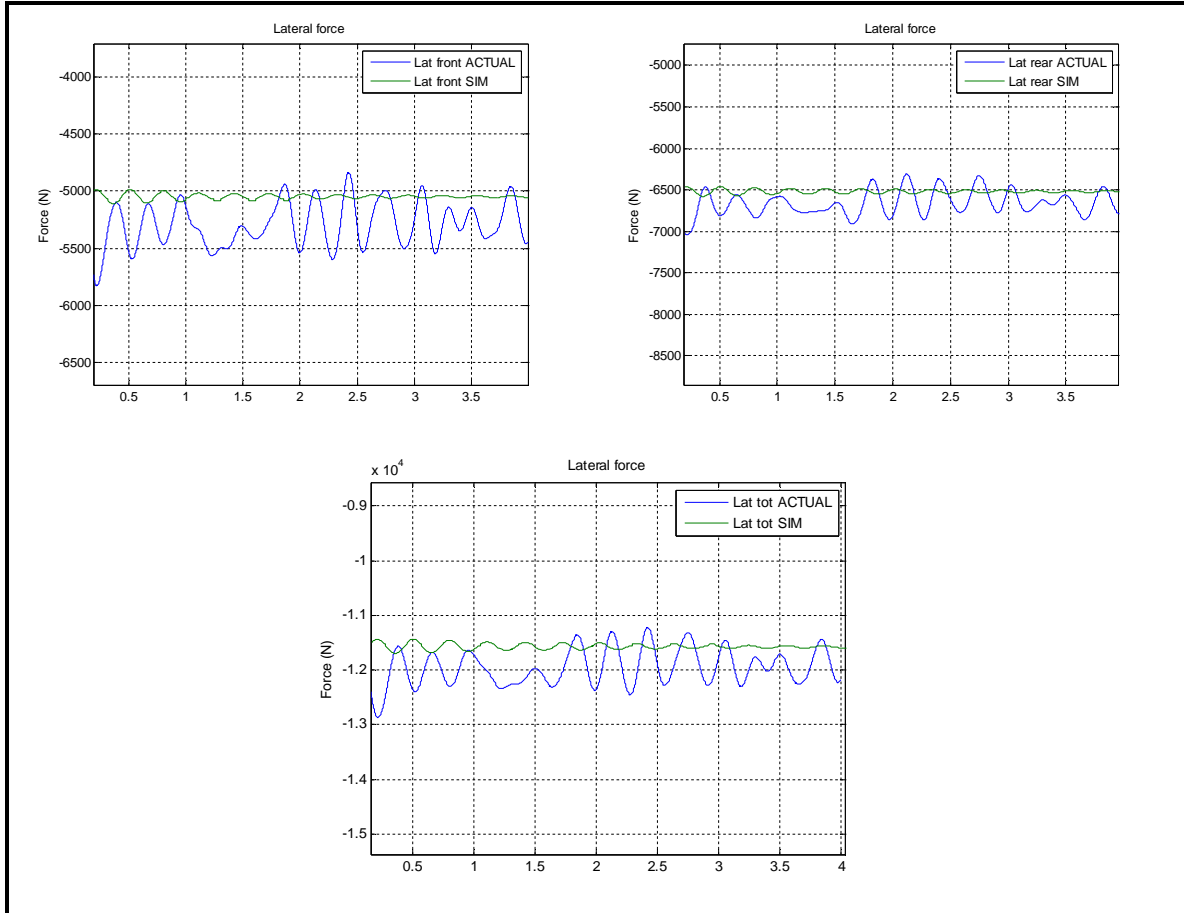


**Figure 69: GoodYear tyre: Lateral load cells data comparison (Pacejka 89, Slip-angle = 4°, load condition: Load 1)**

## Large Tyre Testing and Modelling for Handling

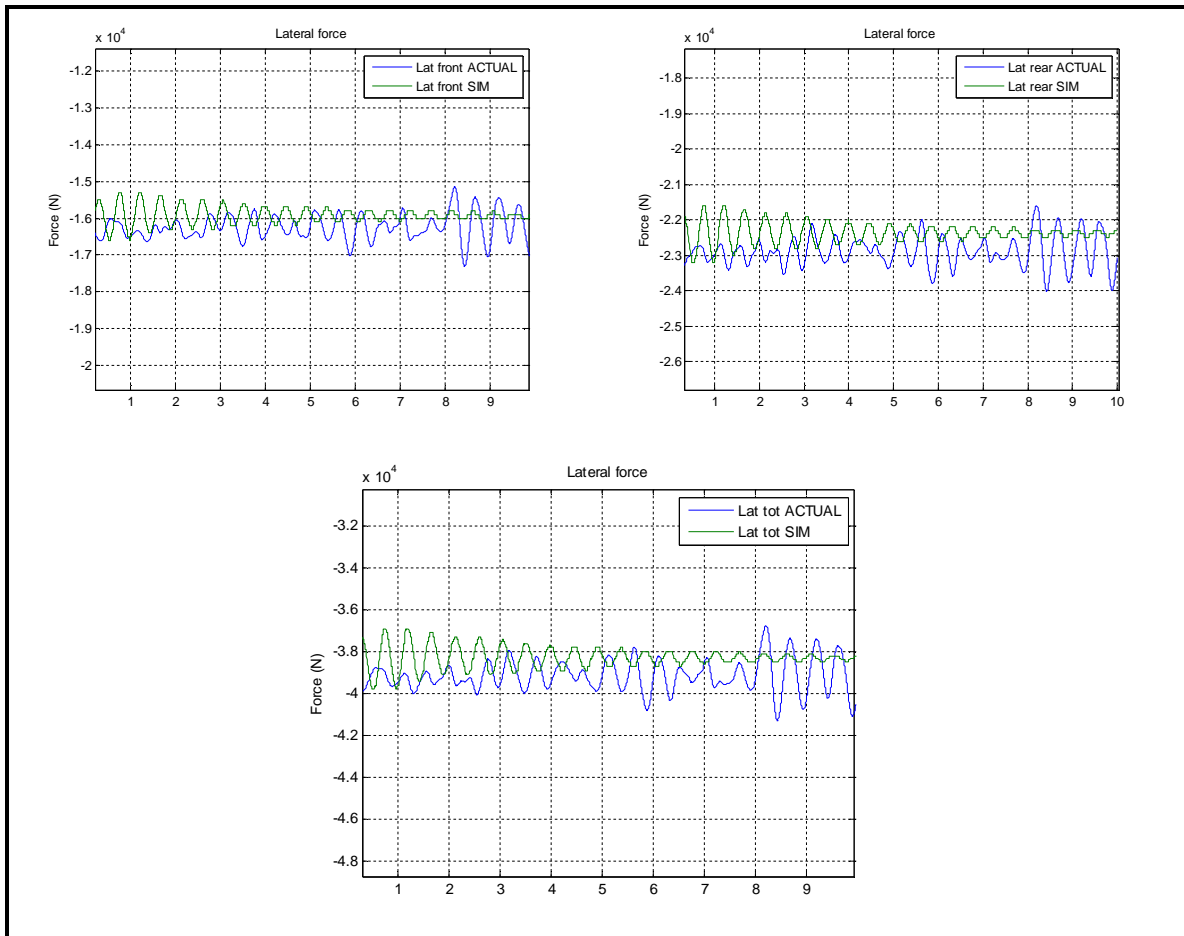


**Figure 70: GoodYear tyre: Lateral load cells data comparison (Pacejka 89, Slip-angle = 10°, load condition: load 3)**

From the simulated data in Figure 69 and Figure 70, the side-force at each slip-angle was incorporated into a side-force versus slip-angle curve. This was done for the Fiala, Pacejka 89, and the UA tyre model. All the tyre model curves and the track testing data curves were overlaid. Figure 71 shows the resulting side-force versus slip-angle comparative curves, for the GoodYear tyre for the load 1 condition. All the tyre models show good correlation with the track test data.

## Large Tyre Testing and Modelling for Handling

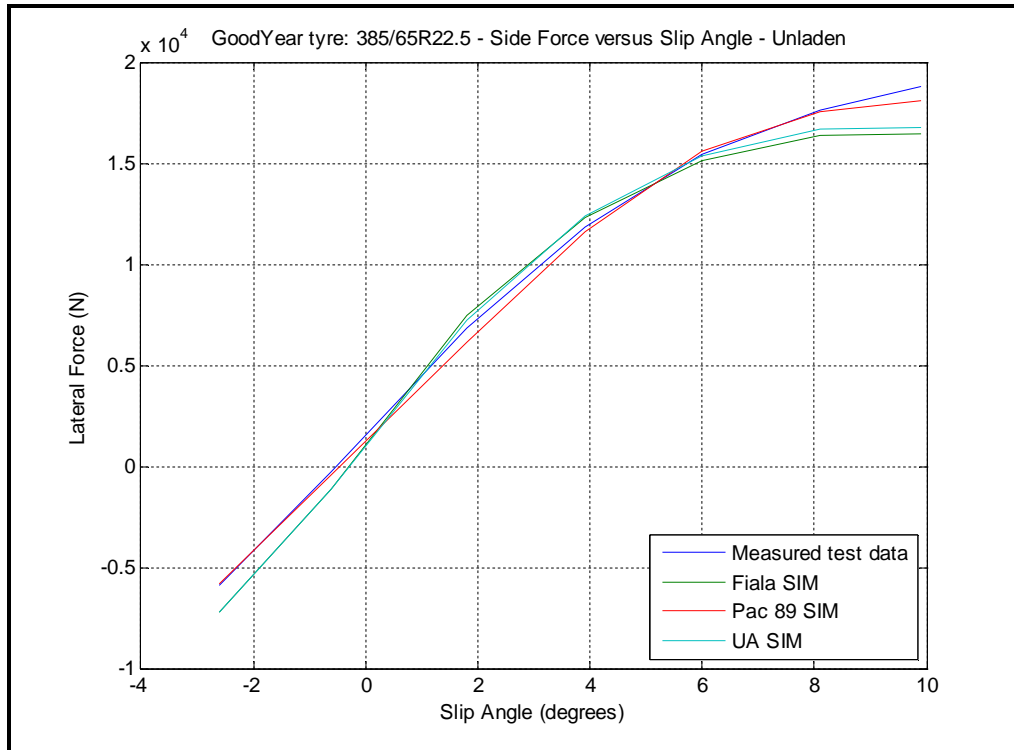


**Figure 71: GoodYear tyre: Side-force versus slip-angle comparison of tyre models and measured data (Load 1)**

The side-force versus slip-angle tyre model curves were also generated for the load 2 and load 3 load conditions. The comparisons of the curves with measured data are shown in Figure 72 and Figure 73 for load 2 and load 3 respectively.

The major observation is that at these higher loads (3 835 kg and 5 235 kg vertical wheel loads), it is only the Pacejka 89 model that shows good correlation with the measured track data. The Fiala tyre model deviates significantly from the measured track data. The UA tyre model fails to simulate successfully at  $-2^\circ$ ,  $0^\circ$  and  $2^\circ$  for load condition 3, and as a result, does not produce data.



## Large Tyre Testing and Modelling for Handling

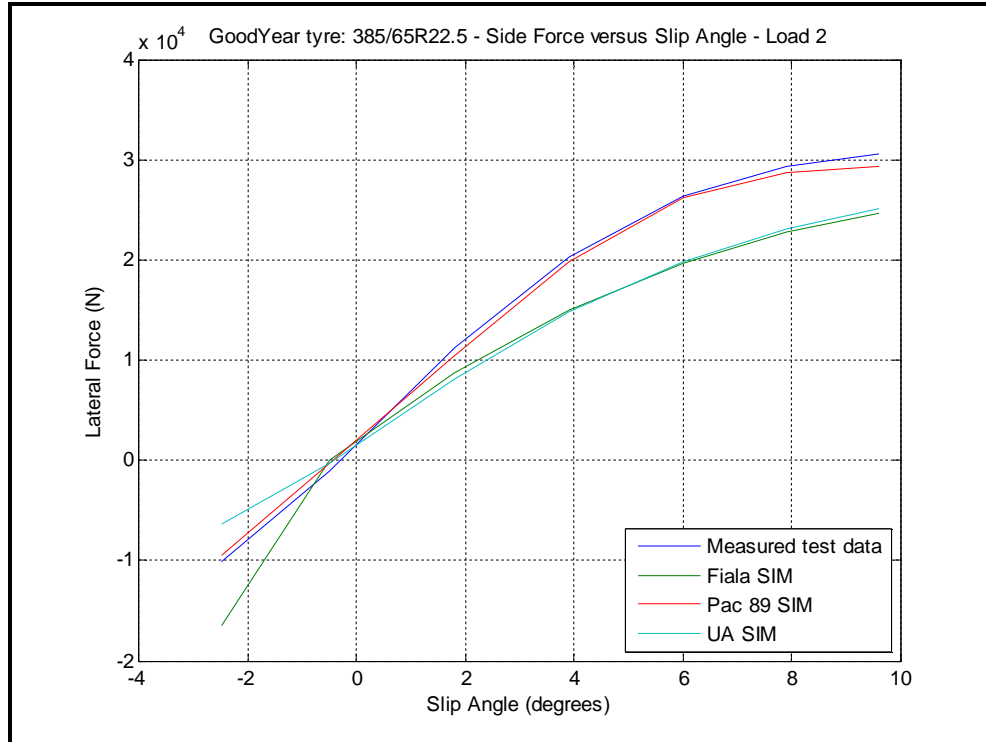


Figure 72: GoodYear tyre: Side-force versus slip-angle comparison of tyre models and measured data (Load 2)

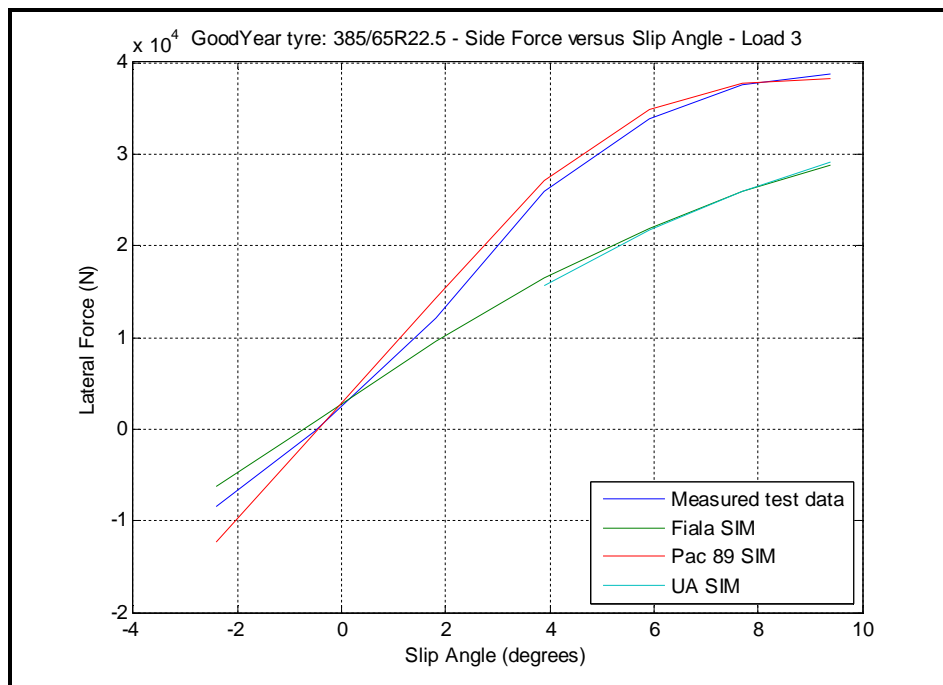


Figure 73: GoodYear tyre: Side-force versus slip-angle comparison of tyre models and measured data (Load 3)

## Large Tyre Testing and Modelling for Handling

In order to determine which tyre model produced the closest fit to the measured data, the Root Mean Squared Error (RMSE), between the tyre model data and track testing data was calculated as follows:

$$RMSE = \sqrt{\frac{1}{n} \sum_{i=1}^n (M_i - S_i)^2}$$

Where:

$M_i$  = Measured track data at slip-angle  $i$

$S_i$  = Simulated tyre model data at slip-angle  $i$

The RMSE was computed for each tyre model, and the results are shown in Figure 74. The overall correlation and deviation for the GoodYear tyre can be quantified by Figure 74, which shows the root mean squared error plots for each tyre model, with reference to the measured track data. The observations are:

- The Pacejka 89 model has the least root mean squared error, over all three load conditions, therefore produces the closest fit to the measured data.
- Fiala tyre model simulates successfully over the three load conditions. However, the Fiala data has proven a result similar to that observed by Blundell (2004), where the Fiala model underestimates lateral forces where high slip-angles co-incide with higher vertical wheel loads.
- The UA (University of Arizona) tyre model is unstable at high vertical wheel loads (load3) with slip-angles close to zero (i.e. at  $-2^\circ$ ,  $0^\circ$  and  $2^\circ$ ). The simulation does not solve.

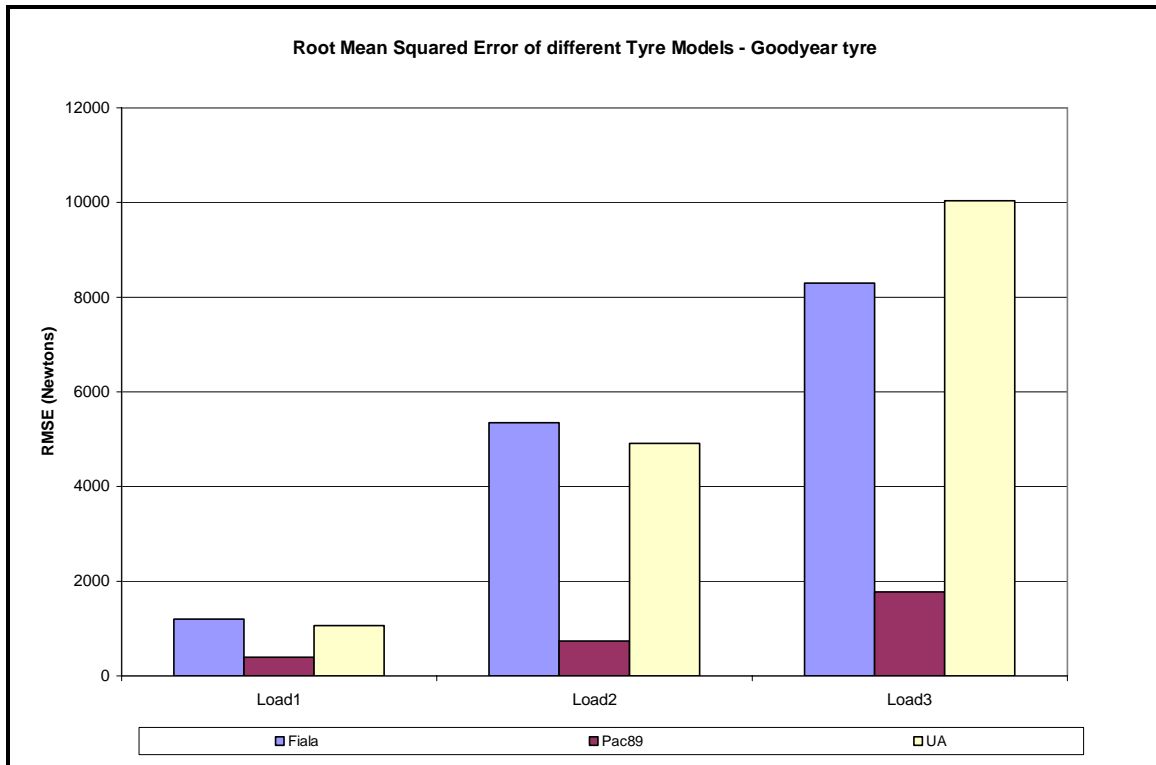


Figure 74: GoodYear tyre: Root mean squared error comparison of tyre models and measured data

## Large Tyre Testing and Modelling for Handling

### 7.2 Simulation results: Michelin tyre – Side-force versus slip-angle tests:

Similarly all the tyre models, (Fiala, UA and Pacejka 89) of the Michelin tyre were simulated with the ADAMS model of the Tyre Tester. Figure 75 shows the comparison of the measured data versus the simulated data of the load cells. This was for the Pacejka 89 tyre model, and for load 1 condition. Again, good correlation on the magnitude of the front, rear and total lateral force was noted.

The frequency of the oscillation noted in the measured signal corresponded with the lateral natural frequency of 2.3 to 2.4 Hz. The lateral natural frequency was calculated during the lateral stiffness tests, where the tyre was pulled laterally and released, then allowed to oscillate.

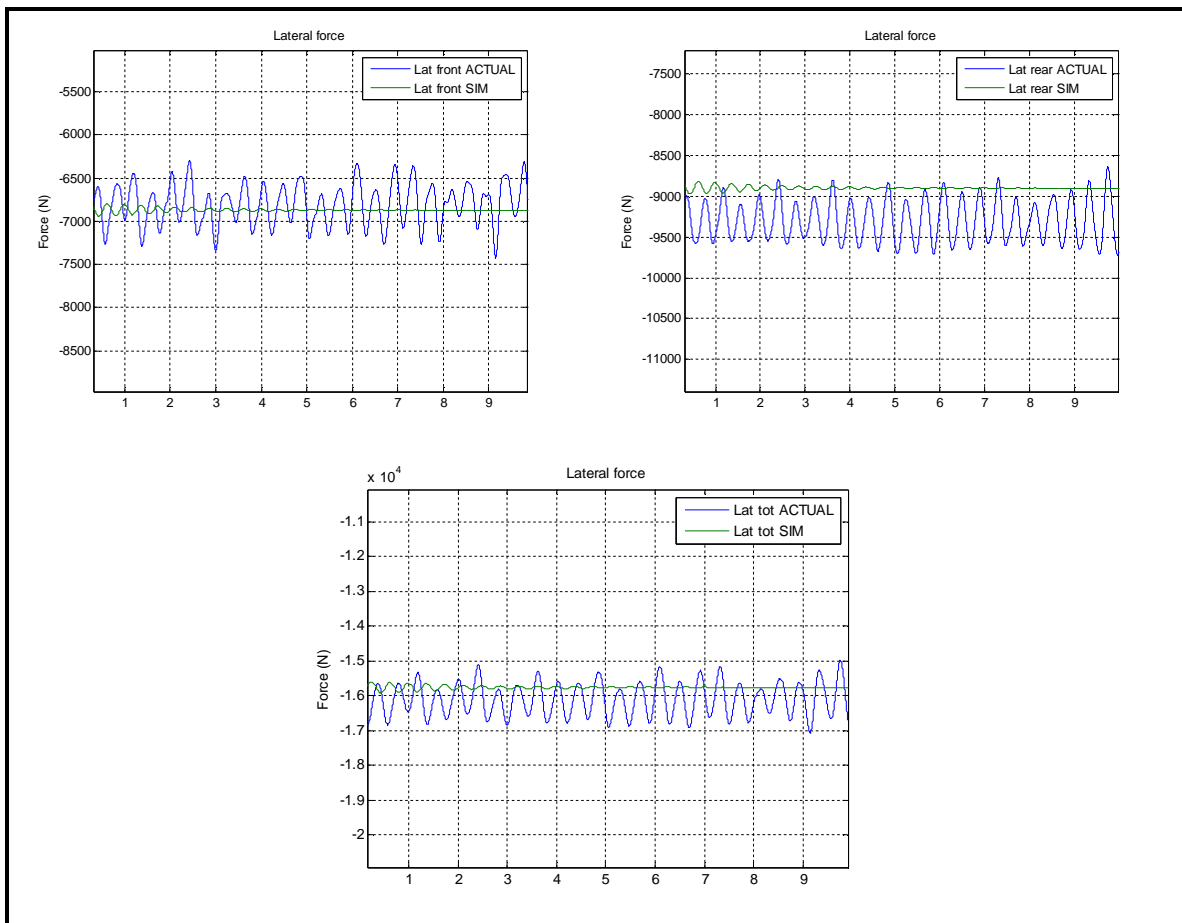


**Figure 75: Michelin tyre: Lateral load cells data comparison (Pacejka 89, Slip-angle = 4°, load condition: Load 1)**

Figure 76 shows the Pacejka 89 tyre model load cell values comparison, at a higher load (load 3). Again good correlation was noted.

## Large Tyre Testing and Modelling for Handling

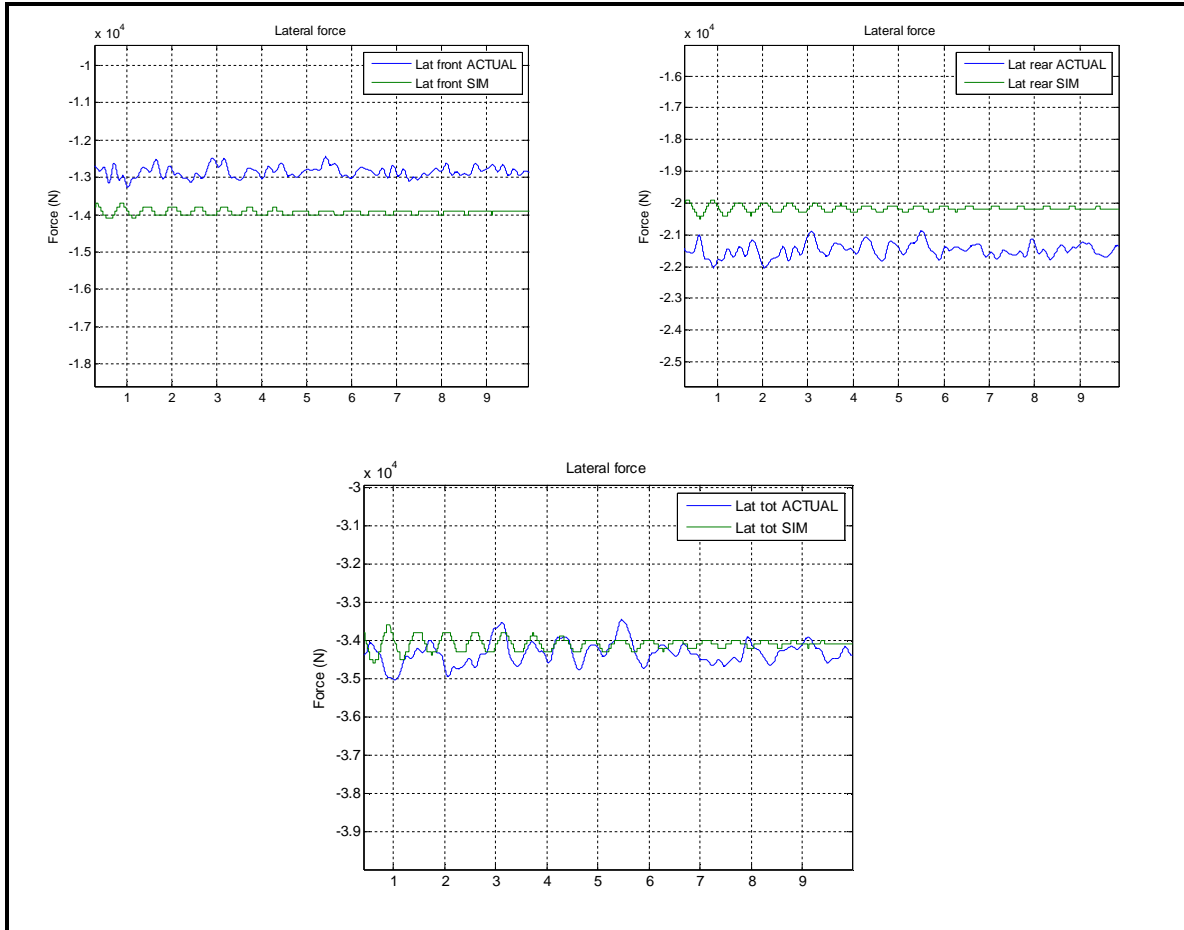


**Figure 76: Michelin tyre: Lateral load cells data comparison (Pacejka 89, Slip-angle = 10°, load condition: load 3)**

### ***Side-force versus slip-angle curves – Michelin tyre***

From the simulated data above, the side-force at each slip-angle was incorporated into a side-force versus slip-angle curve. This was done for the Fiala, Pacejka 89, and the UA tyre model. All the tyre model curves and the track testing data curves were overlayed. Figure 77 shows the resulting side-force versus slip-angle comparative curves, for the Michelin tyre for the load 1 condition. All the tyre models show good correlation with the track test data. This is a similar result to the GoodYear tyre, load 1 condition.

## Large Tyre Testing and Modelling for Handling

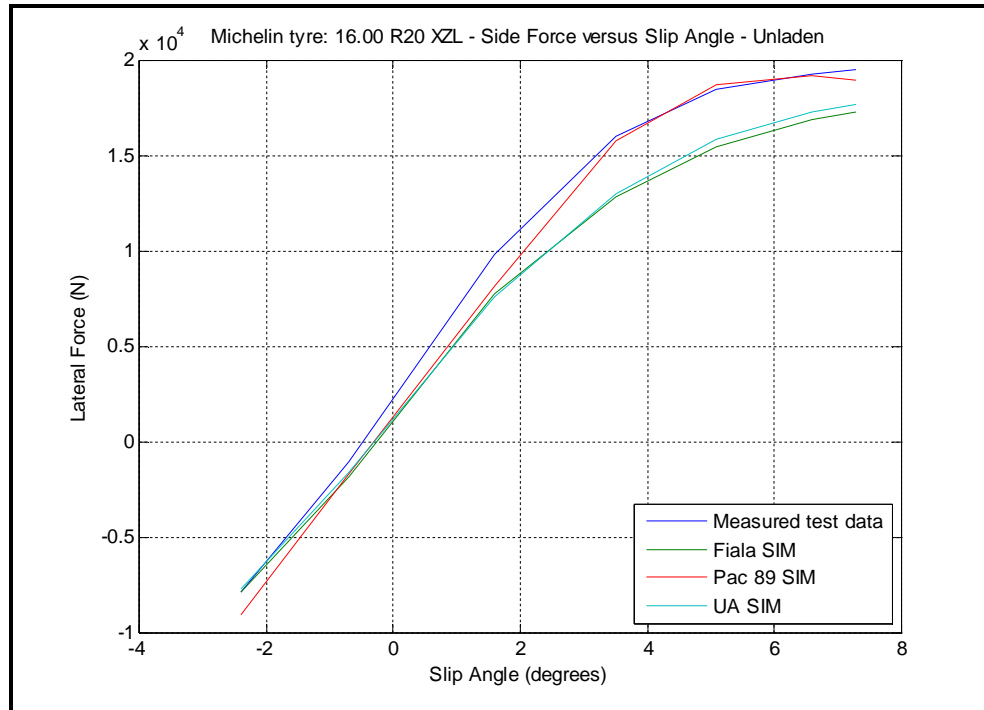


**Figure 77: Michelin tyre: Side-force versus slip-angle comparison of tyre models and measured data (Load 1)**

The side-force versus slip-angle tyre model curves were generated for the load 2 and load 3 load conditions. The comparisons of the curves with measured data are shown in Figure 78 and Figure 79 for load 2 and load 3 respectively.

The same conclusions as produced earlier for the GoodYear tyre is applicable to the Michelin tyre: i.e. the major observation is that at these higher loads (3 940 kg and 5 390 kg vertical wheel loads), it is only the Pacejka 89 model that shows good correlation with the measured track data. The Fiala model deviates significantly from the measured track data. The UA tyre model fails to simulate successfully at  $-2^\circ$ ,  $0^\circ$  and  $2^\circ$  for load condition 3, and as a result, does not produced data.

## Large Tyre Testing and Modelling for Handling

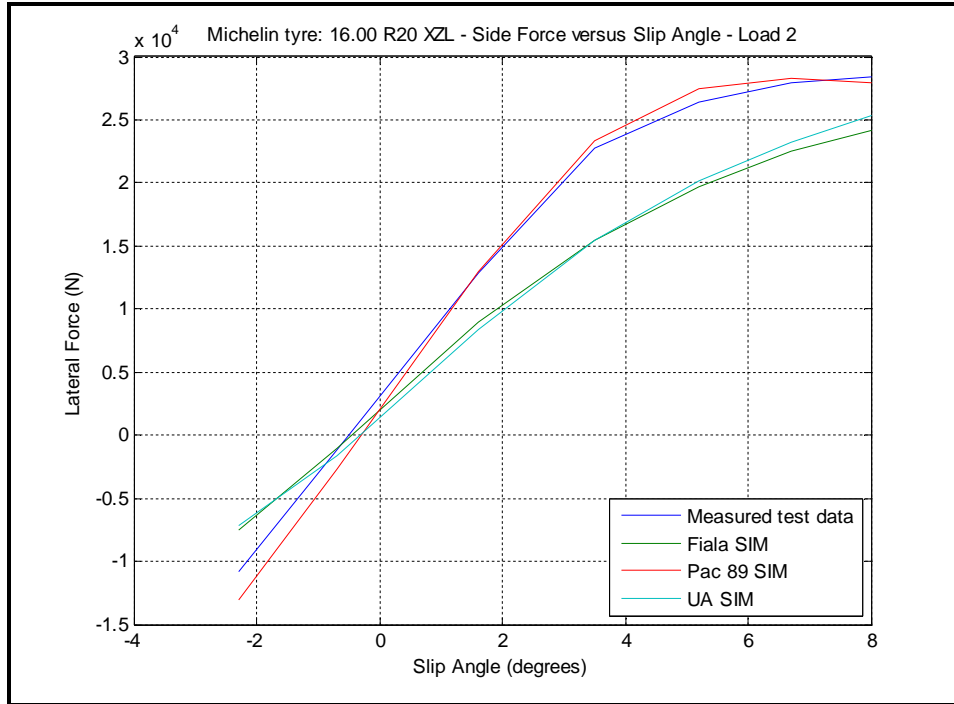


Figure 78: Michelin tyre: Side-force versus slip-angle comparison of tyre models and measured data (Load 2)

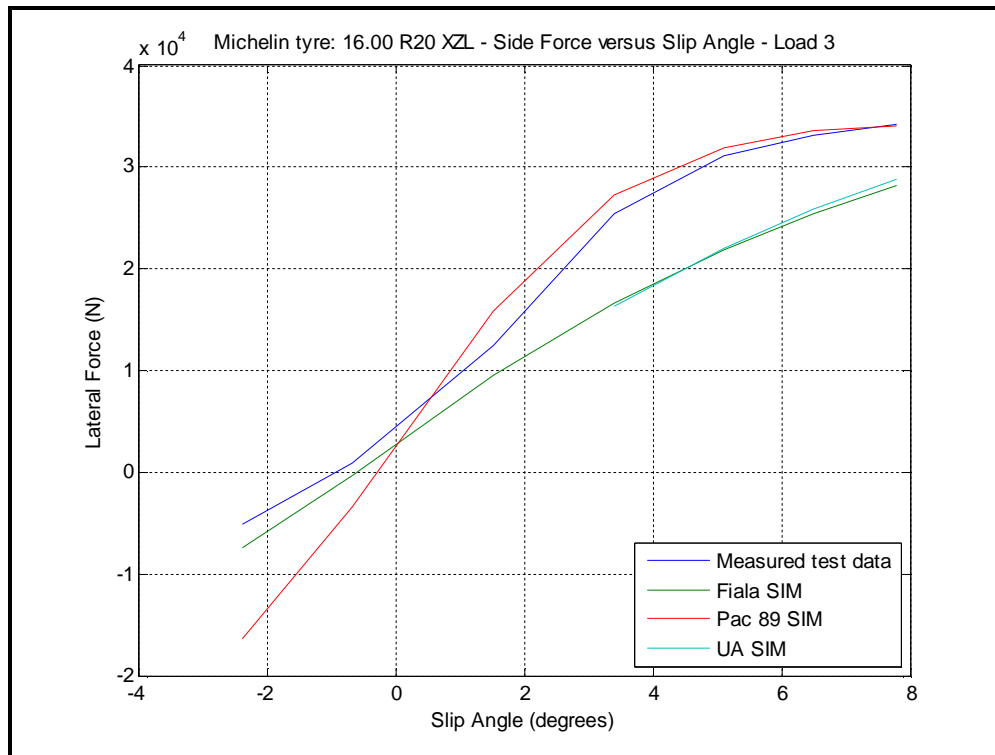
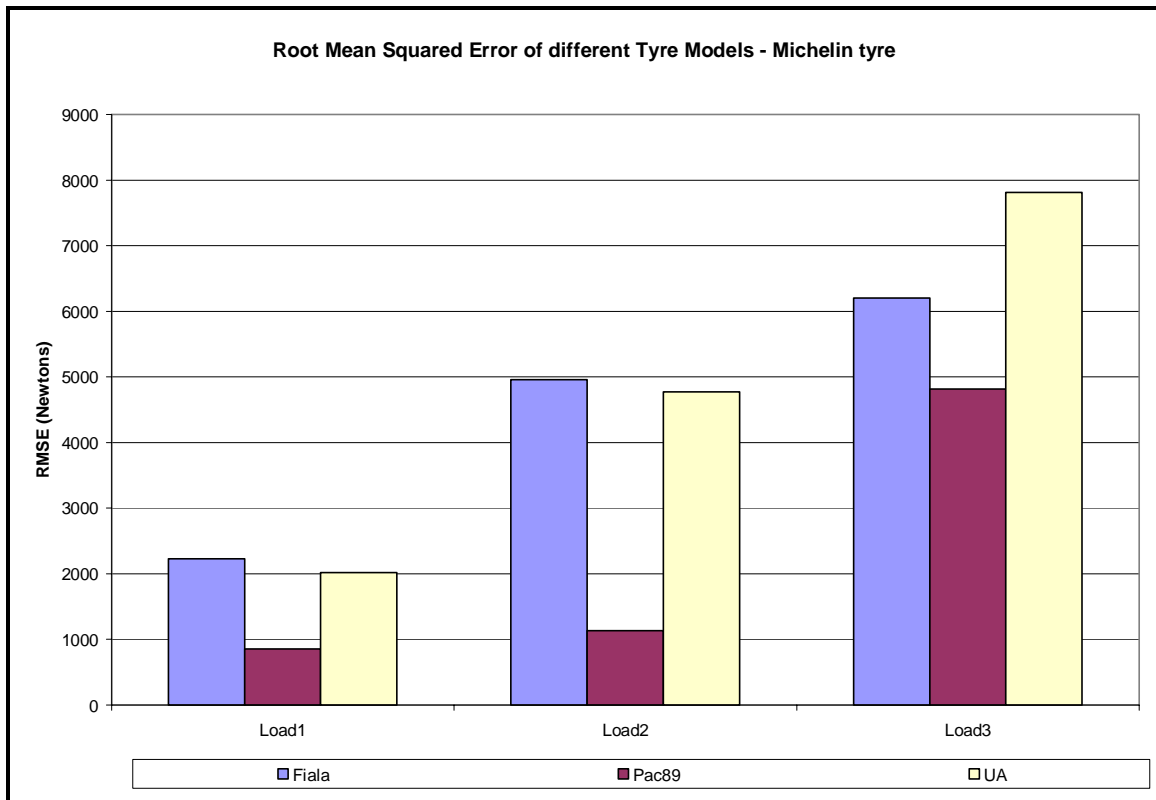


Figure 79: Michelin tyre: Side-force versus slip-angle comparison of tyre models and measured data (Load 3)

## Large Tyre Testing and Modelling for Handling

Similarly a closest fit tyre model to the track test data needed to be established for this Michelin tyre. Again the RMSE was computed for each tyre model, and the results are shown in Figure 80:



**Figure 80: Michelin tyre: Root mean squared error comparison of tyre models and measured data**

This overall correlation and deviation for the Michelin tyre can be quantified by Figure 80, which shows the root mean squared error plots for each tyre model, with reference to the measured track data. The observations are:

- The Pacejka 89 model has the least root mean squared error, over all three load conditions, therefore produces the closest fit to the measured data.
- Fiala tyre model simulates successfully over the three load conditions. However, the Fiala data has proven a result similar to that observed by Blundell (2004), where the Fiala model underestimates lateral forces where high slip-angles co-incide with higher vertical wheel loads.
- The UA (University of Arizona) tyre model is unstable at high vertical wheel loads (load3) with slip-angles close to zero (i.e. at  $-2^\circ$ ,  $0^\circ$  and  $2^\circ$ ). The simulation does not solve.

## Large Tyre Testing and Modelling for Handling

### 7.3 Pacejka 89: RMSE analysis of Curve-fit and Simulated data compared to Measured data

A Root Mean Square Error analysis was performed on the Pacejka 89 “curve-fit” and “Simulated” data compared to the measured data. Figure 81 and Figure 82 depict the results for the GoodYear and Michelin tyre respectively.

It was shown that the “simulated” data had a lower RMSE than the “curve-fit” data, for both tyres and all three load conditions. Therefore the simulated data is closer to the measured data.

However, one would expect that the “curve-fit” data to be closer to the measured data. This unusual (and positive) result has been shown for both tyres and all three load conditions.

The end result shows that the Pacejka 89 simulated data is a closer fit to the measured data, for both GoodYear and Michelin tyres and for all three load conditions.

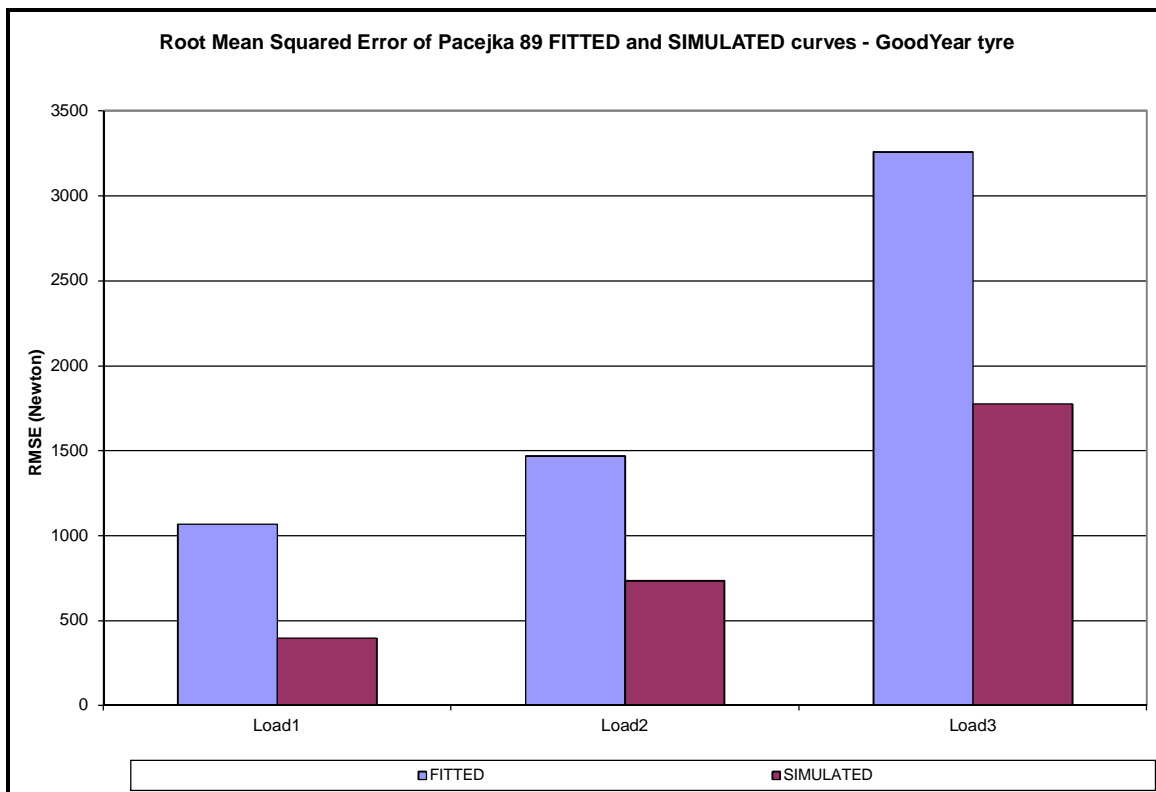
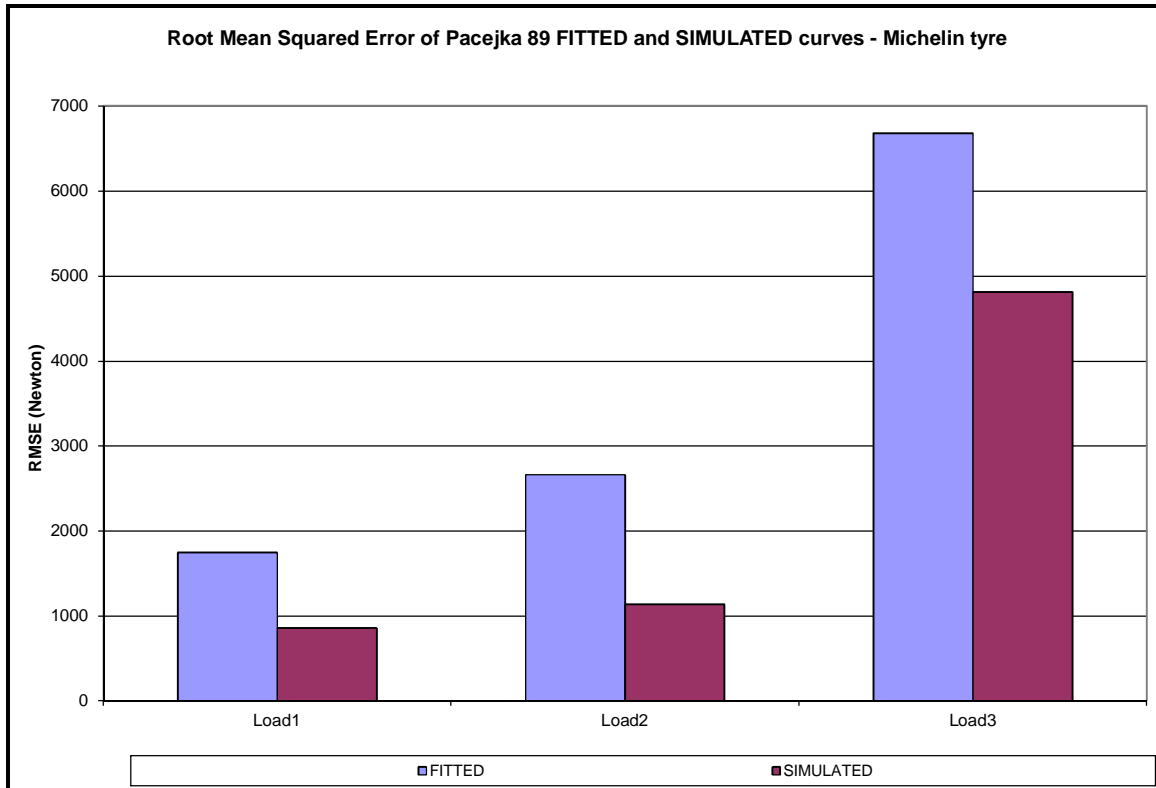


Figure 81: GoodYear tyre: Pacejka 89 tyre model Curve-fit and Simulated data compared to measured data



## Large Tyre Testing and Modelling for Handling



**Figure 82: Michelin tyre: Pacejka 89 tyre model Curve-fit and Simulated data compared to measured data**

### 7.4 Simulation results: GoodYear tyre - Double lane change

The double lane change test was performed as follows: A tow vehicle towed the Tyre Tester (slip-angle set to zero degrees on Tyre Tester) through the double lane change track. The layout of the track is given in section 4.8. The GPS co-ordinates of the actual path traversed by the Tyre Tester were recorded during the test using a VBOX III Differential GPS with base station, for highly accurate measurement. The positional accuracy of the system was 2cm (VBOX III 100Hz GPS Data Logger - User Guide, 2011). This data was used as a spline to drive the ADAMS model Tyre Tester, though the exact path that was traversed by the actual Tyre Tester. In this manner the simulation data could be compared directly with the measured track data. This is important as there are dynamic transients (i.e. changing slip-angles etc.) that occur when entering and exiting the double lane change track, and it was important that these dynamic transients are replicated by the simulation model.

Each tyre model was simulated through the measured lane change track. The lateral acceleration, tyre slip, and force on the lateral load cells were monitored, and compared with the measured track data. Figure 83 shows the results obtained for the GoodYear tyre for the Load 1 condition.

## Large Tyre Testing and Modelling for Handling

The following graphs are presented in Figure 83:

- Lateral acceleration of the Tyre Tester
- Tyre slip-angle
- The force as measured on the front lateral load cell
- The force as measured on the rear lateral load cell
- The total lateral force, which is the sum of the front and the rear lateral load cells.

For each of the above graphs the following data is overlaid

- Measured track data (blue curve)
- Simulated result with Fiala tyre model (green curve)
- Simulated result with Pacejka 89 tyre model (red curve)

Note: the UA tyre model did simulate, but the data appeared very spiky, and as a result did not show good correlation with the measured data, therefore for the comparison purposes, only the Pacejka 89 and Fiala tyre models were used.

## Large Tyre Testing and Modelling for Handling

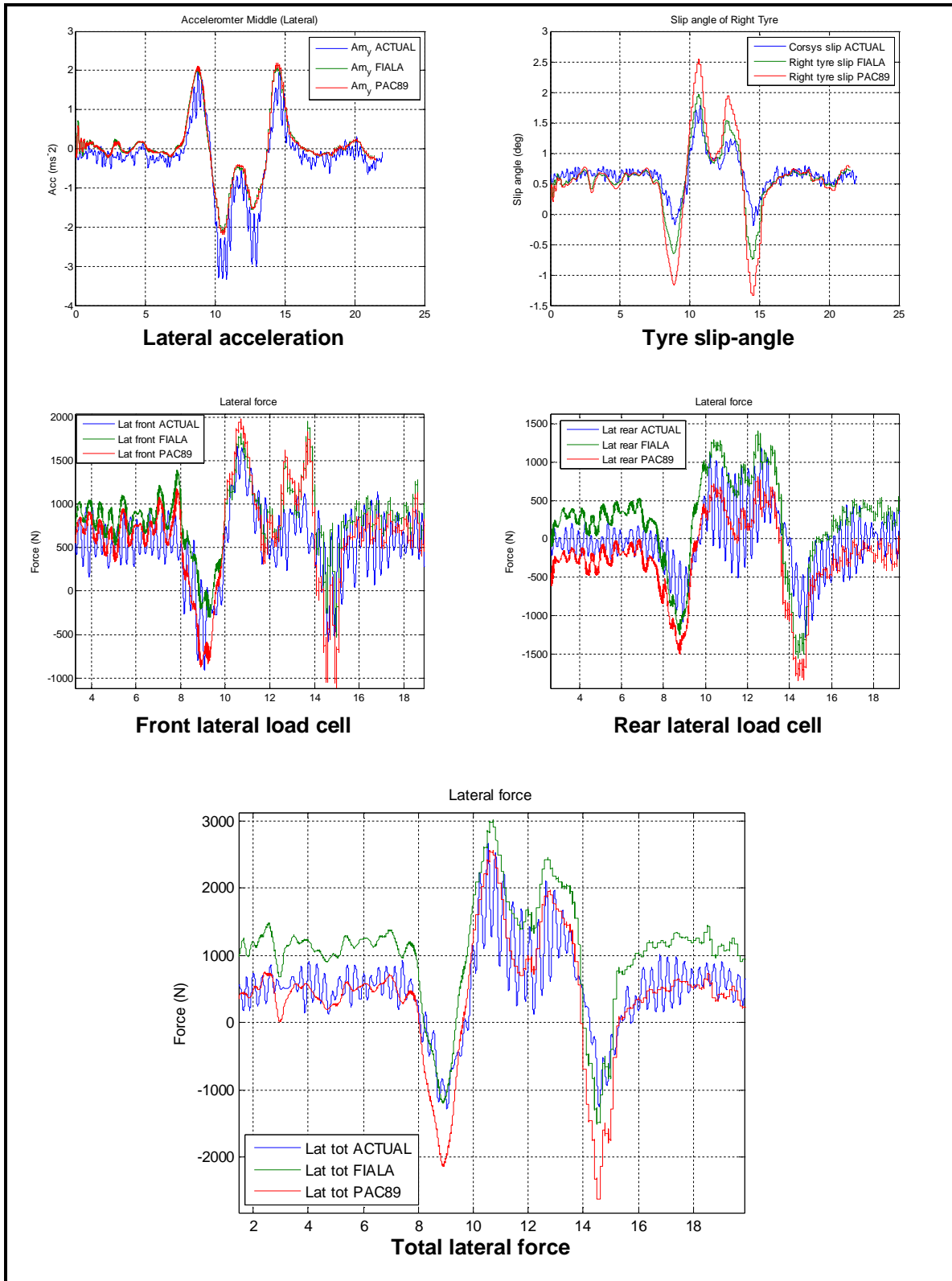
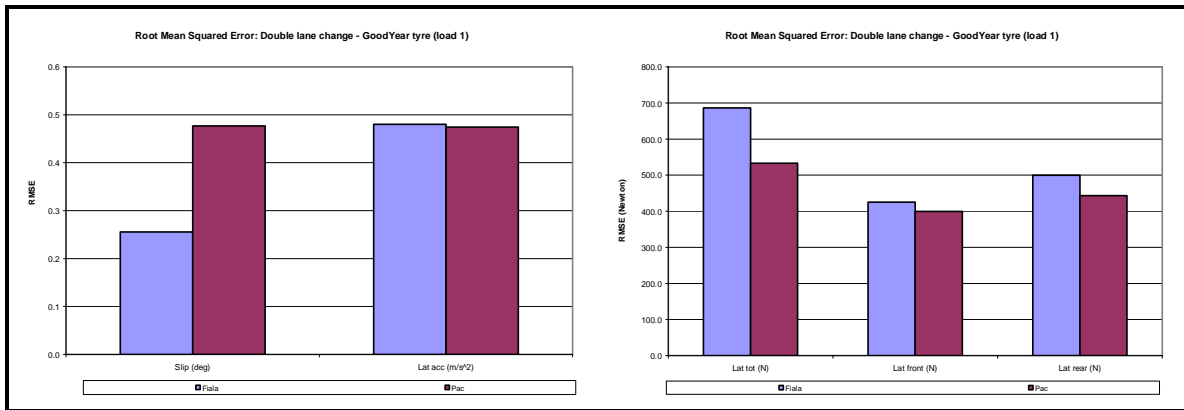


Figure 83: GoodYear tyre: Double lane change data (load condition: load 1)

## Large Tyre Testing and Modelling for Handling



**Figure 84: GoodYear tyre: Root mean squared error comparison for double lane change (load 1)**

From the Root Mean Squared Error, it indicates that the Fiala model predicts the slip-angle more accurately than the Pacejka 89 model. However the Pacejka 89 model predicts the total lateral force more accurately, than the Fiala model.

## Large Tyre Testing and Modelling for Handling

Similarly Figure 85 shows the GoodYear tyre lane change data, with the Load 2 condition.

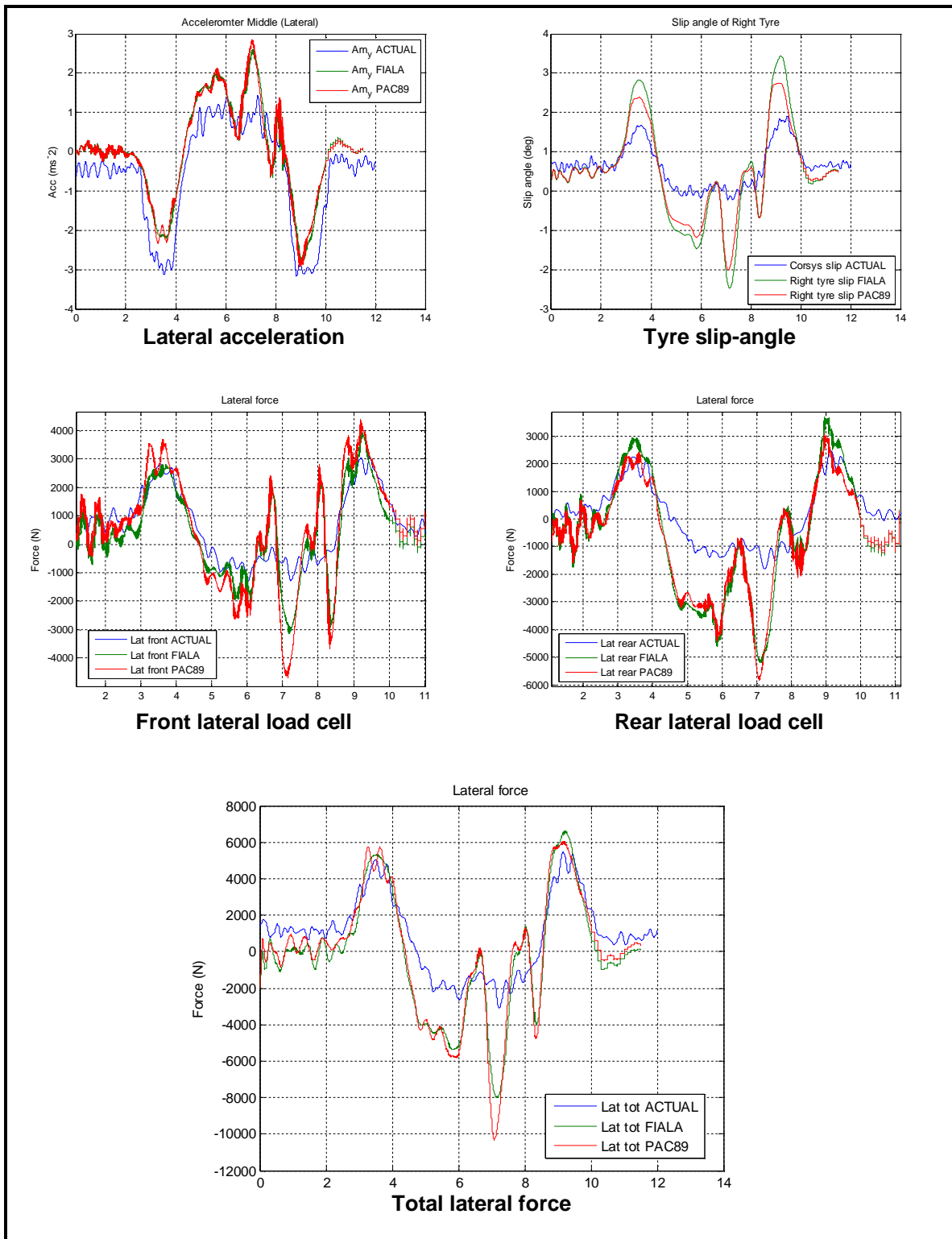
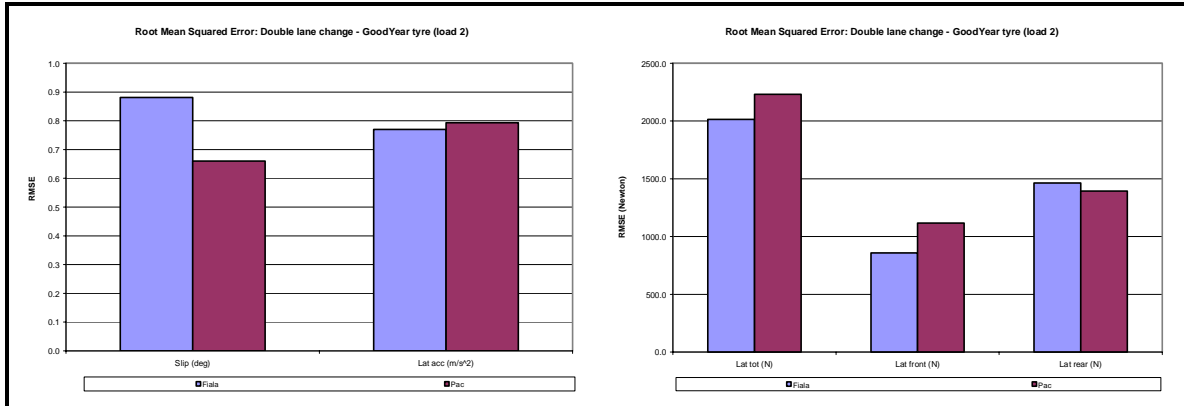


Figure 85: GoodYear tyre: Double lane change data (load condition: load 2)

## Large Tyre Testing and Modelling for Handling



**Figure 86: GoodYear tyre: Root mean squared error comparison for double lane change (load 2)**

From the Root Mean Squared Error, it indicates that the Pacejka 89 model predicts the slip-angle slightly more accurately than the Fiala model. However the Fiala model predicts the total lateral force slightly more accurately than the Pacejka 89 model, though the differences are marginal.

## Large Tyre Testing and Modelling for Handling

### 7.5 Simulation results: Michelin tyre – Double lane change

Similarly Figure 87 shows the Michelin tyre lane change data, for the Load 1 condition.

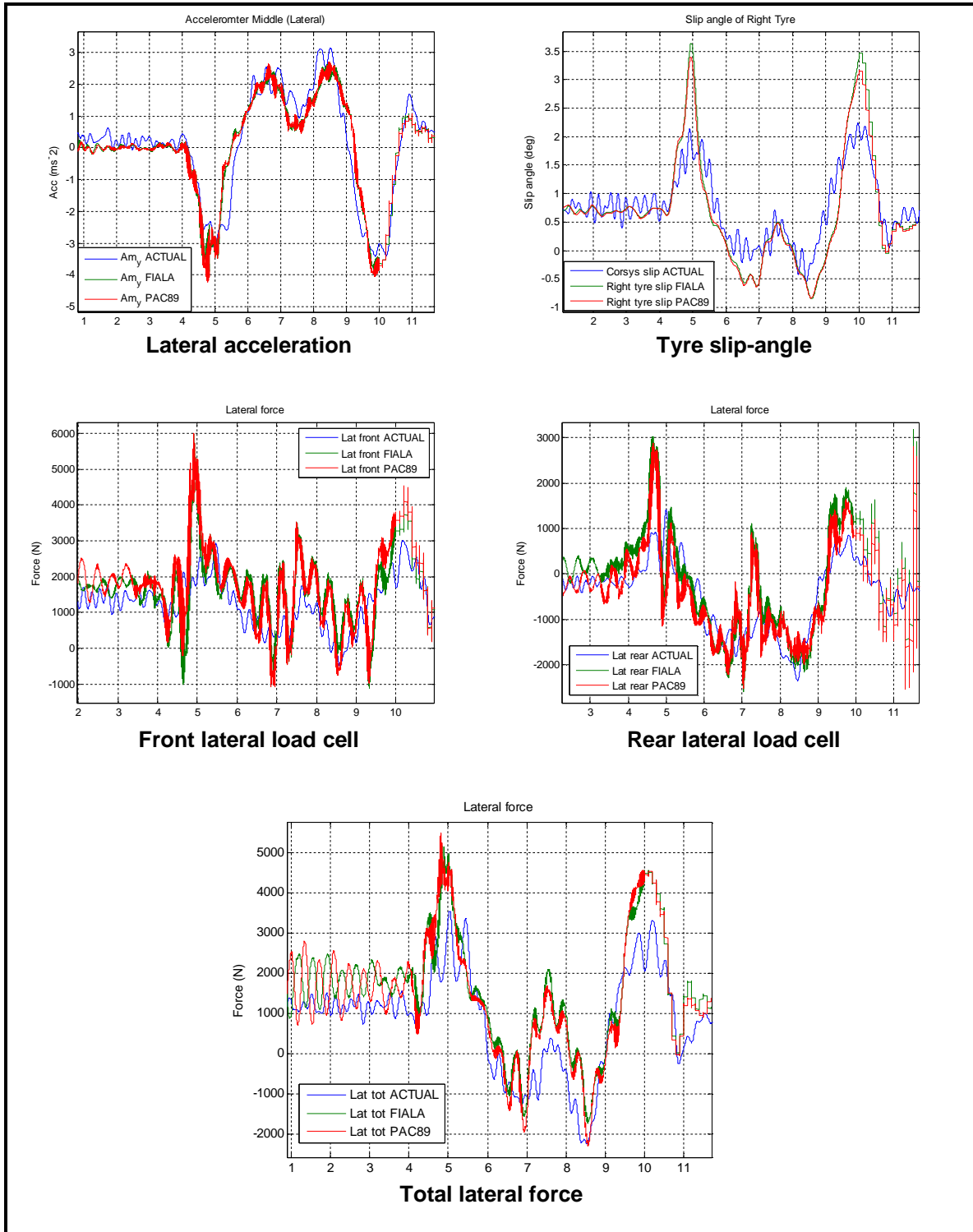
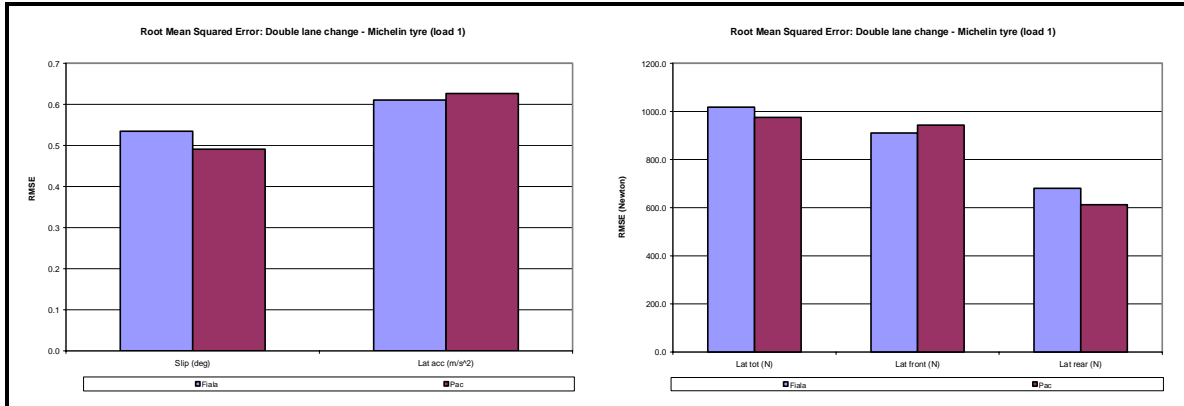


Figure 87: Michelin tyre: Double lane change data (load condition: load 1)

## Large Tyre Testing and Modelling for Handling



**Figure 88: Michelin tyre: Root mean squared error comparison for double lane change (load 1)**

From the Root Mean Squared Error, it indicates that the Pacejka 89 model predicts the slip-angle marginally more accurately than the Fiala model. Also the Pacejka 89 model predicts the total lateral force slightly more accurately, than the Fiala model (also the difference being fairly marginal). Therefore the Pacejka 89 is the better choice for the Michelin tyre at the load 1 vertical wheel load condition, as it is better at slip-angle and lateral force prediction than the Fiala model.



## Large Tyre Testing and Modelling for Handling

Similarly Figure 89 shows the Michelin tyre lane change data, with the load2 load condition.

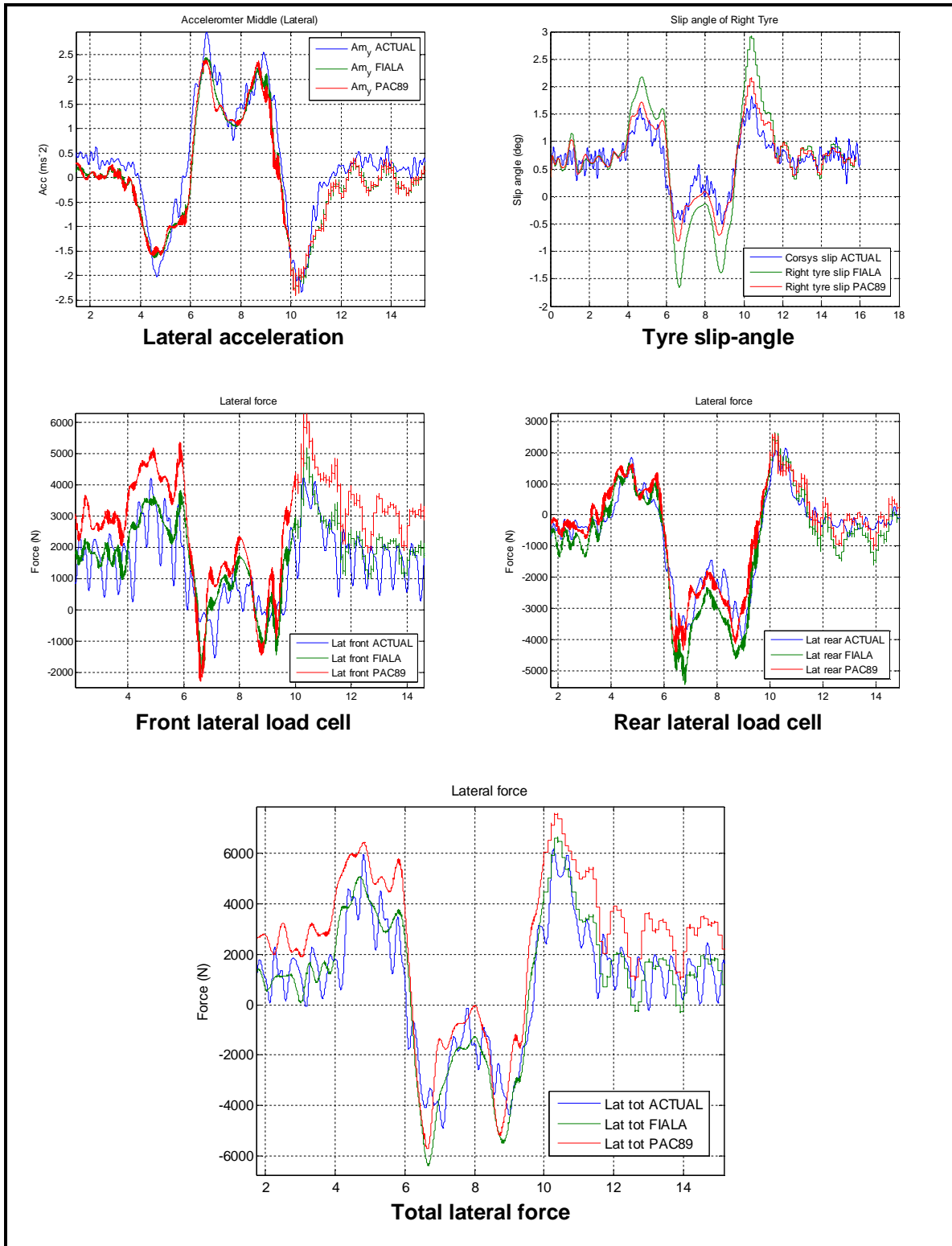
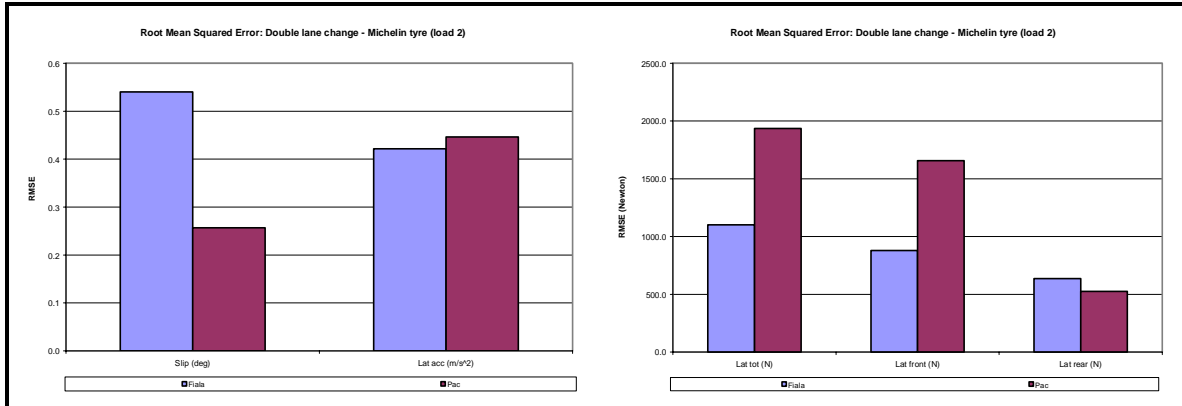


Figure 89: Michelin tyre: Double lane change data (load condition: load 2)

## Large Tyre Testing and Modelling for Handling



**Figure 90: Michelin tyre: Root mean squared error comparison for double lane change (load 2)**

From the Root Mean Squared Error, it indicates that the Pacejka 89 model predicts the slip-angle more accurately than the Fiala model. However the Fiala model predicts the total lateral force more accurately, than the Pacejka 89 model.

### ***Discussion on double lane change results: GoodYear and Michelin Tyres***

It is difficult to pick a tyre model that is a closer fit to the measured data for the double lane change test. The Root Mean Squared Errors have shown that in most cases (3 out of 4), the one model is better for slip-angle prediction and the other is better for the total lateral force prediction, or vice-versa. In one instance, however, the Pacejka 89 model was the better fit in both the slip-angle and total lateral force prediction.

In general the slip-angles are small (less than 2°) and the other possibilities for discrepancies in these sets of tests could be:

- GPS input (speed and position)
- Textures (road surface)
- Dynamic lateral stiffness of the tyre
- Dynamic vertical stiffness of the tyre

What is significant is that both the Fiala and Pacejka 89 tyre models show overall good correlation with the measured data. This result ties up with the steady state tests conducted earlier, where the Fiala and Pacejka 89 models show good correlation at low slip-angle and low vertical wheel loads.

However if the slip-angles experienced were much higher, and the vertical wheel loads were higher, then the Pacejka 89 model would be the model to use, as from the side-force versus slip-angle graphs, the correlation of the Pacejka 89 model is far superior to that of the Fiala tyre model, at higher slip-angles and higher vertical wheel loads.

## Large Tyre Testing and Modelling for Handling

### **7.6 Summary of Simulation results and correlation**

This chapter focussed on simulating the tyre models with the ADAMS model of the Tyre Tester, and the correlation of the simulated results versus the measured results.

#### ***Side-force versus slip-angle tests***

Steady state side-force versus slip-angle simulation was first conducted. The tyre models exhibited the following behaviour. Note, the conclusions are applicable to both GoodYear and Michelin tyres:

Pacejka 89 tyre model:

The Pacejka 89 model has shown the least Root Mean Squared Error, over all three load conditions, therefore produces the closest fit to the measured data.

Fiala tyre model:

The Fiala tyre model simulates successfully over the three load conditions. However, the Fiala data has proven a result similar to that observed by Blundell (2004), where the Fiala model underestimates lateral forces where high slip-angles co-incide with higher vertical wheel loads.

UA tyre model:

The UA (University of Arizona) tyre model is unstable at high vertical wheel loads (load3) with slip-angles close to zero (i.e. at  $-2^\circ$ ,  $0^\circ$  and  $2^\circ$ ). The simulation does not solve.

Conclusion for side-force versus slip-angle tests:

The Pacejka 89 tyre model is the recommended choice.

#### ***Double lane change tests***

Dynamic double lane change tests were conducted. The tyre models exhibited the following behaviour. Note, the conclusions are applicable to both GoodYear and Michelin tyres:

Pacejka 89 and Fiala tyre models:

Both Fiala and Pacejka 89 models showed good correlation on the double lane change simulation results. The low slip-angles encountered in the double lane change contribute to the Fiala models good performance. However if higher slip-angles are to be encountered, then the Pacejka 89 model would be the recommended choice, based on the steady state side-force versus slip-angle results.

UA tyre model:

The UA tyre model did simulate, but the simulation time was much longer than the Pacejka and Fiala models. The data also showed spikes, indicating instability compared to the other two models.

Conclusion for double lane change tests:

The Pacejka 89 tyre model is the recommended choice.

## Large Tyre Testing and Modelling for Handling

### 8. Conclusion and recommendations

#### 8.1 Conclusion

This research project entitled Large Tyre Testing and Modelling for Handling had two major objectives highlighted in its title. The tyre testing aspect involved the side-force versus slip-angle characteristic determination for two large truck tyres, whilst the modelling aspect involved the modelling of the Tyre Tester, and tyre models, and finally correlation between measured and simulated data.

#### **Regarding the tyre testing objective:**

The following is a summary of the targets, together with the supporting evidence of achievements.

1. To develop confidence in local tyre testing equipment  
The following was achieved in this regard:
  - The load cells on the equipment were verified.
  - Laboratory tests were conducted where forces were applied to the wheel hub of the Tyre Tester, and the resulting load cell forces were verified against the applied forces.
  - From the exercises above, enough confidence was developed in the equipment to perform track tests.
2. Conduct successful tyre tests, in order to obtain tyre data, as tyre data is not openly available:  
The following was done in support of this:
  - Conducted the following tests at Gerotek Test Facilities on both GoodYear and Michelin tyres:
    - Steady state tests: Side-force versus slip-angle tests characterisation tests
    - Dynamic tests : Double lane change tests
  - As a result of the above tests, side-force versus slip-angle characteristic curves are available for the GoodYear and Michelin tyres tested.
  - These two sets of data should be of great help to researchers working in this field as data on these tyres are virtually non-existent.

#### **Regarding the Modelling objective:**

Similarly the following is a summary of the targets, together with the supporting evidence of achievements.

1. Modelling of the Tyre Tester  
The following was done in support of this:
  - Mass of the major components of the Tyre Tester were measured (i.e. the mainframe and the subframe)
  - Centre of gravity was measured
  - Moments of inertia were measured
  - The ADAMS model was created with the above parameters incorporated therein.
2. Parameterisation tyre models  
The following lateral tyre models were parameterised, for both GoodYear and Michelin tyres:
  - Fiala tyre model

## Large Tyre Testing and Modelling for Handling

- UA (University of Arizona) tyre model
- Pacejka 89 tyre model
- 3. Correlation with track data
  - The following was done in support of this:
    - Side-force slip-angle tests
      - The Pacejka 89 tyre model has the least Root Mean Squared Error of the three tyre models, therefore has the closest fit to the measured data.
    - Double lane change tests
      - The Pacejka 89 and Fiala tyre models perform similarly, due to smaller slip-angles experienced during testing. The Pacejka 89 tyre model is the recommended tyre model to use, if higher slip-angles and loads are experienced.

So in summary, the Tyre Tester can be used to successfully perform tests to gather tyre data. Note this type of tyre data is not openly available, especially for large tyres. It was envisaged at the beginning of this project that tyre testing should become a commercial business opportunity, with the equipment available being upgraded and utilised for this purpose. At the time of writing, an opportunity for commercial tyre testing has arisen, and a quotation has been issued for the testing to be performed.

It has also been shown that from the data gathered from the track tests, it is possible to parameterise a Pacejka 89 tyre model for large tyres (for both on-road and off-road tread patterns), and produce good correlation with side-force versus slip-angle results and also dynamic tests, such as the double lane change tests.

### ***8.2 Recommendations for future work***

The following recommendations arise from the research work conducted:

A swept slip-angle functionality for the tyre-tester (rather than discrete, as it currently is) should be investigated, as it would provide more data points for the side-force versus slip-angle curves.

The effect of camber change has not been evaluated in these models. The Tyre Tester did not have adjustable camber functionality to explore this effect.

The longitudinal parameters, such as braking and propulsion, have not been explored. This is a possibility for future work in the field of tyre characteristics and modelling.

An upgrade to the Tyre Tester is proposed to investigate the areas highlighted above.

# **APPENDIX A: ADAMS TYRE MODEL FILES**

## A1. Introduction

ADAMS tyre models were developed for the GoodYear and the Michlein tyres. The following models were developed for each tyre:

- Fiala tyre model.
- UA (University of Arizona) tyre model.
- Pacejka 89 tyre model.

The tyre files of each of the models will be presented below:

**Table 1: GoodYear tyre - Fiala Model**

```

$
$Lateral force tyre model for Goodyear Regional RHT
$ 2013-09-07 correct width, aspect ratio, stiffness
$-----MDI_HEADER
[MDI_HEADER]
FILE_TYPE = 'tir'
FILE_VERSION = 2.0
FILE_FORMAT = 'ASCII'
(COMMENTS)
{comment_string}
'Tire - GoodYear Regional RHT 385/65R22.5'
'Pressure - 7.4bar'
'Test Date - 2010/11/24'
'Test tire'
'New File Format v2.1'
$-----units
[UNITS]
LENGTH = 'mm'
FORCE = 'newton'
ANGLE = 'degree'
MASS = 'kg'
TIME = 'sec'
$-----model
[MODEL]
! use mode 1 2
! -----
! smoothing X
!
PROPERTY_FILE_FORMAT = 'FIALA'
FUNCTION_NAME = 'TYR902'
USE_MODE = 2.0
$-----dimension
[DIMENSION]
UNLOADED_RADIUS = 535.0
WIDTH = 385.0
ASPECT_RATIO = 0.65
$-----parameter
[PARAMETER]
VERTICAL_STIFFNESS = 1025.6
VERTICAL_DAMPING = 2.6877
ROLLING_RESISTANCE = 0.015
CSLIP = 0
CALPHA = 4257.5
CGAMMA = 0.0
UMIN = 0.7
UMAX = 0.8
$-----shape
[SHAPE]
{radial width}
0.813 1.000
0.849 0.947
0.886 0.895
0.910 0.842
0.942 0.789
0.985 0.737
0.996 0.684
1.000 0.632
1.000 0.000
  
```

**Table 2: GoodYear tyre - UA Model**

```

$-----MDI_HEADER
[MDI_HEADER]
FILE_TYPE = 'tir' FILE_VERSION = 2.0
FILE_FORMAT = 'ASCII'
(COMMENTS) {comment_string}
'Tire - GoodYear'
'Pressure - XXXXXX'
'TestDate - XXXXXX'
'Test tire'
'New File Format v2.1'
$-----units
[UNITS]
LENGTH = 'meter'
FORCE = 'newton'
ANGLE = 'rad'
MASS = 'kg'
TIME = 'sec'
$-----model
[MODEL]
! use mode          1  2  3
! -----
! relaxation lengths      X
! smoothing              X
!
PROPERTY_FILE_FORMAT = 'UATIRE'
USE_MODE = 2
$-----dimension
[DIMENSION]
UNLOADED_RADIUS = 0.535
WIDTH = 0.385
ASPECT_RATIO = 0.65
$-----parameter
[PARAMETER]
VERTICAL_STIFFNESS = 1025600
VERTICAL_DAMPING = 2687.7
ROLLING_RESISTANCE = 0.015
CSLIP = 0
CALPHA = 243936.8
CGAMMA = 0
UMIN = 0.7
UMAX = 0.8
REL_LEN_LON = 0.0
REL_LEN_LAT = 0.535
$-----shape
[SHAPE]
{radial width}
0.813 1.000
0.849 0.947
0.886 0.895
0.910 0.842
0.942 0.789
0.985 0.737
0.996 0.684
1.000 0.632
1.000 0.000
$-----load_curve
$ For a non-linear tire vertical stiffness (optional)
$ Maximum of 100 points
$[DEFLECTION_LOAD_CURVE]
$(pen fz)
$0.000 0.0
$0.001 212.0
$0.002 428.0
$0.003 648.0
$0.005 1100.0
$0.010 2300.0
$0.020 5000.0
$0.030 8100.0

```



**Table 3: GoodYear tyre - Pacejka 89 Model**

```

$Pacejka '89 Property File
$created 2013-09-07
$correct vert damping - new width, aspect ratio
$-----MDI_HEADER
[MDI_HEADER]
FILE_TYPE = 'tir'
FILE_VERSION = 2.0
FILE_FORMAT = 'ASCII'
(COMMENTS)
{comment_string}
'Tire - GoodYear Regional RHT 385/65R22.5'
'Pressure - 7.4bar'
'Test Date - 2011/18/xx'
'Test tire'
$-----UNITS
[UNITS]
LENGTH = 'mm'
FORCE = 'newton'
ANGLE = 'radians'
MASS = 'kg'
TIME = 'sec'
$-----MODEL
[MODEL]
! use mode 1 2 3 4
! -----
! smoothing X X
! combined X X
! transient X X
!
PROPERTY_FILE_FORMAT = 'PAC89'
USE_MODE = 3.0
TYRESIDE = 'SYMMETRIC'
$-----DIMENSION
[DIMENSION]
UNLOADED_RADIUS = 535.0
WIDTH = 385.0
ASPECT_RATIO = 0.65
$-----PARAMETER
[PARAMETER]
VERTICAL_STIFFNESS = 1025.6
VERTICAL_DAMPING = 2.6877
LATERAL_STIFFNESS = 407.76
ROLLING_RESISTANCE = 0.015

$-----LATERAL_COEFFICIENTS
[LATERAL_COEFFICIENTS]
a0 = 1.30
a1 = -3.2012147546
a2 = 919.3549275

a3 = 16349100436.915
a4 = 249770333.357
a5 = 0

a6 = -0.0273655837
a7 = -1.594630872

a8 = 0
a9 = 0
a10 = 0

a11 = 0
a12 = 0
a13 = 0

$-----longitudinal
[LONGITUDINAL_COEFFICIENTS]
b0 = 0.0
b1 = 0.0
b2 = 0.0
  
```

**Table 3: GoodYear tyre - Pacejka 89 Model**

```
b3 = 0.0
b4 = 0.0
b5 = 0.0
b6 = 0.0
b7 = 0.0
b8 = 0.0
b9 = 0.0
b10 = 0.0
$-----aligning
[ALIGNING_COEFFICIENTS]
c0 = 0.0
c1 = 0.0
c2 = 0.0
c3 = 0.0
c4 = 0.0
c5 = 0.0
c6 = 0.0
c7 = 0.0
c8 = 0.0
c9 = 0.0
c10 = 0.0
c11 = 0.0
c12 = 0.0
c13 = 0.0
c14 = 0.0
c15 = 0.0
c16 = 0.0
c17 = 0.0
$-----shape
[SHAPE]
{radial width}
0.813 1.000
0.849 0.947
0.886 0.895
0.910 0.842
0.942 0.789
0.985 0.737
0.996 0.684
1.000 0.632
1.000 0.000
```

**Table 4: Michelin tyre - Fiala Model**

```

$
$ Lateral force tyre model for Michelin 16.00 R20 XZL
$
$-----MDI_HEADER
[MDI_HEADER]
FILE_TYPE = 'tir'
FILE_VERSION = 2.0
FILE_FORMAT = 'ASCII'
(COMMENTS)
{comment_string}
'Tire - Michelin 16.00 R20 XZL'
'Pressure - 3.0bar'
'Test Date - 2011/08/xx'
'Test tyre'
'New File Format v2.1'
$-----units
[UNITS]
LENGTH = 'mm'
FORCE = 'newton'
ANGLE = 'degree'
MASS = 'kg'
TIME = 'sec'
$-----model
[MODEL]
! use mode 1 2
! -----
! smoothing X
!
PROPERTY_FILE_FORMAT = 'FIALA'
FUNCTION_NAME = 'TYR902'
USE_MODE = 2.0
$-----dimension
[DIMENSION]
UNLOADED_RADIUS = 660.0
WIDTH = 406.4
ASPECT_RATIO = 1.00
$-----parameter
[PARAMETER]
VERTICAL_STIFFNESS = 707.5
VERTICAL_DAMPING = 2.5869
ROLLING_RESISTANCE = 0.015
CSLIP = 0
CALPHA = 5000.6
CGAMMA = 0.0
UMIN = 0.7
UMAX = 0.8
$-----shape
[SHAPE]
{radial width}
0.865 1
0.939 0.95
0.977 0.9
0.982 0.85
0.985 0.8
1.000 0.5
1.000 0
  
```

**Table 5: Michelin tyre - UA Model**

```

$-----MDI_HEADER
[MDI_HEADER]
FILE_TYPE = 'tir' FILE_VERSION = 2.0
FILE_FORMAT = 'ASCII'
(COMMENTS) {comment_string}
'Tire - XXXXXX'
'Pressure - XXXXXX'
'TestDate - XXXXXX'
'Test tyre'
'New File Format v2.1'
$-----units
[UNITS]
LENGTH = 'meter'
FORCE = 'newton'
ANGLE = 'rad'
MASS = 'kg'
TIME = 'sec'
$-----model
[MODEL]
! use mode          1  2  3
! -----
! relaxation lengths      X
! smoothing              X
!
PROPERTY_FILE_FORMAT = 'UATIRE'
USE_MODE = 2
$-----dimension
[DIMENSION]
UNLOADED_RADIUS = 0.660
WIDTH = 0.4064
ASPECT_RATIO = 1.00
$-----parameter
[PARAMETER]
VERTICAL_STIFFNESS = 707500
VERTICAL_DAMPING = 2586.9
ROLLING_RESISTANCE = 0.015
CSLIP = 0
CALPHA = 286513.3
CGAMMA = 0
UMIN = 0.7
UMAX = 0.8
REL_LEN_LON = 0.0
REL_LEN_LAT = 0.66
$-----shape
[SHAPE]
{radial width}
0.865 1
0.939 0.95
0.977 0.9
0.982 0.85
0.985 0.8
1.000 0.5
1.000 0
$-----load_curve
$ For a non-linear tire vertical stiffness (optional)
$ Maximum of 100 points
$[DEFLECTION_LOAD_CURVE]
${pen fz}
$0.000 0.0
$0.001 212.0
$0.002 428.0
$0.003 648.0
$0.005 1100.0
$0.010 2300.0
$0.020 5000.0
$0.030 8100.0
  
```

**Table 6: Michelin tyre - Pacejka 89 Model**

```

$Pacejka '89 Property File
$created 2013-09-07
$ correct damping, aspect ratio, width, shape
$-----MDI_HEADER
[MDI_HEADER]
FILE_TYPE = 'tir'
FILE_VERSION = 2.0
FILE_FORMAT = 'ASCII'
(COMMENTS)
{comment_string}
'Tire - Michelin 16.00 R20 XZL'
'Pressure - 3.0bar'
'Test Date - 2011/18/xx'
'Test tire'
$-----UNITS
[UNITS]
LENGTH = 'mm'
FORCE = 'newton'
ANGLE = 'radians'
MASS = 'kg'
TIME = 'sec'
$-----MODEL
[MODEL]
! use mode 1 2 3 4
! -----
! smoothing X X
! combined X X
! transient X X
!
PROPERTY_FILE_FORMAT = 'PAC89'
USE_MODE = 3.0
TYRESIDE = 'SYMMETRIC'
$-----DIMENSION
[DIMENSION]
UNLOADED_RADIUS = 660.0
WIDTH = 406.4
ASPECT_RATIO = 1
$-----PARAMETER
[PARAMETER]
VERTICAL_STIFFNESS = 707.5
VERTICAL_DAMPING = 2.5869
LATERAL_STIFFNESS = 223.09
ROLLING_RESISTANCE = 0.015

$-----LATERAL_COEFFICIENTS
[LATERAL_COEFFICIENTS]

a0 = 1.30

a1 = -6.3030646310
a2 = 979.2077539

a3 = 1051853672.434
a4 = 11125706.419
a5 = 0

a6 = 0.12686976
a7 = -6.968352745

a8 = 0
a9 = 0
a10 = 0
a11 = 0
a12 = 0
a13 = 0

$-----longitudinal
[LONGITUDINAL_COEFFICIENTS]
b0 = 0.0
b1 = 0.0
b2 = 0.0
  
```

**Table 6: Michelin tyre - Pacejka 89 Model**

```
b3 = 0.0
b4 = 0.0
b5 = 0.0
b6 = 0.0
b7 = 0.0
b8 = 0.0
b9 = 0.0
b10 = 0.0
$-----aligning
[ALIGNING_COEFFICIENTS]
c0 = 0.0
c1 = 0.0
c2 = 0.0
c3 = 0.0
c4 = 0.0
c5 = 0.0
c6 = 0.0
c7 = 0.0
c8 = 0.0
c9 = 0.0
c10 = 0.0
c11 = 0.0
c12 = 0.0
c13 = 0.0
c14 = 0.0
c15 = 0.0
c16 = 0.0
c17 = 0.0
$-----shape
[SHAPE]
{radial width}
0.865 1
0.939 0.95
0.977 0.9
0.982 0.85
0.985 0.8
1.000 0.5
1.000 0
```

# **APPENDIX B: LOAD CELL CALIBRATION CERTIFICATE**



**Apollo**  
**Scientific cc**  
"as precise as it gets"

1997/03888/23  
VAT Reg. 4930167368

P O Box 267  
Northriding  
2162  
South Africa  
Tel: +27 11 466 7666  
Fax: +27 11 466 7672  
E-Mail: info@apollosci.co.za  
Website: www.apollosci.co.za

**CERTIFICATE OF CALIBRATION**

CERTIFICATE NO : 8638FL03P  
PAGE 1 OF 5

DATE OF CALIBRATION : 16 March 2010  
CONTACT PERSON : Ms E Snyder  
CLIENT : GEROTEK  
ADDRESS : CHURCH STREET WEST  
PRETORIA

LOAD CELL & INDICATOR : TDC & HBM  
- Serial Number : 33417 & 262  
AVERAGE TEMPERATURE : 24.0 °C  
CONDITION OF LOAD CELL : Good  
REVISION NO 10.6

**FORCE CALIBRATION**


LOAD CELL RANGE : 100 kN  
- Serial Number : 33417  
RESOLUTION : 0,00001 mV/V  
STANDARD USED : 200 kN 116751  
CALIBRATION PROCEDURE : AP1001  
CALIBRATION PERFORMED IN : COMPRESSION  
CALIBRATION VALUE : N/A  
ADJUSTED BY : N/A  
LINEARITY : N/A

Applied force kN	True force in mV/V			AVERAGE mV/V
	RUN1	RUN2	RUN3	
0	0	0	0	0
10	0.20622	0.20630	0.20660	0.20637
20	0.41185	0.41208	0.41226	0.41206
30	0.61745	0.61759	0.61788	0.61764
40	0.82348	0.82348	0.82366	0.82354
50	1.02947	1.02946	1.02971	1.02955
60	1.23551	1.23565	1.23569	1.23562
70	1.44097	1.44156	1.44174	1.44142
80	1.64684	1.64742	1.64757	1.64728
90	1.85223	1.85286	1.85311	1.85273
100	2.05777	2.05843	2.05859	2.05826

UNCERTAINTY OF CALIBRATION ± 0.36 % OF READING + 1 LSD

The reported expanded uncertainty is based on a standard uncertainty multiplied by the coverage factor  $k = 2$ , providing a level of confidence of approximately 95%. The uncertainty of measurement has been estimated in accordance with the principles defined in the GUM, Guide to Uncertainty of Measurement, ISO, Geneva, 1993'

-- x -- End of page -- x --

Calibrated by:   
DEWALD JACOBS

Technical Signatory:   
JAKES JACOBS

Members: C. Bignonaut, D. Koet, N. Bignonaut



# Apollo

CERTIFICATE NO : 8638FL03P  
PAGE 2 OF 5

## AVERAGE CALIBRATION FACTORS FOR COMPRESSION

Average calibration factors were calculated for each value of force. The coefficients of a third order polynomial equation, fitted through the average calibration data points were calculated using the least square method.

The average of three sets of readings given fitted to a polynomial equation of the form:

$$y = a \cdot x^3 + b \cdot x^2 + c \cdot x + d$$

Where y is the applied load and x is the indicated load.

$$a = 2.26056E-02$$

$$b = -5.25105E-02$$

$$c = 48.6014$$

$$d = -1.141E-02$$

The inverse of the equation above has this form:

$$p = k \cdot q^3 + l \cdot q^2 + m \cdot q + n$$

Where q is the applied load and p is the indicated load.

$$k = -4.0598E-09$$

$$l = 4.58275E-07$$

$$m = 2.057553E-02$$

$$n = 2.351E-04$$

--- x --- End of page --- x ---

Calibrated by:  DEWALD JACOBS

Technical Signatory:  JAKES JACOBS



CERTIFICATE NO : 8638FL03P  
PAGE 3 OF 5

**FORCE CALIBRATION**


LOAD CELL RANGE : 100 kN  
 . - Serial Number : 33417  
 RESOLUTION : 0.00001 mV/V  
 STANDARD USED : 200 kN 116791  
 CALIBRATION PROCEDURE : AP1001  
 CALIBRATION PERFORMED IN : TENSION  
 CALIBRATION VALUE : N/A  
 ADJUSTED BY : N/A  
 LINEARITY : N/A

Applied force kN	True force in mV/V			AVERAGE
	RUN1	RUN2	RUN3	mV/V
0	0	0	0	0
10	0.20117	0.20129	0.20131	0.20126
20	0.40386	0.40394	0.40389	0.40390
30	0.60706	0.60716	0.60710	0.60711
40	0.80987	0.81067	0.81067	0.81040
50	1.01231	1.01360	1.01413	1.01335
60	1.21497	1.21660	1.21720	1.21626
70	1.41798	1.42013	1.42100	1.41970
80	1.62153	1.62421	1.62476	1.62350
90	1.82517	1.82795	1.82849	1.82720
100	2.02900	2.03184	2.03265	2.03116

UNCERTAINTY OF CALIBRATION +/- 0.39 % OF READING + 1 LSD

The reported expanded uncertainty is based on a standard uncertainty multiplied by the coverage factor  $k = 2$ , providing a level of confidence of approximately 95%, the uncertainty of measurement has been estimated in accordance with the principles defined in the GUM, Guide to Uncertainty of Measurement, ISO, Geneva, 1993

--- x --- End of page --- x ---

Calibrated by:   
DEWALD JACOBS

Technical Signatory:   
JAKES JACOBS

# Apollo

CERTIFICATE NO : 8638FL03P  
PAGE 4 OF 5

## AVERAGE CALIBRATION FACTORS FOR TENSION

Average calibration factors were calculated for each value of force. The coefficients of a third order polynomial equation, fitted through the average calibration data points were calculated using the least square method.

The average of three sets of readings given fitted to a polynomial equation of the form:

$$y = a \cdot x^3 + b \cdot x^2 + c \cdot x + d$$

Where y is the applied load and x is the indicated load.

$$a = 2.73073E-02$$

$$b = -1.89391E-01$$

$$c = 49.4983$$

$$d = 1.962E-02$$

The inverse of the equation above has this form:

$$p = k \cdot q^3 + l \cdot q^2 + m \cdot q + n$$

Where q is the applied load and p is the indicated load.

$$k = -4.5940E-09$$

$$l = 1.58024E-06$$

$$m = 2.020224E-02$$

$$n = -3.943E-04$$

--- x --- End of page --- x ---

Calibrated by:



DEWALD JACOBS

Technical Signatory:



JAKES JACOBS

## CONDITIONS OF CONTRACT:

CALCULATIONS OF THE RESULTS AND UNCERTAINTIES ARE RETAINED BY APOLLO SCIENTIFIC ACCREDITED CALIBRATION LABORATORY AND ARE AVAILABLE ON REQUEST. THE PERSON(S) SIGNING THIS CERTIFICATE ACCEPT(S) RESPONSIBILITY FOR THE CONTENTS OF THIS CERTIFICATE.

THE RESULTS GIVEN RELATE ONLY TO THE ITEM(S) CALIBRATED AND CAN ONLY BE GUARANTEED AT THE TIME OF ISSUE. NO RESPONSIBILITY IS ACCEPTED BY APOLLO SCIENTIFIC FOR ANY CLAIMS ARISING FROM READINGS MADE USING THE EQUIPMENT WHICH ARE FOUND TO BE INCORRECT IN ANYWAY DUE TO ANY CAUSE WHATSOEVER OR LIABLE FOR CONSEQUENTIAL LOSS ARISING DUE TO ANY ERROR ON IT'S PART. THIS CERTIFICATE OR REPORT SHALL NOT BE REPRODUCED IN FULL OR IN PART WITHOUT THE WRITTEN PERMISSION OF APOLLO SCIENTIFIC ACCREDITED CALIBRATION LABORATORY.

THE MEASUREMENT RESULTS RECORDED IN THIS CERTIFICATE WERE CORRECTED AT THE TIME OF CALIBRATION. THE SUBSEQUENT ACCURACY WILL DEPEND ON FACTORS SUCH AS CARE, HANDLING AND FREQUENCY OF USE. IT IS RECOMMENDED THAT RECALIBRATION BE UNDERTAKEN AT AN INTERVAL THAT WILL ENSURE THAT THE INSTRUMENT REMAINS WITHIN THE DESIRED LIMITS.

APOLLO SCIENTIFIC ACCREDITED CALIBRATION LABORATORY IS AUTHORISED BY THE SOUTH THE SOUTH AFRICAN NATIONAL ACCREDITATION SYSTEM.

"THE SOUTH AFRICAN NATIONAL ACCREDITATION SYSTEM (SANAS) IS A MEMBER OF THE INTERNATIONAL LABORATORY ACCREDITATION COOPERATION (ILAC) MUTUAL RECOGNITION ARRANGEMENT (MRA). THIS ARRANGEMENT ALLOWS FOR THE MUTUAL RECOGNITION OF TECHNICAL TEST AND CALIBRATION DATA BY MEMBER ACCREDITATION BODIES WORLDWIDE. FOR MORE INFORMATION ON THE ARRANGEMENT PLEASE CONSULT [www.ilac.org](http://www.ilac.org)"

APOLLO SCIENTIFICS' POLICY NO: 3003 TERMS AND CONDITIONS APPLY TO THIS CALIBRATION AND ARE AVAILABLE ON REQUEST.

Please note that all load-cells or tensile testing machines will be calibrated by means of comparison to a standards traceable to the national standard.

--- x --- End of Certificate of Calibration --- x ---

CALIBRATED BY:   
DEWALD JACOBS

CERTIFICATE NO: 8638FL03P

TECHNICAL SIGNATORY:   
JAKES JACOBS

DATE OF ISSUE: 23 March 2010

## References

ADAMS View HELP. 2012. California: MSC Software Corporation.

Bakker, E., Pacejka, H.B. & Lidner, L. 1989. *A New Tire Model with Application in Vehicle Dynamic Studies*. SAE Technical paper, 890087, 101-113.

Blundell, M. 2004. *The Multibody Systems Approach to Vehicle Dynamics*. 1st ed. USA: SAE.

"Car of the Week" Hot Rod Ramblings Part 2 | MyRideisMe.com. 2014. *"Car of the Week" Hot Rod Ramblings Part 2 | MyRideisMe.com*. [ONLINE] Available at: <http://www.myrideisme.com/Blog/car-of-the-week-hot-rod-ramblings-part-2/>. [Accessed 11 March 2014].

Correxit® S-HR Sensors. 2012. 1st ed. [pdf] Winterthur, Switzerland: Kistler Group, p.1. Available at: [http://www.corrsys-datron.com/Support/Data\\_Sheets/CSHRA\\_000-806e.pdf](http://www.corrsys-datron.com/Support/Data_Sheets/CSHRA_000-806e.pdf) [Accessed 6 Sep. 2014].

Ervin, R.D. 1976. *Effects of tire properties on truck and bus handling - Vol 1*. 1st ed. Springfield, VA, 22161: National Technical Information Service.

Flat-Trac® Tire Test Systems. 2005. 1st ed. [pdf] Eden Prairie: MTS Systems Corporation, pp.4&12. Available at: [http://www.mts.com/en/products/producttype/test-systems/simulation-systems/tire/flat-trac/DEV\\_002227](http://www.mts.com/en/products/producttype/test-systems/simulation-systems/tire/flat-trac/DEV_002227) [Accessed 6 Sep. 2014].

Fylstra, D., Lasdon, L., Watson, J. and Waren, A. 1998. *Design and use of the Microsoft Excel Solver*. Interfaces, 28(5), pp.29--55.

GEROTEK. 2013. *GEROTEK*. [ONLINE] Available at: [http://www.armscordi.com/SubSites/Gerotek1/GEROTEK02\\_03\\_019.asp](http://www.armscordi.com/SubSites/Gerotek1/GEROTEK02_03_019.asp). [Accessed 02 December 2013].

Haney, P. 2003. *The racing and high performance tire*. 1st ed. United States of America: Infotire and SAE. pp 111.

INTERNATIONAL ORGANISATION FOR STANDARDISATION. 2011. ISO 10392:2011(E). *Road vehicles – Determination of centre of gravity*. Geneva:ISO.

Jazar, R.N. 2008. *Vehicle Dynamics: Theory and application*. New York, USA: Springer Science + Business Media, LLC. pp 151.

Kutzbach, H.D., Witzel, P. & Schreiber, M. 2009. Single wheel field tester for farm tractor tyres a review. In: *11<sup>th</sup> European Regional Conference of the International Society for Terrain-Vehicle-Systems*. Bremen: ISTVS, pp.1-18.

Pacejka, H.B. 2006. *Tire and Vehicle Dynamics*. 2nd ed. USA: SAE International.

Robert Bosch, 1986. *Bosch Automotive Handbook*. 2nd Edition. VDI Verlag.

Stallmann, M.J. 2014. *Tyre model verification over off-road terrain*. Masters. Pretoria: University of Pretoria.

## References (continued)

Tire vs. tyre - Grammarist. 2013. *Tire vs. tyre - Grammarist*. [ONLINE] Available at: <http://grammarist.com/spelling/tire-tyre/>. [Accessed 30 November 2013].

Uys, P.E., Els, P.S., Thoresson, M.J., Voigt, K.G. & Combrinck, W.C. 2006. *Experimental determination of moments of inertia for an off-road vehicle in a regular engineering laboratory*. International Journal of Mechanical Engineering Education, 34/4, 291 - 314.

VBOX III 100Hz GPS Data Logger - User Guide. (2011). 17th ed. [pdf] Buckingham: Racelogic Ltd, p.20. Available at: [http://www.racelogic.co.uk/\\_downloads/vbox/Manuals/Data\\_Loggers/RLVB3\\_Manual%20-%20English.pdf](http://www.racelogic.co.uk/_downloads/vbox/Manuals/Data_Loggers/RLVB3_Manual%20-%20English.pdf) [Accessed 14 Sep. 2014].

VMI Group | Force and moment testing. 2014. *VMI Group | Force and moment testing*. [ONLINE] Available at: <http://www.vmi-group.com/tire/products/tire-and-compound-testing/force-and-moment-testing/>. [Accessed 11 March 2014].

Wong, J.Y. 2001. *Theory of Ground Vehicles, 3rd Edition*. 3 Edition. Wiley-Interscience, p 29.

www.ika.rwth-aachen.de, 2007. *Dynamic Tire Test Facility*. [online] Available at: [http://www.ika.rwth-aachen.de/pdf\\_eb/gb1-06e\\_tire\\_test\\_facility.pdf](http://www.ika.rwth-aachen.de/pdf_eb/gb1-06e_tire_test_facility.pdf) [Accessed 6 Sep. 2014].

Yunus.hacettepe.edu.tr, (n.d.). *Tyre test rigs*. [online] Available at: <http://yunus.hacettepe.edu.tr/~scaglarb/omu403/test%20rigs.docx> [Accessed 6 Sep. 2014].